POLING OF FERROELECTRIC 0-3 COMPOSITES

SUBMITTED BY

OR YUK TIN

FOR THE DEGREE OF MASTER OF PHILOSOPHY AT

THE DEPARTMENT OF APPLIED PHYSICS

The Hong Kong Polytechnic University

2003

ABSTRACT

Poling of ferroelectric lead titanate / polyvinylidene fluoride - trifluoroethylene (PT/P(VDF-TrFE)) 0-3 composites has been studied. Successful poling of various 0-3 composites like PT, PZT & PLZT dispersed in polymer matrices has been reported in the literature. However, the poling recipes / techniques are still quite empirical because a firm understanding of the physical processes involved in poling has not been established. The present work aims at a systematic study of the physical processes relevant to the poling process. Understanding of the physical processes behind poling will give an idea on the materials selection and the design of poling parameters for tailored applications.

Thick composite films with lead titanate (PT) ceramic volume fractions from 0.05 to 0.3 were fabricated. The PT powder was prepared by the metal alkoxide sol-gel method. The gel was sintered at 600 °C for one hour. The average diameter and standard deviation of the PT particles were determined as 300 nm and 170 nm respectively by a particle size analyzer, and the crystalline structure was characterized by X-ray diffractometry. 30 μm thick composite films were prepared by solution casting followed by compression molding. Uniform dispersion of the ceramic particles

in the copolymer matrix was confirmed by examining fracture surfaces of the samples under a scanning electron microscope. Gold electrodes were deposited on both surfaces of the composite samples.

The dielectric properties of the composite samples were studied from -20 °C to 120 °C in the frequency range of 100 Hz to 1 MHz. The capacitance and loss factor were measured as a function of both temperature and frequency. The results were compared with a prediction by the Bruggeman model and good agreement is found. Curie's transitions were identified at 106 °C and 65 °C in the heating and cooling curve respectively.

The polarization development in the composite film under poling conditions was extensively studied. Composite films were polarized at an elevated temperature of 120 °C under a high d.c. electric field of 50 MV/m for different poling times to polarize the ceramic phase only. Unpoled samples were measured for reference: the pyroelectric and piezoelectric coefficients, the pyroelectric profiles across the film thickness and the XRD patterns showed null polarization consistently. The samples were then subjected to the poling process for different poling times. The pyroelectric and piezoelectric coefficients were measured at various poling times and the pyroelectric profile along the sample thickness direction was measured by the laser

intensity modulation method (LIMM). Pyroelectric profiles also revealed the composite with 30 vol-% PT can be uniformly polarized along the thickness direction in 10^3 s. The XRD patterns of the unpoled and poled samples were compared. Peak intensity changes in (002) and (200) were observed and the poling ratio of the inclusions could therefore be estimated. The result shows that higher poling ratio under the same poling condition can be obtained in the composites with higher ceramic volume fraction. Both measurements, LIMM and XRD show that the inclusions can be polarized to a saturated state in 10^3 s, which is found to be several times shorter than the time scale reported previously.

Theoretical modeling has been developed to study the effective polarization response of the composite systems under an arbitrary applied electric field. The model intends to explain the physical features related to the poling process. The electric fields acting in the constituent phases, remanent polarization in the ceramic particles and interfacial compensating charges as a function of poling time have been evaluated. Both experimental observation and theoretical simulation indicate that the PT ceramic inclusions can be fully polarized fairly quickly at an elevated temperature where the conductivity of the polymer matrix is high enough to provide a desirable condition for the build-up of high electric field acting in the ceramic phase. Model predictions on the

piezoelectric and pyroelectric activities of the 0-3 composites based on the calculated polarization behaviour of the inclusions as a function of poling time were also discussed.

ACKNOWLEDGEMENTS

I would first like to thank my thesis supervisors Dr. B. Ploss and Prof. F. G. Shin for their guidance, support and patience throughout the course of this thesis work. Without their motivation and insight, this thesis would not have been completed.

My thanks are also extended to Dr. N. Chong, Dr. Y. W. Wong, Dr. K. H. Pang and Mr. M. N. Yeung for their support and fruitful discussions.

For those friendly helping hands in dealing with the practical details, I am thankful to Miss W. M. Fung, Mr. C. K. Wong, Dr. R. Zeng, Mr. K. Li, Mr. S. U. Akidary, Mr. K. W. Tang, Mr. L. S. Tai, Mr. K. C. Cheng, Mr. C. H. Tsang, Mr. K. H. Lam, Mr. D. Y. Wang, Mr. S. F. Wong, Mr. C. W. Tsang, Mr. K. P. Kwok and Mr. T. T. Leung.

Most of all I would like to thank my parents for their continued love, support, understanding and patience. It is to them I owe my deepest thanks and appreciation. Without them this accomplishment would not have been fulfilled.

Support from the Materials Research Centre and The Hong Kong Polytechnic University are gratefully acknowledged.

TABLE OF CONTENTS

Chapter 4 Modeling Studies

Chapter 5 Conclusion and Suggestions for Future Work

LIST OF FIGURE CAPTIONS

LIST OF TABLE CAPTIONS

CHAPTER 1
INTRODUCTION

1.1 Ferroelectric Composites

Composite systems with ferroelectric ceramics and ferroelectric polymers may combine the high piezoelectric and pyroelectric activities of the ceramic with the excellent mechanical properties of the polymer and have therefore received great attention due to their advantages for sensor and transducer applications.

Piezoelectric materials not only have the ability to convert mechanical to electrical energy but also develop strain upon application of an electric field [Moulson, 1990]. Thus piezoelectric materials can be utilized to provide both sensing and actuating capabilities, which, along with their fast response characteristics are some of the reasons why these materials have been used extensively in the development of smart composite structures. Polymer based piezoelectric composite materials can offer additional advantages, such as compatibility to the host matrix and ease of embedding. Ferroelectric ceramic/polymer composites can take advantage of the favorable properties of their constituents while reducing the detrimental ones. The high piezoelectric, pyroelectric and electromechanical properties of the ceramic phase

combined with the mechanical properties and low relative permittivity of the polymer matrix can enhance the overall performance of a composite. Thus, desirable properties for specific applications can be achieved by the appropriate choice of constituents, their relative amount and their connectivity.

The different ways of connectivity of the ceramic and polymer phases of composites were classified by Newnham *et al.* [Newnham, 1978]. The simplest type of piezo- / pyroelectric composite consists of a polymer matrix embedded with ceramic particles. In a composite with 0-3 connectivity, the ceramic particles are not in contact with each other while the polymer phase is self-connected in all three dimensions. Figure 1.1 shows the schematic diagram of a ceramic/polymer 0-3 composite. One of the most attractive features of the 0-3 design is its versatility in fabricating a variety of forms including thin film, extruded bar and fibers, and molded shapes, and has the ability to conform to curved surfaces. This type of composite is also easy to manufacture in large sizes and capable of mass production [Safari, 1986].

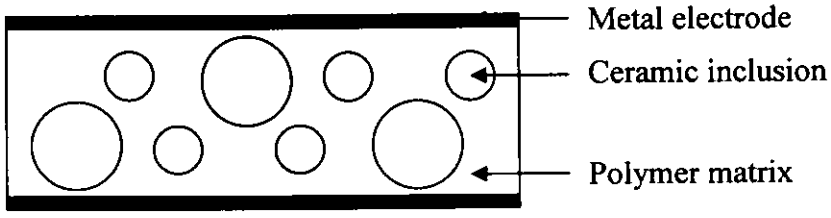

Figure 1.1 Schematic diagram of ceramic/polymer 0-3 composite.

Ferroelectric materials have a spontaneous polarization but usually show no net macroscopic polarization due to the different orientations of the individual domains. In order to impart piezoelectric and pyroelectric activities, they must be subjected to a poling process, to give orientation to the spontaneous polarization in the ferroelectric phase(s) [Furukawa, 1986]. Polarization methods for ferroelectrics are generally based on the application of an electric field to the dielectric material. Although the poling process is conceptually simple, it can be quite complex in practice. For example, for some ferroelectric materials, a problem is caused by the fact that the coercive field strength required for the orientation of the polar groups is only slightly lower than the electrical breakdown field [Ploss, 1996]. On the other hand, the relative permittivity of ceramics is usually much larger than that of polymers, say by at least a factor of ten. Consequently, the applied electric field is, at least instantaneously, greatly reduced in the ceramics phase, which seems to make the polarization (poling) of a 0-3 composite impossible [Furukawa, 1986].

Poling of composites has been extensively studied by several research groups. Yamazaki *et al.* have studied the polarization ratio and pyroelectric coefficient of the PT/PVDF 0-3 composite as a function of poling field [Yamazaki, 1981]. A linear dependence between the pyroelectric coefficients of the composites and the poling field was reported. Furukawa *et al.* have studied the piezoelectric properties of

PZT/polymer 0-3 composites as a function of poling field and poling time [Furukawa, 1976, 1979, 1986]. Safari *et al.* [Safari, 1986] have studied the piezoelectric properties of carbon doped PZT/polymer 0-3 composite as a function of poling electric field and time. A duration of 5 minutes is reported to be sufficient for full poling of the carbon-doped composites under a field of 4 MV/m at 100 °C. Ploss *et al.* [Ploss, 1996] have studied the poling of the P(VDF-TrFE) copolymer by using the ferroelectric crystal electrodes. Chan *et al.* [Chan, 1999] and have studied poling procedures to produce 0-3 composites with only the ceramic phases polarized and with both phase polarized in the same direction and in opposite directions. When the two phases are polarized in the same direction, the piezoelectric activities of the two phases partially cancel each other while the pyroelectric activities reinforce, or vice versa, due to the same sign of the pyroelectric coefficient but opposite signs of the piezoelectric coefficient of the two phases.

Various studies have demonstrated the successful poling of composites with 0-3 connectivity. However, in many of these works the poling recipes or schedules adopted rely mostly on experience or trial and error and the physical basis is not usually been guided by technical aspects only and the scientific knowledge is usually not investigated in sufficient detail. Therefore, there is significant interest to a systematic study of the physical processes relevant to the poling of ferroelectric

composites. A fundamental understanding of poling of the composites would be helpful in modeling the polarization behaviour of any combination of ceramic/polymer 0-3 composites, thus allowing the design of practical criteria for materials selection and optimum poling conditions for tailored applications.

There is a large number of ferroelectric materials which exhibit piezoelectricity and/or pyroelectricity. Some typical examples are listed in Table 1.1.

Table 1.1 Materials parameters of commonly used piezo-/pyroelectric materials.

Property	$BaTiO_3$[a]	$Pb(Zr_{0.48}Ti_{0.52})$[c]	$PbTiO_3$[b]	P(VDF-TrFE)[c]
Density (kg/m^3)	5700	7600	7120	1790
Curie Point (°C)	130	386	494	–
d_{33} (pC/N)	190	223	47	-33
d_{31} (pC/N)	-79	-93.5	-7.4	9
p ($\mu C/cm^2K$)	–	–	300	28
k_{33}	0.49	0.67	0.46	22.8
$tan\ \delta$	0.007	0.004	0.022	0.02-0.11
k_p	0.38	0.52	–	–
k_t	0.38	0.51	0.46	0.25-0.30
Q_m	500	500	326	10
ε_3^T	1900	730	203	7.9
ε_3^S	1420	399	–	–
s_{33}^D	6.76	9.35	6.3	–
s_{33}^E	9.6	17.1	8.0	300

where

k_{33} = longitudinal electromechanical coupling coefficient

$tan\ \delta$ = dielectric loss tangent

k_p= planar electromechanical coupling coefficient

k_t = thickness electromechanical coupling coefficient

Q_m = mechanical quality factor

ε_3^T = free relative permittivity

ε_3^S = clamped relative permittivity

s_{33}^D = elastic compliance coefficient at constant electric displacement

s_{33}^E = elastic compliance coefficient at constant electric field

[a] Jaffe, 1971

[b] Channel Industrials, 1998

[c] Atomchem, 1991

Various combinations of ceramic/polymer 0-3 composites have been studied in the literature. Early attempts to fabricate flexible 0-3 composites of piezoelectric lead zirconate titanate (PZT) ceramic particles and polymer were made by Kyiatama [Kyiatama, 1979], Pauer [Pauer, 1973] and Harrison [Harrison, 1976]. The piezoelectric charge coefficients (d_{33}) of these composites were comparable with stretched polyvinylidene fluoride (PVDF), but the hydrostatic strain coefficients (d_h) was lower than those of solid PZT and stretched PVDF polymer. An improved version of the 0-3 composites was synthesized by Banno and Saito [Banno, 1983]. Rather than using PZT as the ceramic filler, pure or modified lead titanate was employed because of its greater piezoelectric anisotropy. The composites were fabricated by mixing 5 μm fillers produced by water-quenching of the ceramic with chloroprene rubber and rolled into 0.5 mm thick sheets. The composites were poled in an electric field of 100-150 kV/cm for 30 minutes. It was found that the d_h value could be as large as 35 pC/N and independent of pressure up to 40 MPa. Barium titanate (BT)/rubber 0-3

composites have been synthesized by Amin and coworkers [Amin, 1988]. The pyroelectric coefficient (p) was found to be approximately 60 $\mu C/cm^2K$ for a 30 % ceramic volume fraction loading. The relative permittivity (ε) was found to be around 17 and thus the pyroelectric figure of merit ($FOM_p = p/\varepsilon$) was 3.5 $\mu C/cm^2K$ which was a quite high value. The pyroelectric coefficients of composites of PZT, lanthanum modified PZT (PLZT) and calcium modified PT (PTCa) with polyvinylidene fluoride-trifluoroethylene (PVDF-TrFE) were investigated by Dias *et al.* [Dias, 1992, 1993]. They reported that the pyroelectric coefficients of PT composites were about 50% and 150% higher than those of PZT and PLZT composites, respectively, at room temperature.

Here we summarize the piezoelectric and pyroelectric coefficients of selected composites in Table 1.2 and Table 1.3 respectively.

Table 1.2 Piezoelectric properties of selected composites

Composite		ceramic vol. fraction	d_{33} (pC/N)	d_h (pC/N)
ceramic	polymer			
PZT[a]	PVDF	0.67	48.3	–
PT[b]	P(VDF-TrFE)	0.4	28	–
PLZT[b]	P(VDF-TrFE)	0.4	29	–
PTCa[c]	epoxy	0.5	–	22
PTCa[d]	P(VDF-TrFE)	0.5	–	8.5

[a] Yamada, 1982
[b] Ngoman, 1990
[c] Garner, 1989
[d] Dias, 1996

Table 1.3 Pyroelectric properties of selected composites

Composite		ceramic vol. fraction	ε	pyroelectric coefficient ($\mu C/m^2K$)	pyroelectric FOM ($\mu C/m^2K$)
ceramic	polymer				
PZT[a]	epoxy	0.4	110	40	0.35
PZT[b]	PVDF	0.5	90	10	0.11
PZT[c]	P(VDF-TrFE)	0.5	118	39	0.33
PTCa m[c]	P(VDF-TrFE)	0.5	56	50	0.99
PTCa q[c]	P(VDF-TrFE)	0.3	28	29	1.03
PTCa q[c]	P(VDF-TrFE)	0.5	40	44	1.10
PLZT[c]	P(VDF-TrFE)	0.5	80	17	0.21
BT[d]	rubber	0.3	17	60	3.5
TGS[e]	PVDF	0.8	12	90	3.3
PT[f]	PVDF	0.62	54	130	2.4

The m and q suffixes stand for milled and quenched powder respectively.

[a] Bhalla, 1981
[b] Abdullah, 1989
[c] Dias, 1992
[d] Amin, 1989
[e] Fang, 1991
[f] Yamasaki, 1981

In the present study on ferroelectric 0-3 composites, PT is selected as the ceramic inclusions because it not only has high piezo- and pyroelectric activities but also a relatively low relative permittivity among the conventional ferroelectric ceramics. Banno and Saito [Banno, 1983] have reported that 0-3 composites with PT as the inclusion material has a superior piezoelectric response compared with those made with PZT as inclusion material. This is attributed to the large c/a ratio of 1.06 in the PT. Figure 1.2 shows the variation of lattice constant with temperature for PT. On the other hand, Gururaja *et al.* [Gururaja, 1985] reported that there are two reasons that large spontaneous strain may be advantageous. First, it makes it easy to obtain a loose ceramic powder of extremely fine grain size. The second reason is that a large spontaneous strain in the ceramic will result in a higher hydrostatic sensitivity, and contribute to a better performance in transducer applications. However, PT is a dense, brittle ceramic, which undergoes a large volume change at the Curie temperature; this often causes fracture during bulk preparation.

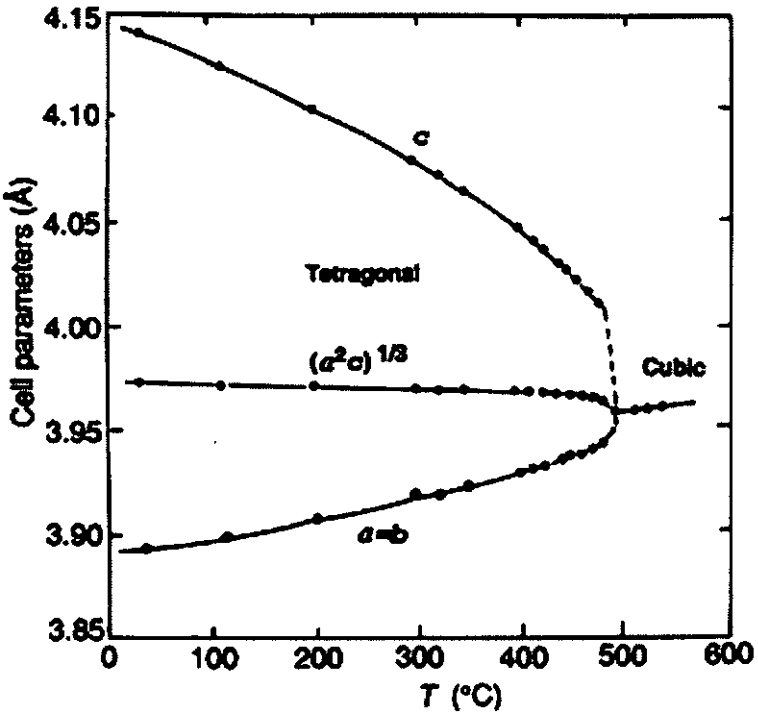

Figure 1.2 Lattice constant with temperature for PT [Jaffe, 1971].

P(VDF-TrFE) 70/30 mol-% is chosen as the copolymer matrix in our study because it has relatively high permittivity (ε~14) among typical polymers such as epoxy (ε~5) [Wada, 1976], which as pointed out before enhances the poling efficiency of the ceramic phase [Dias, 1994]. On the other hand, it has low density, high flexibility and lower coercive field than stretched PVDF. Also, P(VDF-TrFE) copolymer with TrFE content higher than 20 mol-% is known to crystallize from a melt or a solution in the polar β phase and can thus be poled without prior stretching.

1.2 Objectives of Thesis

The aim of the present project is to study the physical processes relating to the poling of ceramic/polymer composite systems.

The main objectives are:

1. To prepare PT/P(VDF-TrFE) 0-3 composites with nanosized PT particles derived from sol-gel method.
2. To study experimentally and theoretically the polarization of the composites as a function of poling time, especially in the short poling time regime.
3. To study the dielectric, piezo-/pyroelectric properties, polarization ratio and polarization profile along the thickness direction of the composites versus ceramic volume fraction.

1.3 Outline of Thesis

This thesis describes the fabrication, microstructure, dielectric, ferroelectric, piezoelectric and pyroelectric properties of PT/P(VDF-TrFE) 0-3 composites. The polarization behaviour of the composite structures is also elaborated.

The first chapter provides a general introduction to ferroelectric composites. A brief overview of the properties of ferroelectric ceramic, polymer and composites is given.

The second chapter introduces the sample preparation and characterization of the constitutive materials and the composites. The microstructure, dielectric and ferroelectric properties of the composites are also described.

Chapter 3 reports on a brief expedition on thermal poling. This chapter introduces the thermal poling procedures, and reports the characterization of the poling state of the composites.

A theoretical approach to study the poling of composite structures is given in the fourth chapter. Poling behaviour of multi-layered composite and predictions on polarization, piezoelectric and pyroelectric properties of the 0-3 composite are also discussed.

Finally, in the last chapter some conclusions are drawn.

CHAPTER 2
SAMPLE PREPARATION AND CHARACTERIZATION

2.1 Introduction

In the preparation of the ceramic/polymer 0-3 composites for this study, it is imperative to use ceramic particles with high piezo-/pyroelectric activities because the ceramic contributes substantially to the gross properties of the composites. Lead titanate (PT) is a good candidate to be incorporated into the composite because it has high piezo- and pyroelectric activities but relatively low permittivity. A fine scale of ceramic powder is required for producing homogenous 0-3 composites with moderate ceramic volume fraction. Therefore, a metal alkoxide sol-gel method instead of the conventional mixed oxide method is employed in the present study. This chapter describes the sol-gel processing and the solution chemistry. The crystal structure and microstructure of the powder is also characterized. The procedures for the preparation of the PT composites are described. The microstructure, dielectric properties and ferroelectric properties of such composites are also discussed.

2.2 Sol-Gel Processing Review

The sol-gel technique offers a unique approach to the creation of fine scale ceramic powders, films and fibers. This technology is based on the chemistry of metal ions in solution in which a network of metal-oxygen-metal bonds is produced. The process by which the solution converts to gel can be utilized to form ceramics and ceramic composites by dip coating, impregnation, spinning and fiber drawing. For this reason, sol-gel technology has received enormous attention in the last decade. The sol-gel route to ceramics offers high purity and excellent control of homogeneity in multi-component systems by the mixing of metal cations at a molecular level [Blum, 1985]. The network of metal-oxygen-metal (M-O-M) bonding in the gel state provides shorter diffusion lengths and requires lower energies to convert the amorphous solid into a crystalline ceramic [Budd, 1995].

2.2.1 Solution Chemistry

The transformation from solution to gel is governed by hydrolysis and condensation reactions in metal alkoxides. An understanding of these reactions is necessary in order to tailor the gelation process to produce the correct rheology,

viscosity, and gel network for the desired application. In multi-component systems, the hydrolysis and condensation reactions are also important for controlling gel homogeneity. Gel homogeneity is important in preventing phase separation during pyrolysis [Meyer, 1998].

Gelation proceeds with the addition of water to the system. Hydrolysis reactions can be summarized as follows:

$$M(OR)_n + xH_2O \rightarrow M(OH)_x(OR)_{n-x} + xROH \qquad (2.1)$$

After hydrolysis, the gel network grows by oxolation. Oxolation is the generation of an M-O-M bond through the elimination of a water group and can be written as

$$M(OH) + M(OH) \rightarrow M\text{-}O\text{-}M + H_2O \qquad (2.2)$$

The final gel structure and morphology is highly dependent upon the relative contributions of the above reactions and their rates.

2.2.2 Gel to Ceramic Conversion

Heat treatment of the gel is necessary for conversion to the ceramic. With alkoxide based processes, organic contents in the gel can range from 15 to 30 wt-%, thus control of the burnout process is essential. Successful burnout consists of

producing a dense, crack free part with no residual carbon ceramic.

Gel decomposition consists of both endothermic and exothermic reactions involving the evolution of the organics as a gas. Factors affecting the reaction rates include surface area, the chemistry / molecular weight of the organics, density of the parts, local atmosphere, heating rates and total volume fraction of organics.

2.3 Preparation of Nanosized PT Powder by Sol-Gel Method

Lead (II) acetate trihydrate [$Pb(CH_3COO)_2 \cdot 3H_2O$] and titanium (IV) butoxide $Ti[O(CH_2)_3CH_3]_4$ with 1:1 molar ratio were dissolved in the 2-methoxyethanol [$C_3H_8O_2$] at 100 °C. The precursor solution was stirred for half an hour for complete reaction. The solution was filtered, followed by hydrolysis for 2 days at room temperature. The yellowish PT gel was pyrolysed at about 300 °C and sintered at different temperatures from 500 °C to 800 °C to form PT powders with various crystallite sizes and particle sizes. The sol-gel process for preparing the PT powder is summarized in Figure 2.1.

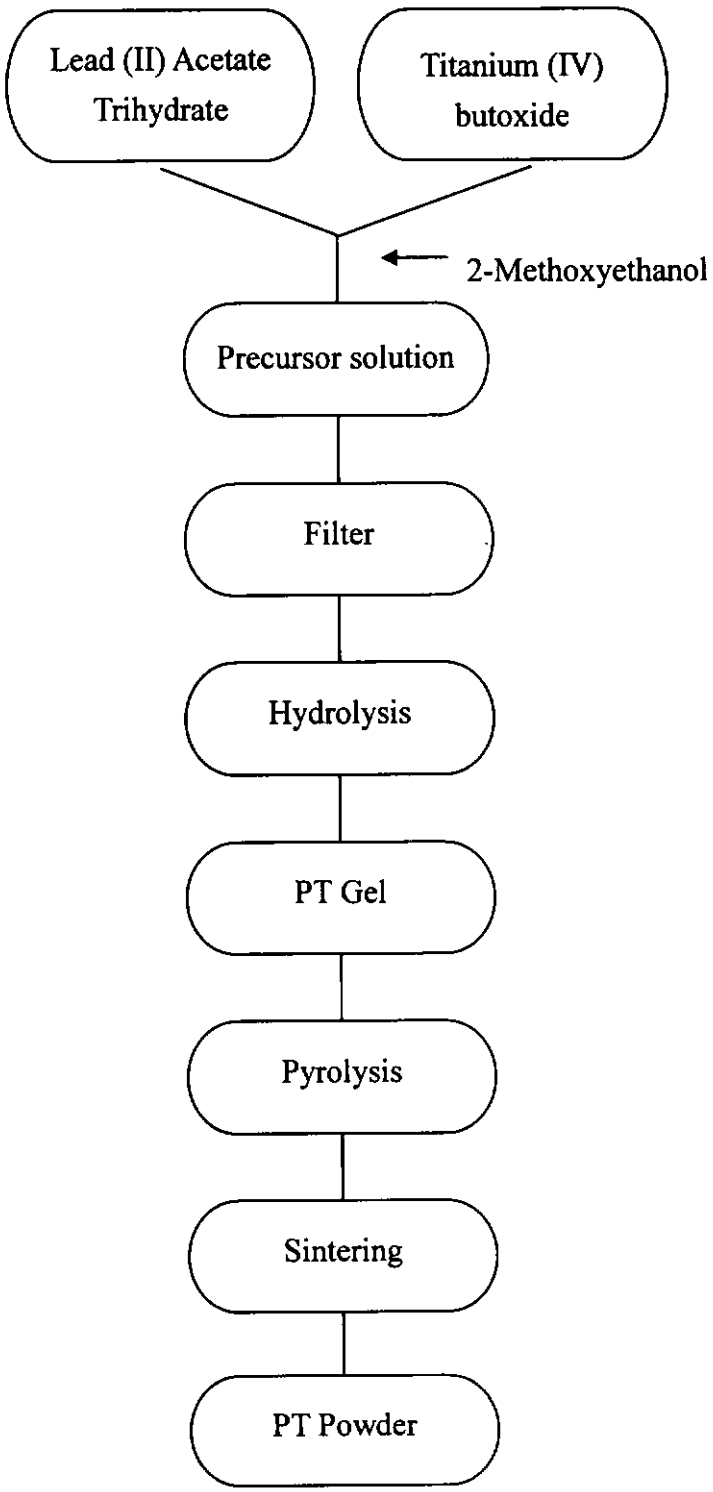

Figure 2.1 A flowchart showing the sol-gel process for preparing the nanosized PT powder.

2.4 Characterization of Nanosized PT Powder

The nanocrystalline PT powder was characterized by use of X-ray diffraction (XRD), particle size distribution measurement and scanning electron microscopy (SEM).

2.4.1 X-Ray Diffractometry (XRD) and Crystalline Size Measurement

In order to probe the crystal structure of materials it is possible to use electromagnetic radiation whose wavelength is of the order of crystal parameters. In the case of inorganic materials with lattice dimensions in the angstrom range, X-ray radiation can be utilized.

The PT powder sintered at various temperatures was examined under the X-ray diffractometer (Philips x'pert XRD system) with Ni filtered CuKα radiation of wavelength λ=1.54 Å. Figure 2.2 shows the XRD patterns of PT powder sintered at temperature from 500 °C to 800 °C for 1 hour. The PT gel sintered at 500 °C shows weak XRD diffraction patterns, which imply that a poor crystallite structure was formed in PT powder sintered at this temperature. When the sintering temperature increases from 600 °C up to 800 °C, the diffraction peak intensity rises rapidly.

Moreover, the double peaks including (001)/(100), (101)/(110), (002)/(200) and (112)/(211) split wider when the sintering temperature increases, which indicates that the c/a ratio increases with sintering temperature.

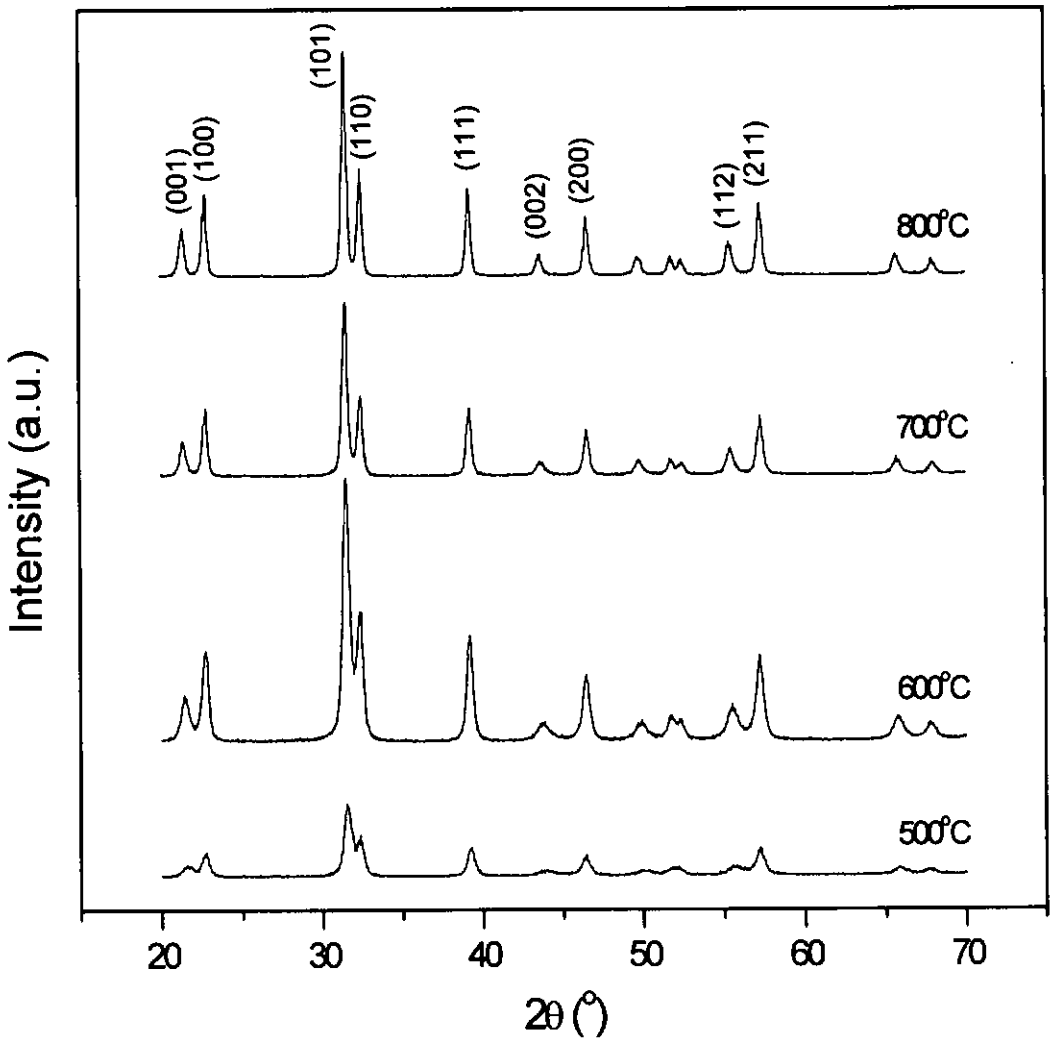

Figure 2.2 The XRD pattern of the PT powder sintered in the temperature range from 500 °C to 800°C. The numbers in brackets indicate the diffraction lattice planes.

The average crystallite size (D) of the PT powder was calculated from the full width at half maximum (FWHM) of the (110) and (111) diffraction peaks using Scherrer's equation [Birks, 1946]

$$D = \frac{K\lambda}{B\cos\theta} \tag{2.3}$$

where λ is the X-ray wavelength, θ is the diffraction angle, B is the FWHM of the diffraction peak and K is Scherrer's constant (K=0.89).

Comparing with the widths of the diffraction peaks of a standard material, i.e. silicon, the width due to the instrument can be evaluated, and the true width arising from the finite crystallite size can be obtained. The calculated D value of the PT powder sintered at various temperatures is given in Table 2.1. The results indicate that PT powder derived from sol-gel method has a low crystallization temperature and small crystallite size.

Table 2.1 The average crystallite diameter of PT powder versus the sintering temperature.

Sintering temperature T (°C)	500	600	700	800
Crystallite diameter D (nm)	32	47	55	60

2.4.2 Particle Size Distribution Analysis

The particle size distributions were measured using a centrifugal automatic particle size analyzer (Horiba CAPA-700). This equipment is based on the principle of liquid-phase sedimentation, which is measured by optical transmission.

A particle having diameter (d) and density (ρ) in a solvent with density (ρ_o) and viscosity coefficient (η_o) will settle at a constant velocity according to Stokes' sedimentation. The sedimentation velocities differ depending on the particle size. Particles with a larger diameter will settle first, followed by successively smaller particles. The sedimentation velocity v is given by

$$v = \frac{d^2(\rho - \rho_o)r\omega^2}{18\eta_o} \tag{2.4}$$

where r and ω denote the radial distance from the axis of rotation and the angular velocity, respectively.

In the present study, a small amount of PT powder was dispersed in ethanol by ultrasonic agitation. The mean particle size of the PT powder falls in the range of 270 nm to 520 nm corresponding to 500 °C to 800 °C sintering temperatures, indicating that each PT particle consists of several crystallites. The PT mean particle size as a function of sintering temperature is given in Table 2.2.

Table 2.2 The mean particle size of PT powder versus the sintering temperature.

Sintering temperature T (°C)	500	600	700	800
Mean particle size (nm)	270	310	360	520
Standard deviation (nm)	150	170	230	240

It is found that the higher the sintering temperature, the larger the mean particle size. In the present study, a sintering temperature of 600 °C has been chosen as it generates good crystallite structure confirmed by XRD and relatively small mean particle size. It is a common experimental fact that a small particle size variance would not give rise to a noticeable difference in the physical properties of composites with randomly distributed inclusions such as considered in the present work.

2.4.3 SEM Characterization

The PT powder sintered at 600 °C was examined under the scanning electron microscope (Leica Stereoscan 440). The SEM micrograph in Figure 2.3 shows that the PT particles have a roughly "spherical" shape (rounded; no sharp corners) and the

diameter is quite close to the result obtained by the particle size distribution analysis.

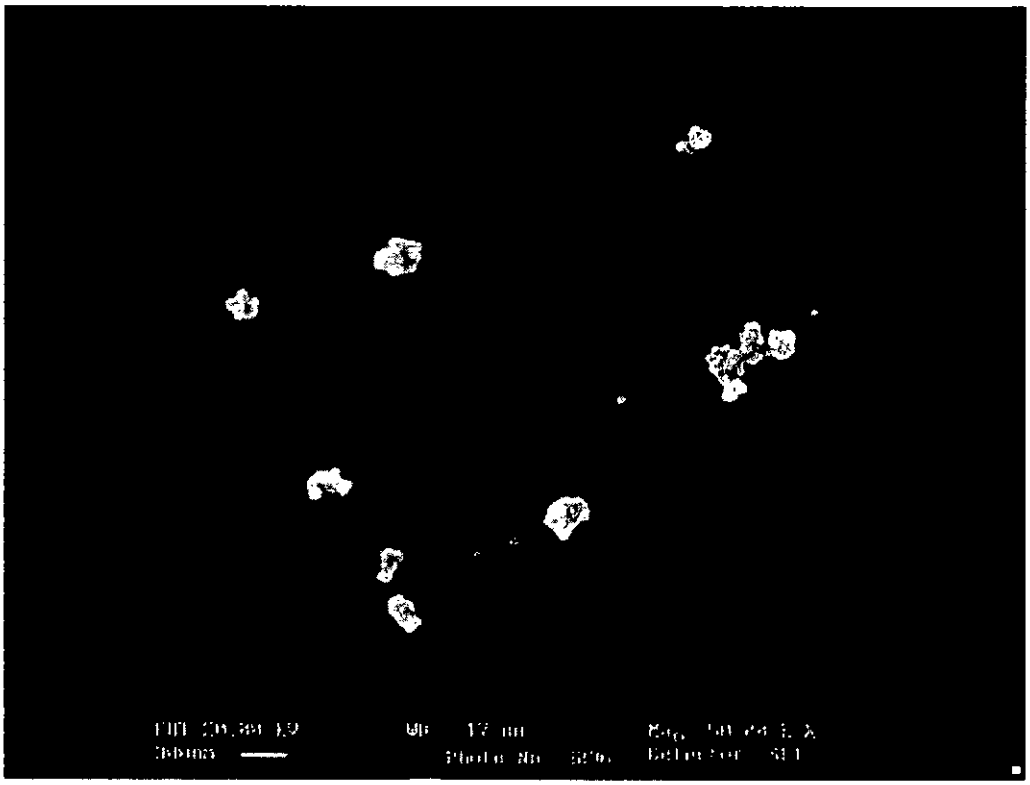

Figure 2.3 The SEM micrograph of PT powder sintered at 600 ˚C.

2.5 Characterization of P(VDF-TrFE) 70/30 mol-% Copolymer

2.5.1 X-Ray Diffractometry (XRD)

P(VDF-TrFE) 70/30 mol-% copolymer film was prepared from solution casting of P(VDF-TrFE) powder (supplier: Piezotech, France) followed by compression molding. Figures 2.4(a) and (b) shows the XRD pattern of unannealed P(VDF-TrFE) 70/30 mol-% copolymer and anannealed sample (annealed at 120 °C for 2 hours), respectively. The single peak at $2\theta = 19.8^{\circ}$ corresponds to reflections of the (110) and (200) planes and shows that the molecular chains of the copolymer are packed in a hexagonal structure [Tashiro, 1984]. The strong diffraction peak corresponding to the (110) and (200) planes is usually employed to estimate the degree of crystallinity (x_c) of the copolymer. The sharp peak which corresponds to the crystalline phase while the shoulder at its low angle corresponds to the noncrystalline phase. The curve can therefore be resolved into two Gaussian peaks [Tajitsu, 1987]. The areas under the "crystalline" and "noncrystalline" curves are labelled by C and N respectively. Therefore, the x_c can be estimated by

$$x_c = \frac{C}{C+N} \tag{2.5}$$

Figures 2.4 (a) and (b) show the XRD diffraction pattern of the unannealed

and the annealed copolymer sample, respectively. It is found that x_c is increased from 0.71 (unannealed) to 0.85 (annealed).

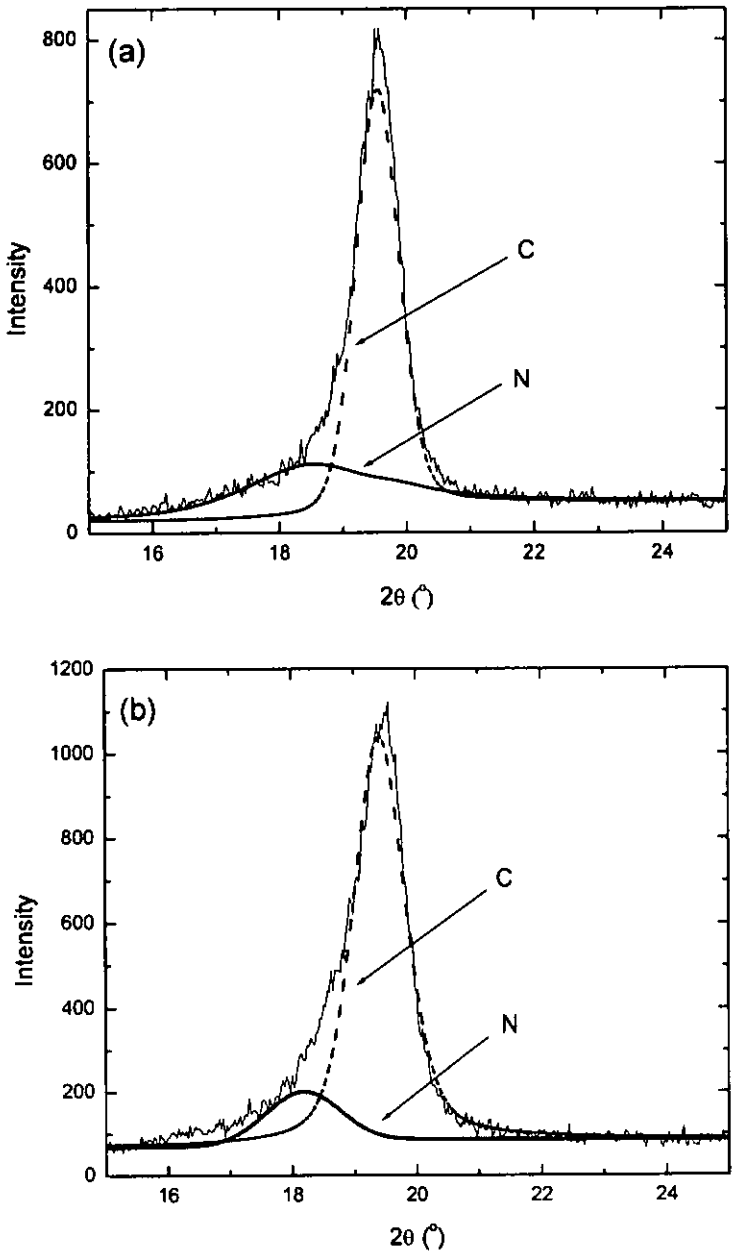

Figure 2.4 The XRD pattern of an (a) unannealed (b) annealed P(VDF-TrFE) 70/30 mol-% copolymer.

2.5.2 Differential Scanning Calorimetry (DSC)

An important characteristic of ferroelectrics is the temperature at which a ferroelectric-to-paraelectric phase transition occurs, and it is called the Curie temperature T_c. When the temperature decreases through the Curie temperature, a ferroelectric crystal undergoes a structural phase transition from a paraelectric phase to ferroelectric phase. When the temperature is in the vicinity of T_c, thermodynamic properties such as dielectric, elastic, optical and thermal properties show anomalies and the structure of the crystal changes [Xu, 1991].

Phase transition of P(VDF-TrFE) 70/30 mol-% copolymer can be observed by differential scanning calorimetry (DSC). Figures 2.5(a) and (b) show the DSC results of the copolymer obtained in a heating and a cooling cycle between room temperature and 170 °C. The heating curve in Figure 2.5(a) exhibits a broad endotherm peak near 106 °C ($T_c\uparrow$) which corresponds to the ferroelectric-paraelectric transition and a sharp peak near 149.5 °C corresponding to the crystalline melting temperature (T_m). The cooling curve in Figure 2.5(b) shows a peak at the 135 °C crystallization temperature (T_s). A double peak appearing around the paraelectric-ferroelectric transition temperature upon cooling ($T_c\downarrow$ 65 °C and 60 °C) which indicates a strong thermal hysteresis arising from the first order nature of the

Curie transition in the copolymer [Lines and Glass, 1977].

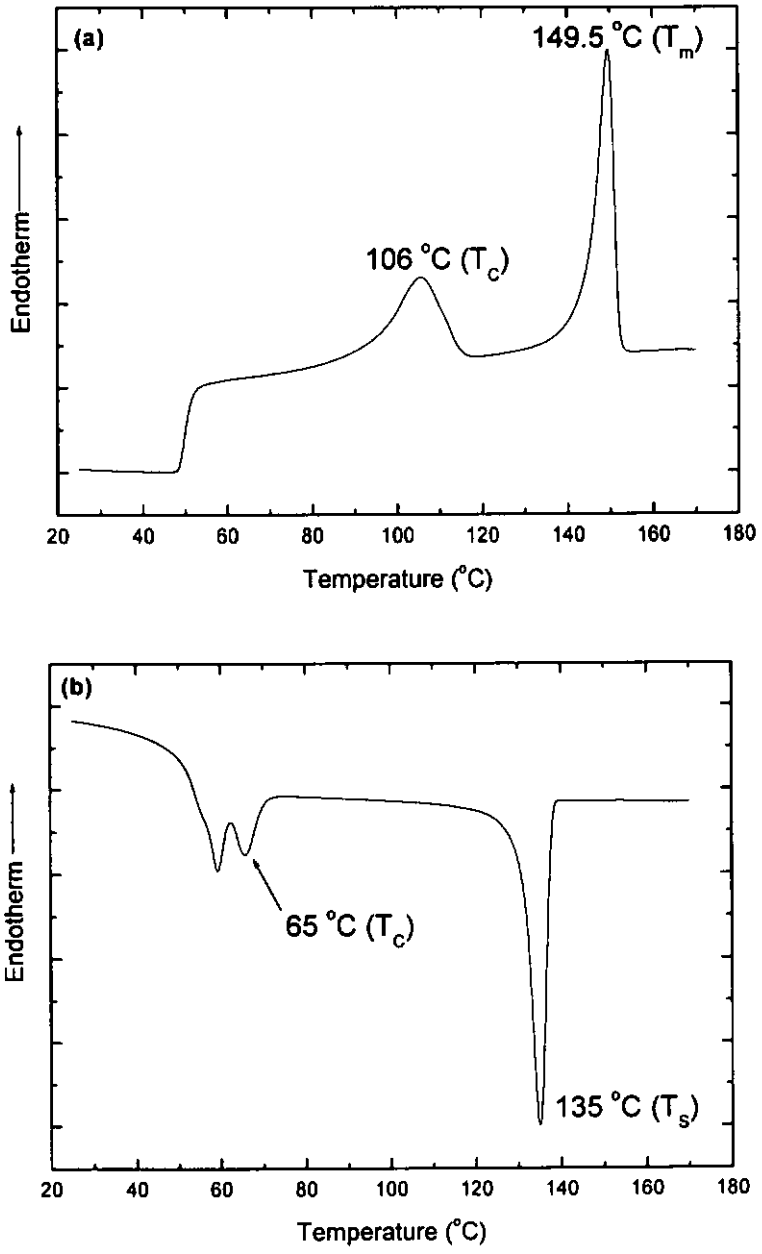

Figure 2.5 DSC endotherms of the P(VDF-TrFE) 70/30 mol-% upon (a) heating (b) cooling.

The observed values including $T_c\uparrow$ and T_m were compared with the literature values for the composition 70/30 (=VDF/TrFE) [Bloomfield, 1986] given in Table 2.3.

Table 2.3 Comparison of the measured $T_c\uparrow$ and T_m of P(VDF-TrFE) 70/30 mol-% with the literature values.

	Heating		Cooling	
Mole-% VDF	T_m (°C)	$T_c\uparrow$ (°C)	T_s (°C)	$T_c\downarrow$ (°C)
70	149.5	106	135	65
70#	147	108	–	–

Results from Bloomfield *et al.*

In Table 2.3, we found that our measured results of $T_c\uparrow$ and T_m of P(VDF-TrFE) 70/30 mol-% by DSC are quite close to the literature values investigated by Bloomfield *et al.* Therefore, we have confirmed that the VDF content of the copolymer used in the present study is near 70 mol-%.

2.5.3 Ferroelectric Hysteresis Loop

The most important characteristic of ferroelectrics is the ferroelectric hysteresis loop. A crystal is said to be ferroelectric if it has a spontaneous polarization P_s, which can be reversed in sense or reoriented by the application of an electric field larger than the coercive field [Xu, 1991]. A ferroelectric hysteresis loop can be observed by means of a Sawyer-Tower circuit. Figure 2.6 shows the schematic diagram of a Sawyer-Tower circuit.

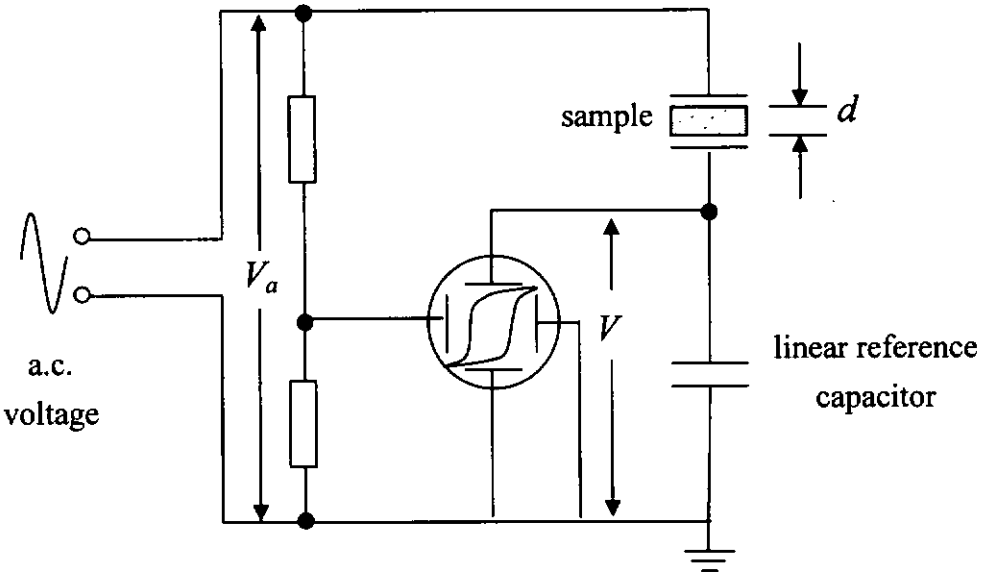

Figure 2.6 Schematic diagram of the Sawyer-Tower Circuit.

An alternating voltage V_a is imposed across a pair of electrodes on the surfaces of a ferroelectric sample, and a linear reference capacitor is connected in series with the sample. The voltage across the reference capacitor is therefore proportional to the electric displacement of a (perfectly insulating) ferroelectric sample, which can be written as

$$D = \frac{CV}{A} \tag{2.6}$$

where D, C, V and A denote the electric displacement of the sample, capacity of the reference capacitor, voltage across the reference capacitor of larger capacitance and electrode area, respectively.

The hysteresis loop of the P(VDF-TrFE) 70/30 mol-% copolymer sample was first measured at room temperature under a sinusoidal electric field of 130 MV/m at frequency 10 Hz. The voltages across the sample and the reference capacitor were monitored by a digital storage oscilloscope (DSO). The hysteresis loop of the copolymer is shown in Figure 2.7.

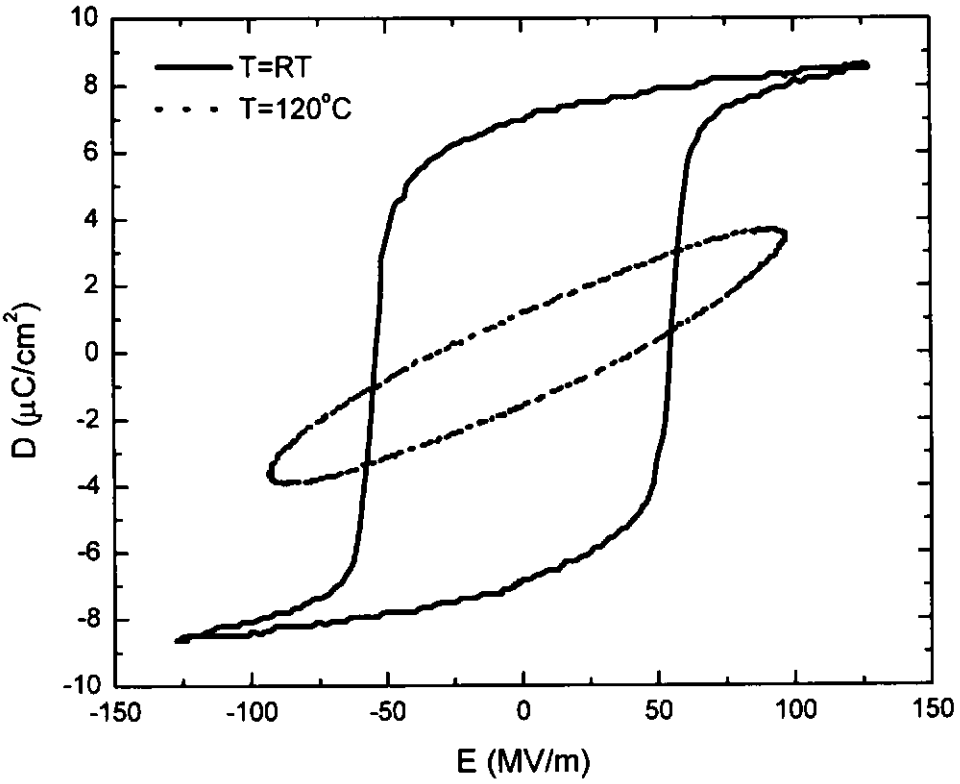

Figure 2.7 The hysteresis loop of P(VDF-TrFE) 70/30 mol-% copolymer measured at room temperature RT (solid line) and 120 °C (dotted line).

The saturation hysteresis loop of the copolymer measured at room temperature is observed under the a.c. electric field of 130 MV/m. It is found that the remanent polarization P_r and the coercive field E_c are equal to 7 μC/cm^2 and 54.5 MV/m, respectively. The spontaneous polarization P_s is obtained by extrapolation of the linear segment of the electric displacement near the maximum applied electric field to the vertical axis x = 0, which is found to be 7.45 μC/cm^2.

The same sample was heated to 120 °C which is above the Curie temperature

of P(VDF-TrFE) 70/30 mol-% ($T_c\uparrow$=106 °C). An a.c. electric field of 95 MV/m was then applied to the copolymer sample. There the copolymer is in its paraelectric phase and the "loop" is caused by dielectric loss [Lines, 1971]. It is expected that ferroelectricity is not retained in the copolymer sample at such high temperatures.

2.6 Preparation of PT / P(VDF-TrFE) 0-3 Composites

The predetermined amount of nanosized PT powder and P(VDF-TrFE) 70/30 mol-% copolymer powder were dissolved in methylethylketone (MEK) solvent to form 0-3 composite with different ceramic volume fractions ϕ. The volume fraction of PT ceramic was determined using the specific gravities 1.90 g/cm^3 of P(VDF-TrFE) 70/30 mol-% and 7.60 g/cm^3 of PT ceramic. The solution was heated and stirred to a slurry. The gel-form composite was then agitated in the ultrasonic bath for 30 minutes in order to improve the dispersion of the ceramic particles in the polymer matrix, and was dried at 85 °C in the oven for 12 hours in order to remove the solvent completely.

The thick composites were cut into small pieces and compression molded into 30 μm thick composite films. The films were annealed at 120 °C for 2 hours. Chromium / gold electrodes were then deposited on both sides of the samples. The procedure for the preparation of the 0-3 composites is summarized in Figure 2.8.

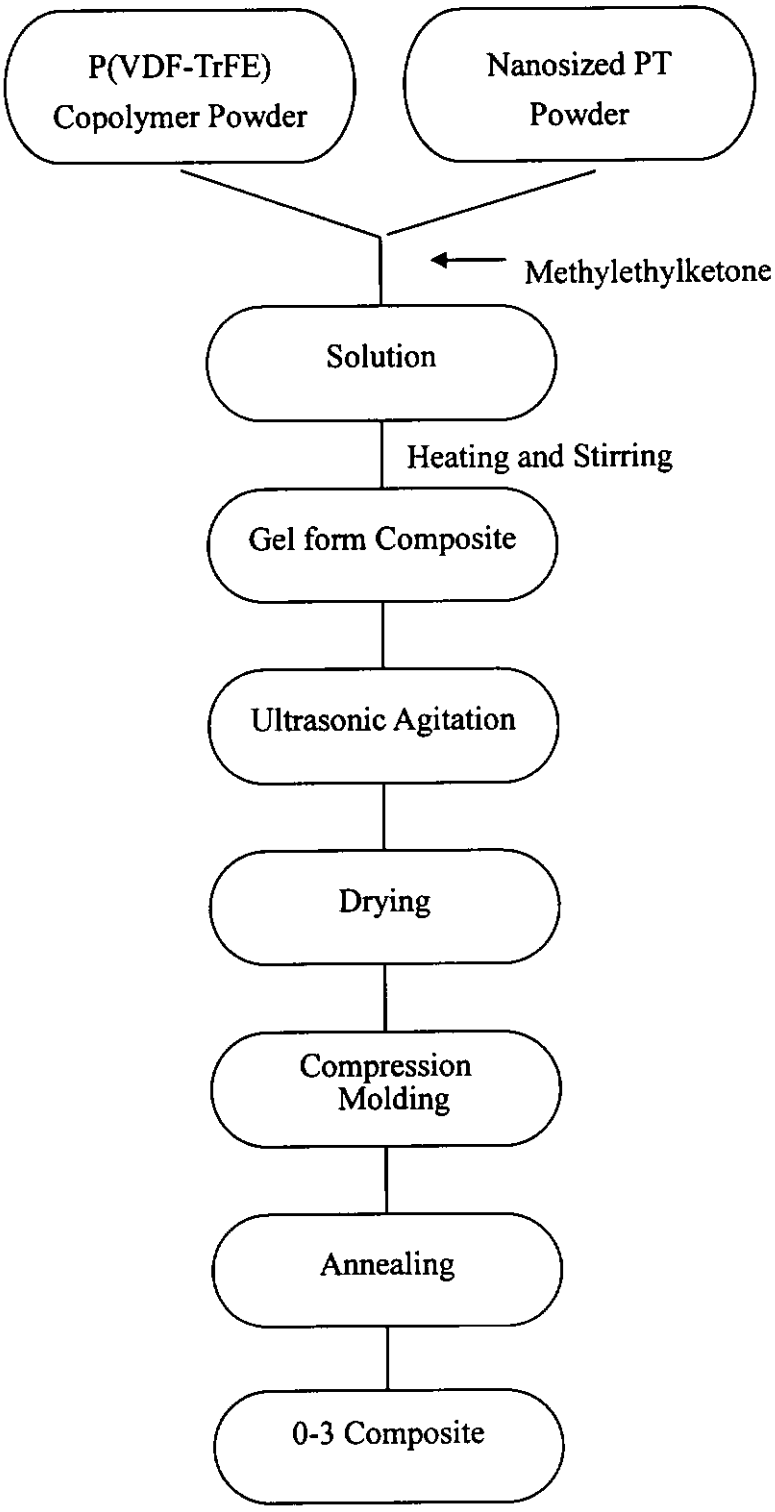

Figure 2.8 A flowchart showing the procedure for preparing PT / P(VDF-TrFE) 0-3 composites.

2.7 Microstructure of the PT/P(VDF-TrFE) 0-3 Composite

To examine the microstructure of the PT / P(VDF-TrFE) 0-3 composites, the sample was dipped into liquid nitrogen for embrittlement and then fractured. The fractured surface was observed under the SEM. The micrograph of the PT/P(VDF-TrFE) composite with ϕ = 0.2 is shown in Figure 2.9. It is seen that the PT powder was dispersed quite uniformly in the polymer matrix and no serious agglomeration was observed.

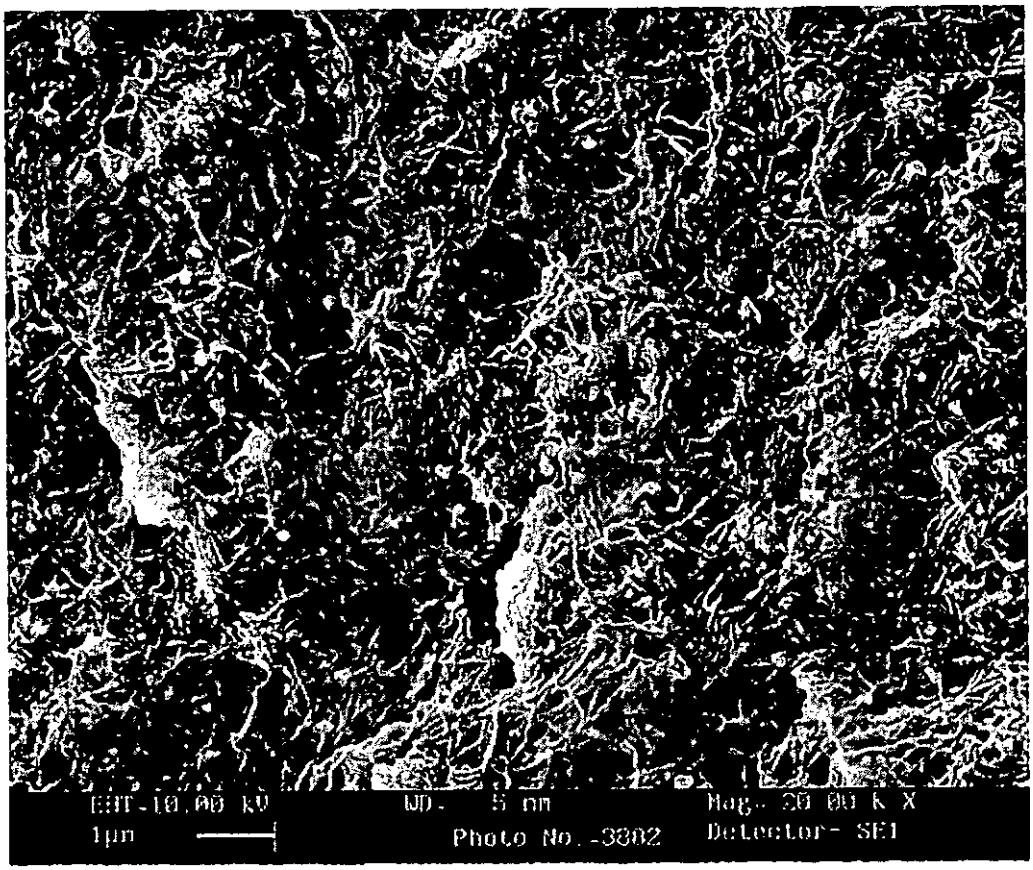

Figure 2.9 SEM micrograph of the fracture surface of the PT/P(VDF-TrFE) composite with ϕ = 0.2.

2.8 Dielectric Properties of PT / P(VDF-TrFE) 0-3 Composites

To study the poling process of the composites (which will be explained in a later chapter), the permittivities of the P(VDF-TrFE) copolymer and PT/P(VDF-TrFE) composites have been characterized as a function of temperature .

The relative permittivity ε_r or $\varepsilon/\varepsilon_o$, sometimes called dielectric constant, can be understood as the ratio between the charge storage on an electroded slab of a material subjected to a given voltage and the charge stored on a set of identical electrodes separated by vacuum. The relative permittivity of the sample is determined using the following equation:

$$\varepsilon_r = \frac{Cd}{\varepsilon_o A} \tag{2.7}$$

where C is the capacitance of the sample, ε_o is the permittivity of free space (=8.852×10^{-12} F/m). A is the electrode area and d is the sample thickness. The absorption of electrical energy by a dielectric material that is subjected to an alternating electric field is termed dielectric loss. The dielectric constant can be written in complex notation:

$$\varepsilon_r = \varepsilon_r' - i\varepsilon_r'' \tag{2.8}$$

where ε_r' is the real part and ε_r'' is the imaginary part. The loss tangent tan δ can be

written as

$$\tan\delta = \frac{\varepsilon_r''}{\varepsilon_r'} \tag{2.9}$$

In the present study, the capacitance C and the dielectric loss tangent of the unpoled P(VDF-TrFE) copolymer and PT / P(VDF-TrFE) 0-3 composites with ϕ from 0.05 to 0.3 were measured as a function of temperature from -20 ˚C to 120 ˚C in the frequency range of 100 Hz to 1 MHz using a HP4194A impedance analyzer. The sample was heated and cooled at a rate of ~1 ˚C/min in a temperature controlled oven (ESPEC SU-240) until a given temperature was reached, and then kept at that temperature for 3 minutes before the measurement was made.

The schematic diagram of the dielectric measurement setup is shown in Figure 2.10. Figures 2.11(a) and (b) shows the relative permittivity of the PT/P(VDF-TrFE) 0-3 composite with ϕ from 0 to 0.3 as a function of temperature from -20 ˚C to 120 ˚C measured at frequency 1 kHz in a heating and cooling cycle, respectively.

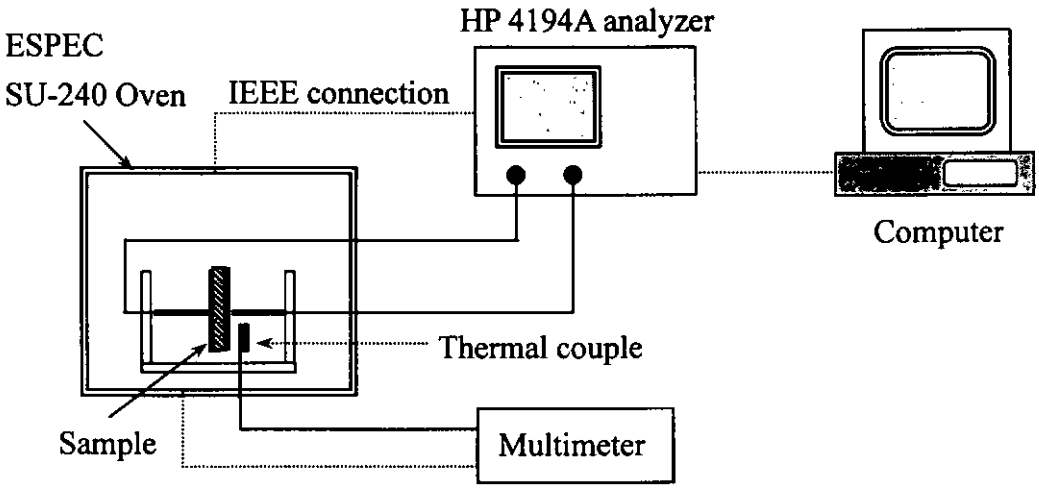

Figure 2.10 Schematic diagram of the measurement setup for the temperature dependent permittivity.

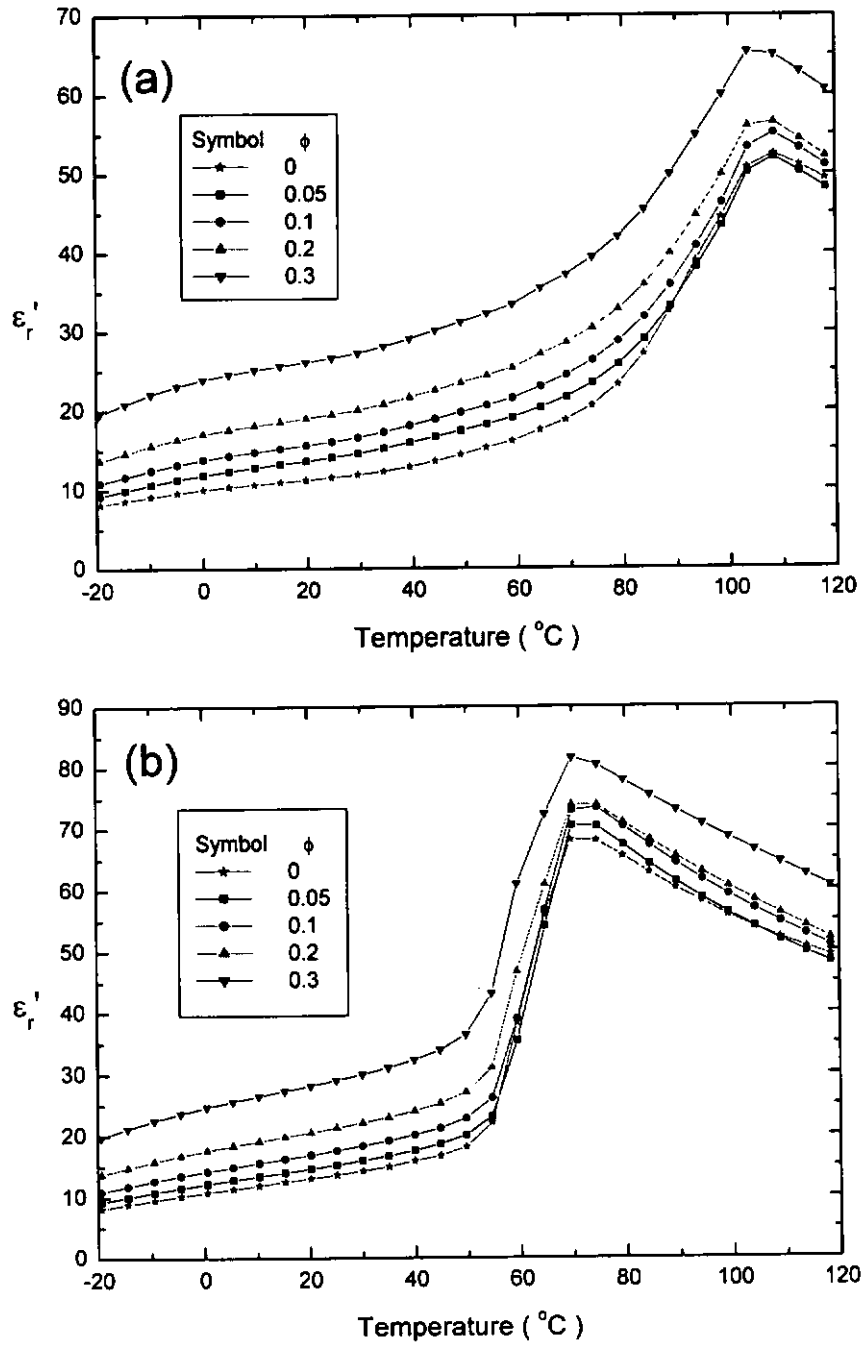

Figure 2.11 The relative permittivity of the PT/P(VDF-TrFE) 0-3 composite with ϕ from 0 to 0.3 as a function of temperature from -20 °C to 120 °C measured at frequency 1 kHz during (a) heating and (b) cooling.

As mentioned before, when the temperature is in the vicinity of Curie temperature T_c, the thermodynamic properties show anomalies and the structure of the crystal changes. In Figure 2.11, a peak was identified at 107 °C and 69 °C during heating and cooling, respectively, which is quite close to the Curie transition temperatures observed in the DSC measurement ($T_c\uparrow$=106 °C and $T_c\downarrow$=65 °C). The observation of two different peaks at heating and cooling is typical for a first order transition where the Curie transition temperatures are different from the Curie temperature.

The permittivity of diphasic composites has been studied by several researchers. The Wagner model [Wagner, 1914] is well known in describing the relative permittivity of a binary system containing dispersed spheres. In that model, the system contains spheres of radius r and permittivity ε_2, sparsely distributed in a continuous medium with permittivity ε_1. In order to facilitate the calculation, the arrangement as shown in Figure 2.12 was considered, in which a sphere with radius $r_o >> r$ supposed to typify the composite material in question, was placed in an infinite matrix. The permittivity of the composite ε is given by

$$\varepsilon = \varepsilon_1 \frac{2\varepsilon_1 + \varepsilon_2 + 2\phi(\varepsilon_2 - \varepsilon_1)}{2\varepsilon_1 + \varepsilon_2 - \phi(\varepsilon_2 - \varepsilon_1)} \tag{2.10}$$

An application of this model is limited to small concentrations of the dispersed particles because the immediate neighborhood of a particle can no longer

be considered as a continuous medium when the concentration of particles is high [Scaife, 1989].

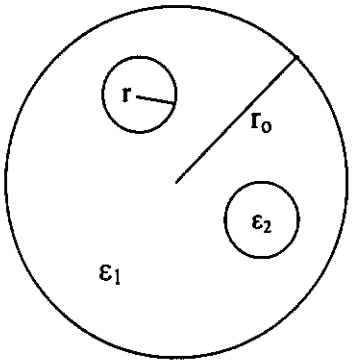

Figure 2.12 Wagner's model of a dielectric with permittivity ε_1 containing dispersed spheres of permittivity ε_2 and radius r.

The concentration of dispersed particles in the immediate neighborhood of a certain particle was taken into account by the use of an integration scheme that was first introduced by Bruggeman [Bruggeman, 1935]. In Bruggeman's scheme the initially low concentration was gradually increased by infinitesimal additions of the dispersed component ε_2. In that process the permittivity of the medium around a particle slowly changes from ε_1 to ε. The studies of 0-3 composite systems such as PZT/P(VDF-TrFE) [Chan, 1997], PCT/P(VDF-TrFE) [Chan, 1998] and PT/P(VDF-TrFE) [Chen, 1998] have shown that the Bruggeman model fits the experimental results very well even for high concentrations of ceramic particles.

$$\frac{\varepsilon_2' - \varepsilon'}{(\varepsilon')^{\frac{1}{3}}} = \frac{(1-\phi)(\varepsilon_2' - \varepsilon_1')}{(\varepsilon_1')^{\frac{1}{3}}} \tag{2.11}$$

$$\varepsilon'' = \frac{(\varepsilon_2' - \varepsilon')(\varepsilon_2' + 2\varepsilon_1')\varepsilon'}{(\varepsilon_2' - \varepsilon_1')(\varepsilon_2' + 2\varepsilon')\varepsilon_1'}\varepsilon_1'' + \frac{3(\varepsilon' - \varepsilon_1')\varepsilon'}{(\varepsilon_2' - \varepsilon_1')(\varepsilon_2' + 2\varepsilon')}\varepsilon'' \tag{2.12}$$

Figure 2.13 shows ε' and ε" of the PT/P(VDF-TrFE) 0-3 composites with different ϕ measured at room temperature at frequency 1 kHz. The calculations of ε' and ε" using equations (2.11) and (2.12) with ε_1'=11.6, ε_1" = 0.018 (measured in the present study), ε_2'=200 [Xu, 1991], and ε_2"=1.8 [Xu, 1991] were compared with the measured data. A good agreement is found for ϕ up to 0.3.

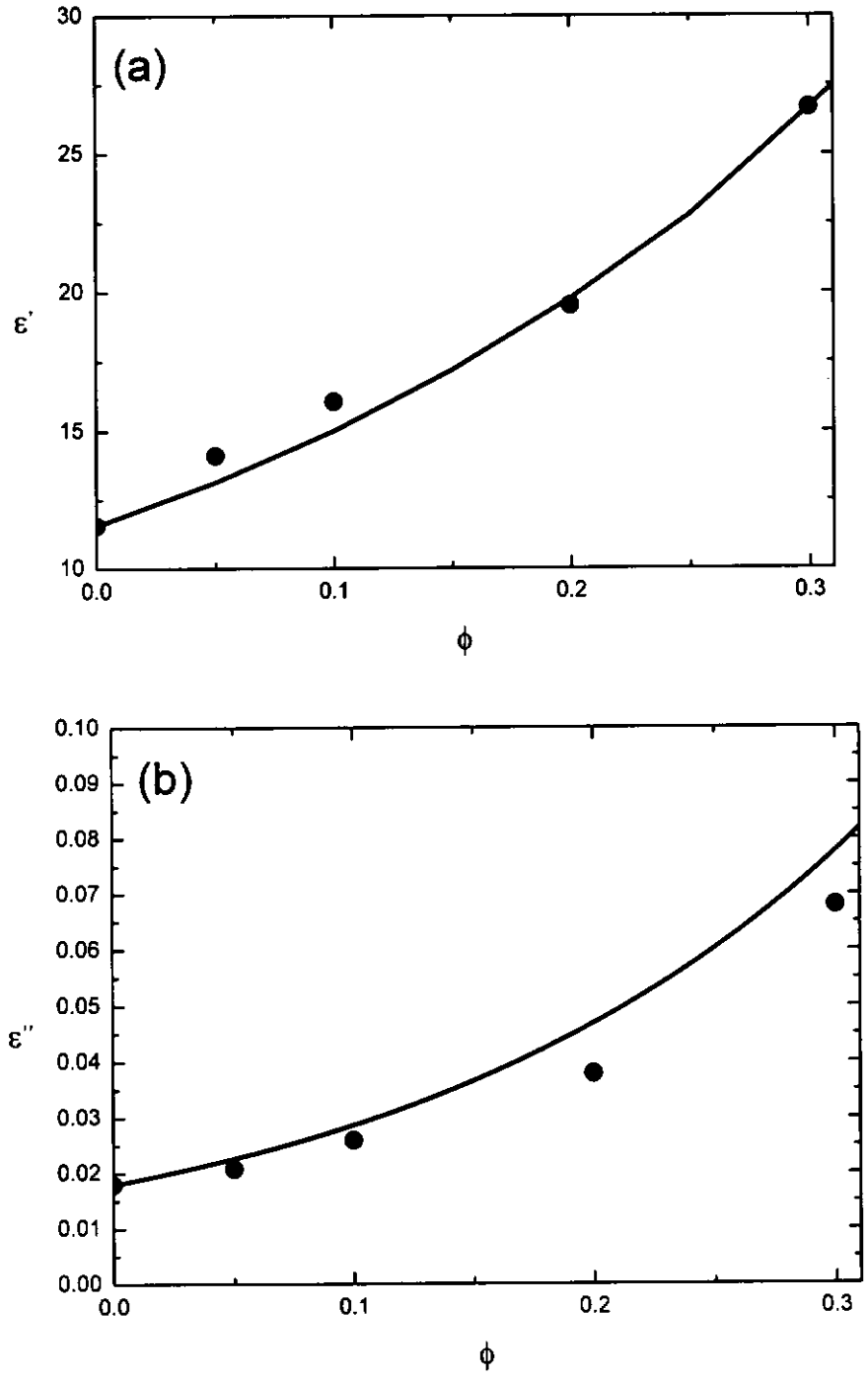

Figure 2.13 (a) ε' and (b) ε" of the composite as a function of ϕ at room temperature at frequency of 1 kHz. Circle and solid line denote the experimental results and calculated curve based on Bruggeman's model respectively.

2.9 Conclusion

Nanosized PT powder was prepared by a sol-gel process. The crystal structure, microstructure and the particles size of the PT powder was characterized by XRD, SEM and particle size analyzer respectively. The PT particles were embedded into the P(VDF-TrFE) copolymer to form 0-3 composite film by solution casting followed by compression molding. A good dispersion of the PT particles in the polymer matrix was confirmed by investigating the cross-section surface with a SEM. On the other hand, crystallinity, ferroelectric-paraelectric transition and ferroelectric properties of the P(VDF-TrFE) copolymer were studied by XRD, DSC and hysteresis *D-E* measurement. The crystallinities of the unannealed material and a sample annealed at 120 °C were found to be 0.71 and 0.85 respectively. The Curie transition temperatures of the copolymer were identified as 106 °C during heating and 65 °C during cooling. The dielectric properties of the PT composites with different ceramic volume fractions were measured between -20 °C to 120 °C. The measured permittivity of the composites with different ceramic volume fractions at room temperature at frequency 1 kHz was compared with the predictions based on Bruggeman's model, and a good agreement is found.

CHAPTER 3
POLING OF FERROELECTRIC PT / P(VDF-TrFE) 0-3 COMPOSITES

3.1 Introduction

The composite systems of polymers and ferroelectric ceramics reveal piezoelectric and/or pyroelectric properties if they have been subjected to a high electric field. This process, called poling, to give the orientation of the spontaneous polarization in the ferroelectric phase(s). As a result, the composites show an electrical response under mechanical or thermal excitation. Such composites are useful for technical applications as flexible transducer with piezoelectric and pyroelectric activities.

In this chapter, thermal poling (poling at elevated temperature) of PT/P(VDF-TrFE) 0-3 composites is employed for polarizing the ceramic inclusions. Methods of characterization of the poling state of the composites, including piezoelectric and pyroelectric measurements, X-ray diffraction and the laser intensity modulation method (LIMM) are also elaborated.

3.2 D.C. Poling of PT / P(VDF-TrFE) 0-3 Composites

Poling of ferroelectrics is generally based on the application of an external electric field to the material. Generally speaking, the higher the electric field, the larger the polarization that can be obtained. Usually, to polarize the sample well, the poling field should be 3 to 4 times higher than the coercive field [Xu, 1991]. However, the maximum applied electric field is usually limited by dielectric breakdown. When a very high electric field is applied across a dielectric material, a large number of electrons may suddenly be excited to energies within the conduction band. As a result, the current through the dielectric by the motion of these electrons increases dramatically. Local melting, burning, vaporization produces irreversible degradation and even failure of the material [Callister, 1997]. The dielectric strength, sometimes called the breakdown strength, represents the magnitude of the electric field necessary to produce breakdown. In our case, the breakdown strength of the 0-3 composite depends on factors such as homogeneity, porosity, composition and impurity etc.

Many efforts have been put to the study of poling of composite structures. Here are some results from previous works.

For a 0-3 composite consisting of spherical inclusions embedded in a matrix, the electric field acting on an isolated inclusion is given by [Safari, 1986]

$$E_i = \frac{3\varepsilon_m}{\varepsilon_i + 2\varepsilon_m} E_o \tag{3.1}$$

where ε_i and ε_m denote the permittivities of the ceramic inclusion and the polymer matrix respectively, and E_o is the externally applied electric field. Equation (3.1) is approximately true for the type of composites considered here.

For a 0-3 composite with PT powder and P(VDF-TrFE) copolymer at room temperature, ε_i is about 200 and ε_m is about 10. In such a composite with an external field of 10 MV/m, the electric field acting on the grain is just 1.36 MV/m which is insufficient to pole the inclusion effectively. In equation (3.1), $E_i \sim E_o$ if the permittivity of the ceramic inclusion approach to that of polymer. Most ferroelectric ceramic materials such as PT ceramic have quite a high permittivity and hence this is not a realistic case.

The importance of conductivity to poling can be assessed by applying the Maxwell-Wagner model [Hippel, 1954] to 0-3 composites. A 0-3 composite with alternating ferroelectric ceramic grains and thin layers of polymer can be approximated to a two-layer Maxwell-Wagner interfacial polarization model. When a d.c. poling voltage is applied on the composite for a period longer than the relaxation time, the voltage acting on the ceramic layer is given by

$$\frac{V_i}{V} = \frac{1}{(\sigma_i / \sigma_m)(d_m / d_i)+1} \tag{3.2}$$

where subscript i and m refer to the ceramic and polymer respectively, and σ and d denote the conductivity and thickness. Equation (3.2) gives $V_i \sim V$ if $\sigma_m >> \sigma_i$ or $d_i >> d_m$.

To facilitate poling of the ceramic inclusions, we borrowed the idea from the above model. It is known that the conductivity of the copolymer rises dramatically when temperature increases [Chan, 1997]. In equation (3.2), it is seen that the "voltage" or field acting on the inclusion would increase if the conductivity of the matrix increases. Therefore, thermal poling was employed in the present study. A higher temperature would tend to increase the conductivity of the host polymer matrix in relation to the conductivity of the ceramic inclusion materials so as to enhance the electric field acting on the inclusions and thus a higher remanent polarization can be achieved. The experimental setup for thermal poling is shown in Figure 3.1. To polarize the ceramic inclusions in the composite, the samples were kept at 120 °C in the silicone oil bath, which was higher than the Curie transition temperature of the copolymer phase (T_c↑=106 °C) and a high d.c. electric field of 50 MV/m was applied on the samples for different poling times. After poling, the electric field was released and the poled samples were cooled down to 60 °C and kept under short-circuit condition for 18 hours for subsequent measurements.

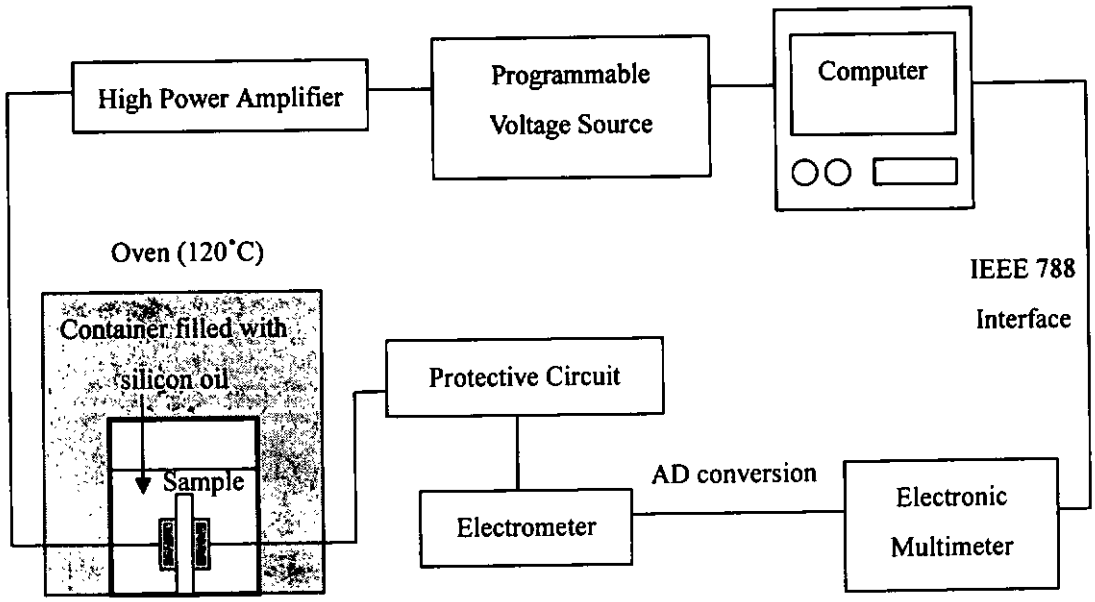

Figure 3.1 Schematic diagram of the thermal poling setup.

3.3 Characterization of the Poling Degree of the 0-3 Composite

3.3.1 Piezoelectric Measurement

As mentioned in the previous section, after the poling process piezoelectric effect will be elicited in the 0-3 composites. The direct piezoelectric effect is due to the development of polarization upon the action of pressure. When a stress is applied to certain crystals they develop an electric moment whose magnitude is proportional to the applied stress. In contrast, when an electric field is applied to a piezoelectric crystal the shape of the crystal changes slightly. This is known as the converse piezoelectric effect.

When a mechanical stress is applied on the sample with no electric field at constant temperature, we have the following equation [Xu, 1991]

$$D_m = d_{mj} X_j \quad (\text{m=1,2,3; j=1,2...6}) \tag{3.3}$$

where D, d and X denote the electric displacement, the piezoelectric coefficient and the stress respectively.

If the direction of the applied stress is in the direction of the polarization axis (thickness direction in the present study), only the X_3 component of the stress exists and

$$D_3=d_{33}X_3 \tag{3.4}$$

If the total force corresponding to the component X_3 is F_3, the total charge produced on the surface electrode is

$$Q=d_{33}F_3 \tag{3.5}$$

Suppose C is the static capacity of the sample having a charge Q, a voltage $V=Q/C$ will be built up across the two electrodes of the sample. Then we have

$$d_{33} = Q/F_3 = CV/F_3 \tag{3.6}$$

In this study, the piezoelectric coefficient d_{33} was measured by using a piezo d_{33} meter (ZJ-3B, Institute of Acoustic, Academia Sinica). The schematic diagram of a d_{33} meter is shown in Figure 3.2.

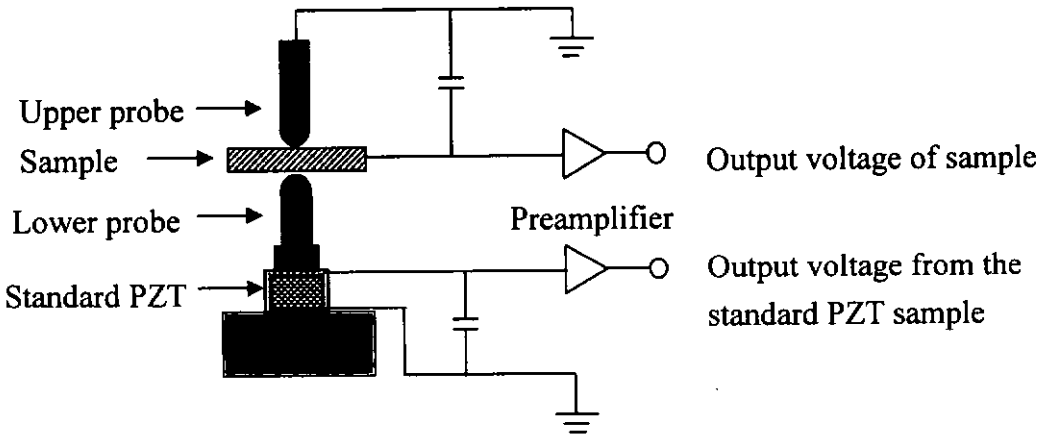

Figure 3.2 Schematic diagram of the piezo- d_{33} meter.

In the piezoelectric measurement, a quasi-static force of 0.250 $N_{r.m.s.}$ with frequency of 110 Hz which is well below the resonant frequencies of the sample, was applied to the electrode surfaces of the sample by two vertical probes which served as supports to the test specimen and also making electrical connection. An internal calibration piezoelectric PZT ceramic element is wired mechanically in series with the sample and they were subjected to the same mechanical excitation. Charge generated by the sample was collected on a capacitor which connected in parallel with the sample, at the same time the charge developed by the internal calibrated piezoelectric ceramic was also collected in another capacitor. The voltages developed from the two capacitors were then compared and thus provide a direct readout of d_{33} coefficient of the sample.

The piezoelectric coefficient of the composites with ceramic volume fraction of 0.05, 0.1, 0.2 and 0.3 as a function of poling time is shown in Figure 3.3.

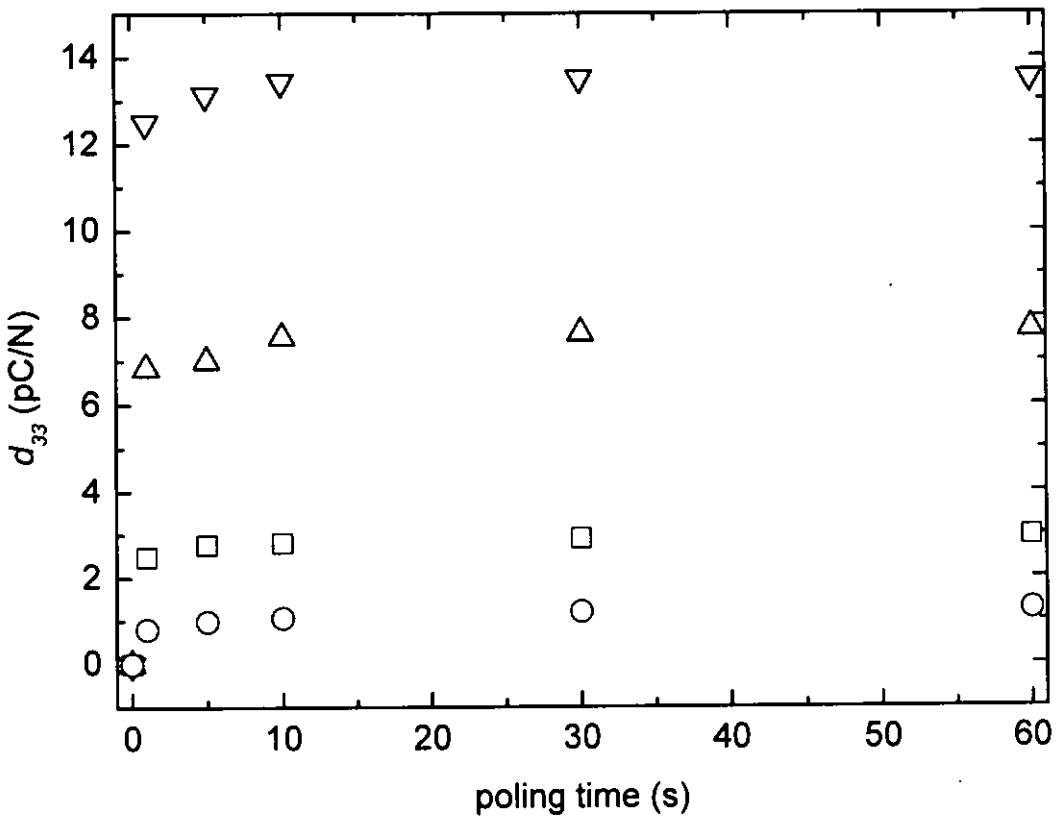

Figure 3.3 Piezoelectric coefficient of the PT/P(VDF-TrFE) 0-3 composites with ceramic volume fraction of 0.05 (circle), 0.1 (square), 0.2 (triangle) and 0.3 (inverted triangle) as a function of poling time.

It is found that the piezoelectric coefficient d_{33} of the composites increases fairly quickly when poling time increases, and the composites with higher ceramic volume fraction show higher piezoelectric coefficient under the same poling condition. A poling time of the order of 10 s is found to be sufficient to achieve a steady piezoelectric coefficient in the present study. This time scale is much shorter

than the poling times of says 10^{3} s in the literature. This significant finding will be discussed in the next chapter.

3.3.2 Pyroelectric Measurement

Pyroelectricity arises from changes in the polarization of a dielectric material for small changes in temperature [Das-Gupta, 1992]. To observe pyroelectricity we can heat the dielectric material uniformly and observe the charge generated. This work can be done in two different ways, either the shape and size of the materials can be held fixed during the heating, or alternatively, the material may be allowed to undergo thermal expansion freely. In the first case, with the material clamped, the effect observed is called primary pyroelectricity. In the second case, with free expansion, which is much easier to achieve experimentally, there is an additional effect called secondary pyroelectricity; what is observed in this case is the primary effect plus the secondary effect. The expression given in the following applies equally well to both primary and secondary pyroelectricity, and to the sum of the two.

If there is a small temperature change ΔT uniform over the sample, the change in the polarization vector ΔP_i is given by [Nye, 1957]

$$\Delta P_i = p_i \Delta T \quad \text{with i=1,2,3} \tag{3.7}$$

where p_i is the pyroelectric coefficient.

In this study, the dynamic method is employed for evaluating the pyroelectric

properties of the composite. The schematic diagram of the dynamic pyroelectric measurement setup is shown in Figure 3.4.

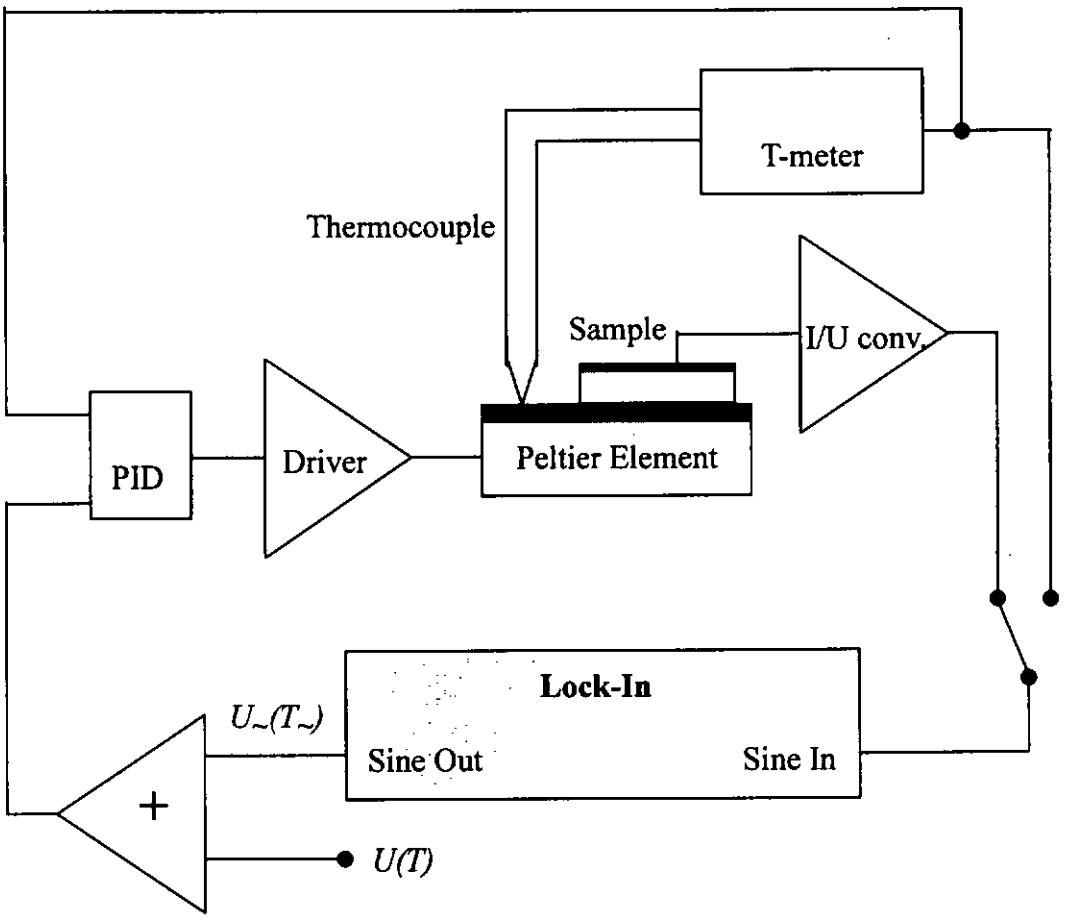

Figure 3.4 Schematic diagram of the dynamic pyroelectric measurement setup.

An a.c. method was used to measure the pyroelectric coefficient. At a certain temperature T_0 the sample temperature was sinusoidally modulated $T(t) = T_o + T_\sim \sin 2\pi ft$ with f = 5 mHz and amplitude $T_\sim$ = 1K using a Peltier element [L.E. Garn, 1982]. The pyroelectric current signal was amplified with an

electrometer and the 90 ° out of phase component of the current with respect to the temperature modulation was measured with a lock-in amplifier.

The pyroelectric coefficient p can be found by [Dias, 1996]

$$p = \frac{1}{A}\frac{I_{\sim}}{2\pi f T_o} \tag{3.8}$$

where A is the electrode area, f is the modulation frequency and T_0 is the measuring temperature.

It is noted that this procedure is the same as that for thermally stimulated discharge current (TSDC) measurement. One has to ensure that this kind of contribution to the total current is negligible or can be properly eliminated. Using the property that the pyroelectric current is a reversible current while TSDC is an irreversible one, this is accomplished by heating and cooling several times until a reproducible current is measured. On the other hand, the samples were annealed at a temperature of 60 °C higher than the highest temperature of measurement (26 °C in the present study) for an extended period of time until the level of TSDC current subsides to negligible values relative to those which are to be measured.

The modulation frequency must be low enough so that the temperature across the sample is uniform, following Dias [Dias, 1996]

$$f << \frac{D}{2\pi d^2} \tag{3.9}$$

where D is the thermal diffusivity of the sample and d is the sample thickness.

Otherwise current due to temperature gradient in the sample will also add to the measured current.

The (primary plus secondary) pyroelectric coefficients of the composites with ceramic volume fraction of 0.05, 0.1, 0.2 and 0.3 as a function of poling time are shown in Figure 3.5.

It is seen that the pyroelectric coefficient of the composites, similar to the piezoelectric measurement results, increase fairly quickly with the poling time. Composites with higher ceramic volume fraction of PT show a higher pyroelectric coefficient under the same poling condition. Overall speaking, the time scale for the achievement of the steady pyroelectric coefficient is found to be 10-30 s. This finding together with the piezoelectric measurement results will be discussed in the next chapter.

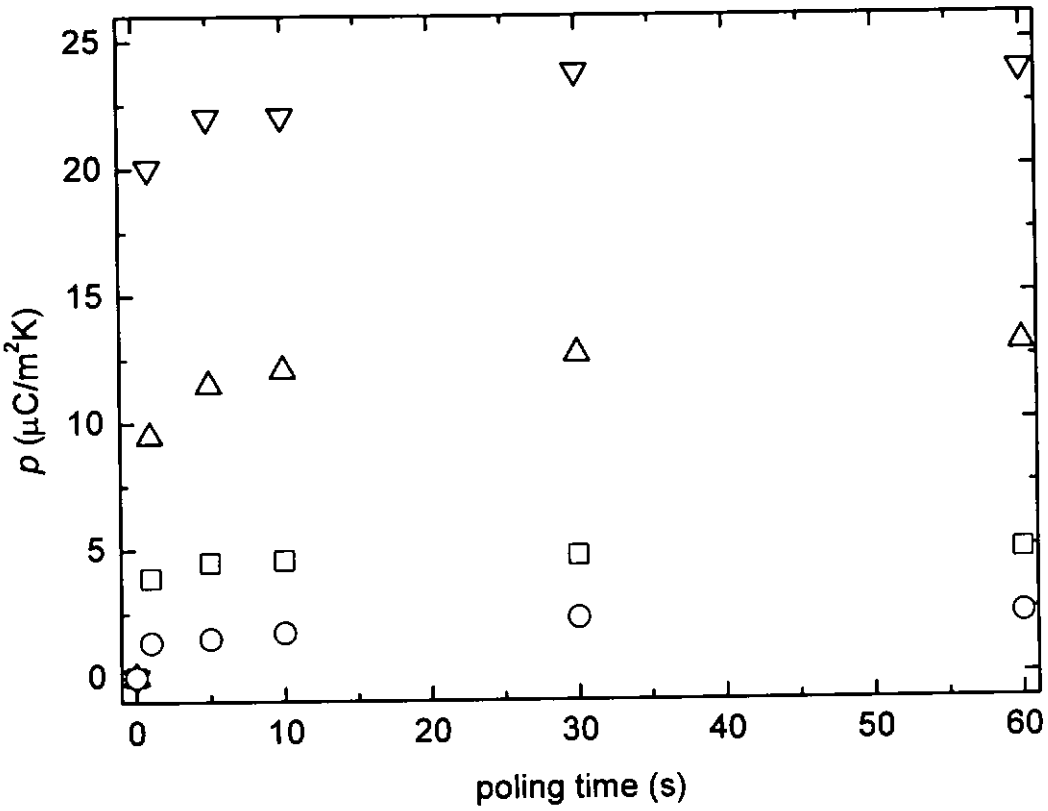

Figure 3.5 Pyroelectric coefficient of the PT/P(VDF-TrFE) 0-3 composites with ceramic volume fraction of 0.05 (circle), 0.1 (square), 0.2 (triangle) and 0.3 (inverted triangle) as a function of poling time.

3.3.3 X-Ray Diffractometry (XRD)

The crystalline orientation of the PT ceramic inclusion after poling was examined by X-ray diffraction.

It is known that in tetragonal crystals such as PT, both 180° and 90° domains

can be reoriented under the influence of strong electric field [Berlincourt *et al.*, 1959]. The 180° domain reorientation can be performed by switching a domain orientation from a direction initially anti-parallel to the electric field, without any dimensional change of the unit cell (see Figure 3.6 (a)). However, 90° domain reorientation results from a switching of perpendicular to parallel direction with respect to the applied electric field during poling. This is achieved by shortening the axis of the unit cell which was perpendicular to the applied field, but elongating the axis that was parallel to the field direction (see Figure 3.6 (b)). As a result, the population of (00h) planes increases but (h00) planes will decrease. Therefore, by comparing the X-ray diffraction intensities of (00h) and (h00) planes, one can estimate the "degree of poling" of the ceramic phase inside the composite after poling. In this study, the diffraction peak intensities of the (002) and (200) were used to estimate the degree of poling of the ceramic phase.

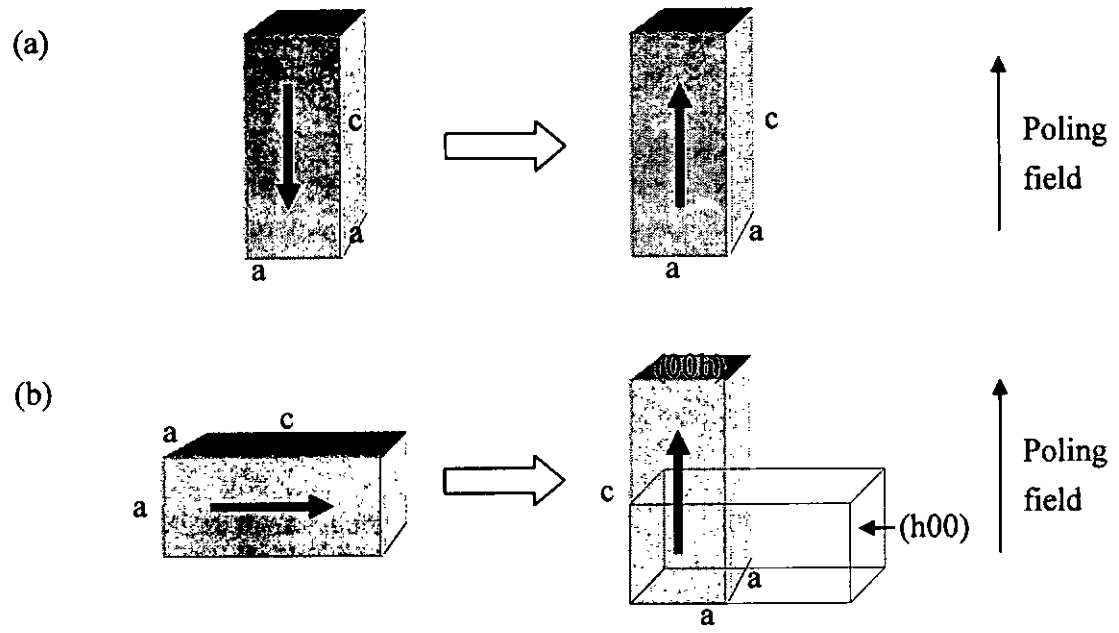

Figure 3.6 The schematic diagram showing (a) 180° (b) 90° domain switching.

The polarization ratio α_c can be expressed as follows [Yamazaki, 1981]

$$\alpha_c = 1 - \left(\frac{I^b_{(002)}}{I^b_{(200)}}\right)\left(\frac{I^a_{(200)}}{I^a_{(002)}}\right) \tag{3.10}$$

where $I_{(002)}$ and $I_{(200)}$ are the intensities of the X-ray diffraction peak of (002) and (200) planes; superscript a and b denote the states after poling and before poling. It is noted that α_c is less than one as many domains cannot be reoriented due to a complex set of internal stresses and electric fields in grains and because some domains will switch back after the poling field is removed [Damjanovic, 1998].

In this study, the XRD patterns of the unpoled composites with ceramic volume fraction of 0.05, 0.1, 0.2 and 0.3 were first measured for reference. These

samples were then polarized under the same poling condition that we mentioned above. And the XRD patterns of these composites were measured again. Figures 3.7, 3.8, 3.9 and 3.10 show XRD spectra of composites with 5 %, 10 %, 20 % and 30 % volume fraction of PT before and after poling at a field of 50 MV/m for different poling times, respectively. Figure 3.11 shows the poling ratio α_c (equation (3.10)) of the PT inclusion in the composites with different ceramic volume fractions, after poling. It is seen that a higher poling ratio of the PT inclusion can be achieved in the composite with higher ceramic loading. For the composites with 30 % volume fraction of PT, the poling ratio attains a high value of 0.85.

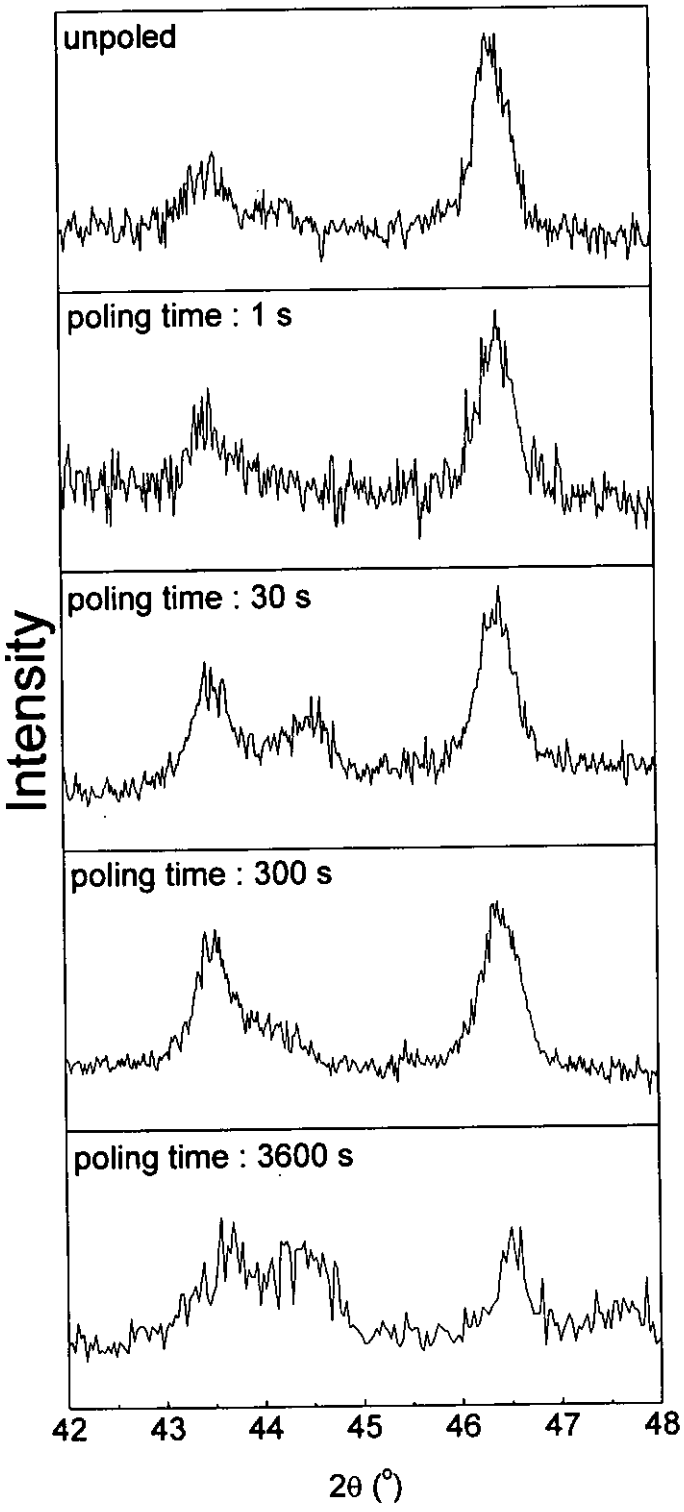

Figure 3.7 X-ray diffraction patterns of the composite film with 5 % PT ceramic volume fraction after poling for different poling times.

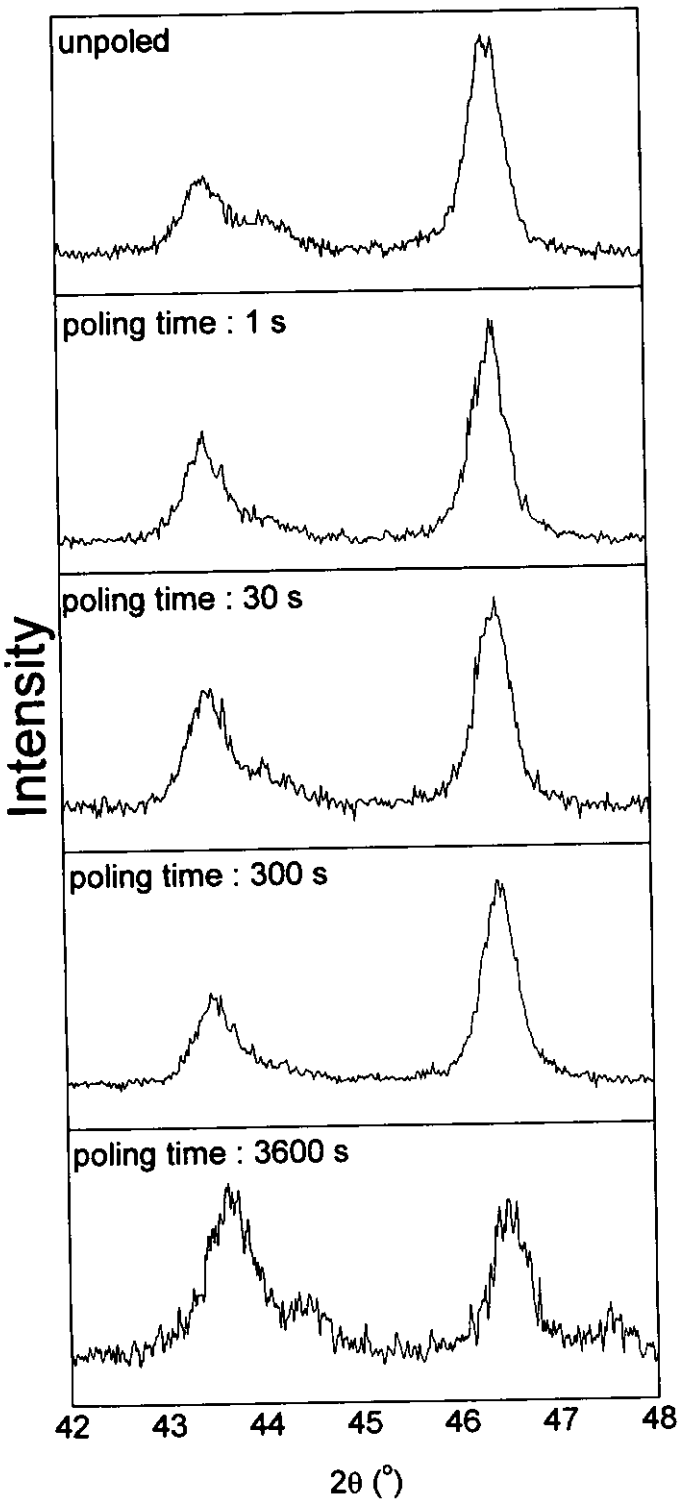

Figure 3.8 X-ray diffraction patterns of the composite film with 10 % PT ceramic volume fraction after poling for different poling times.

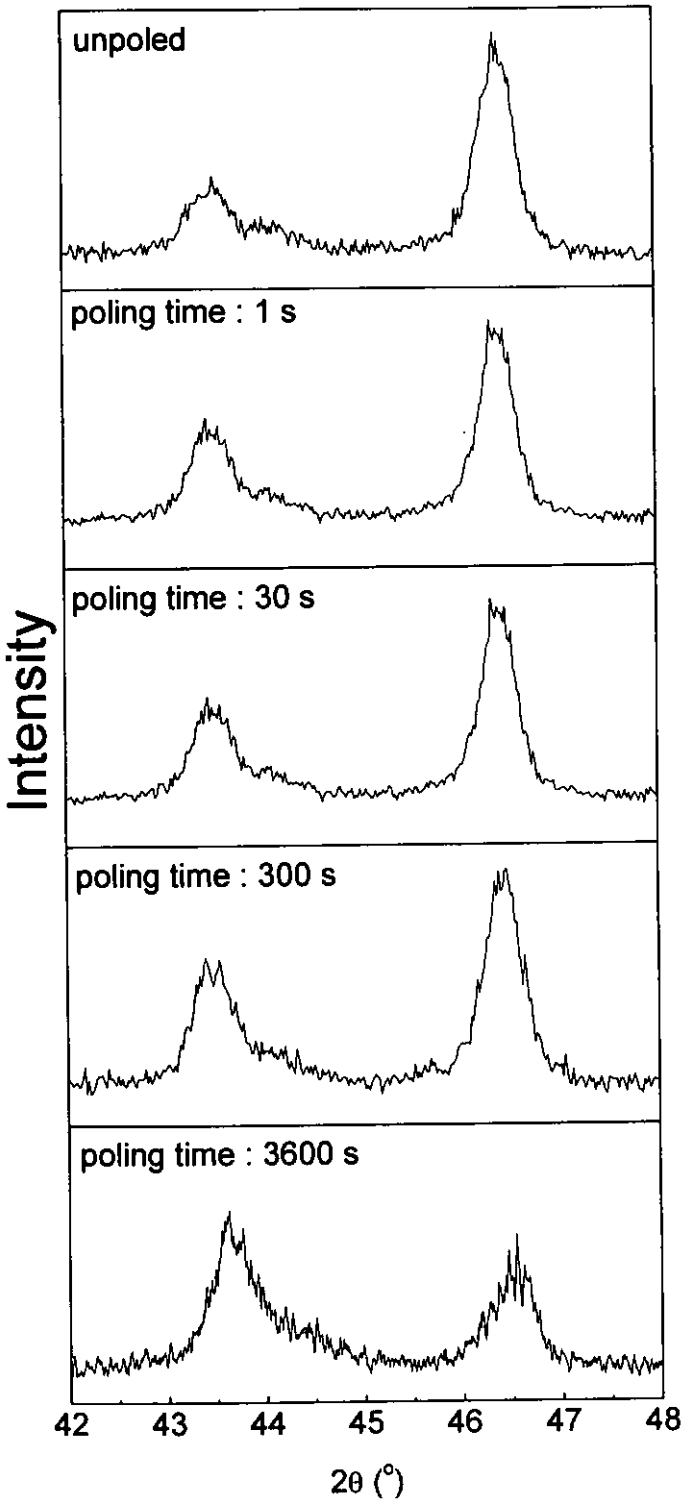

Figure 3.9 X-ray diffraction patterns of the composite film with 20 % PT ceramic volume fraction after poling for different poling times.

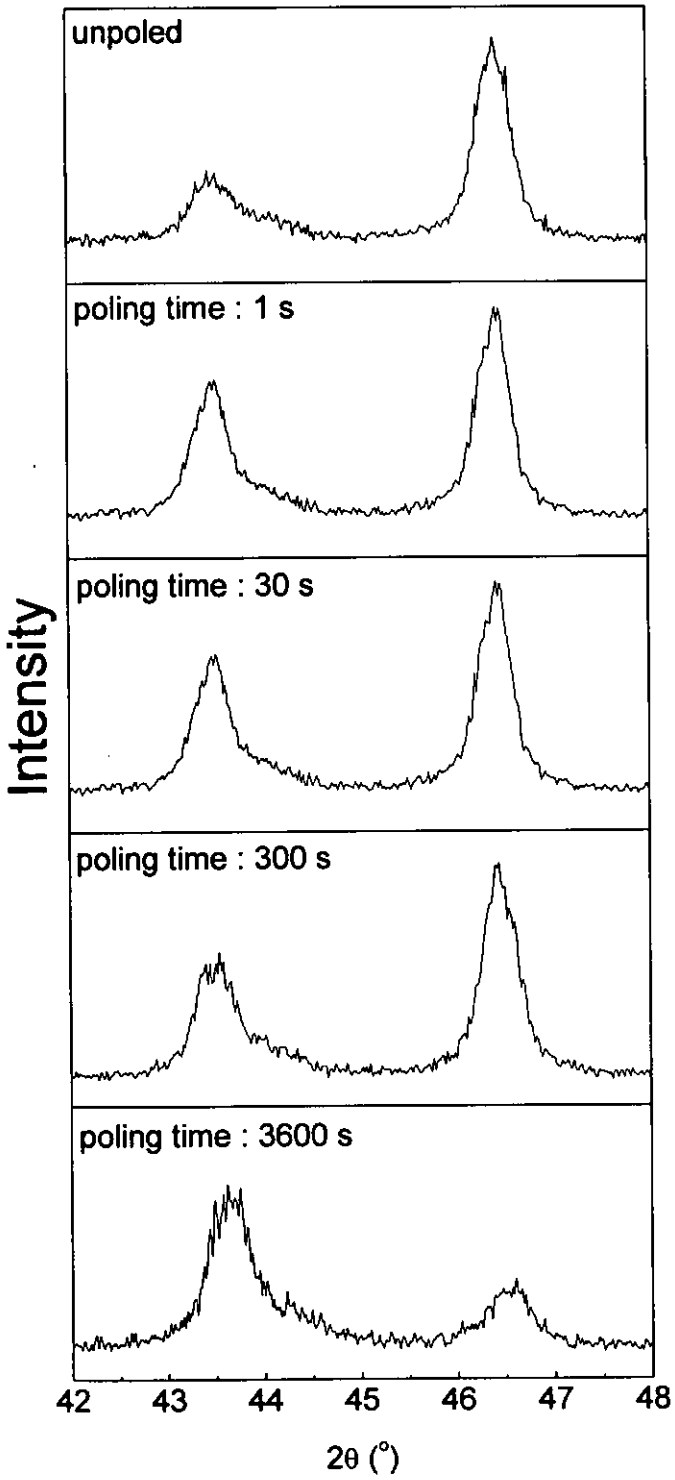

Figure 3.10 X-ray diffraction patterns of the composite film with 30 % PT ceramic volume fraction after poling for different poling times.

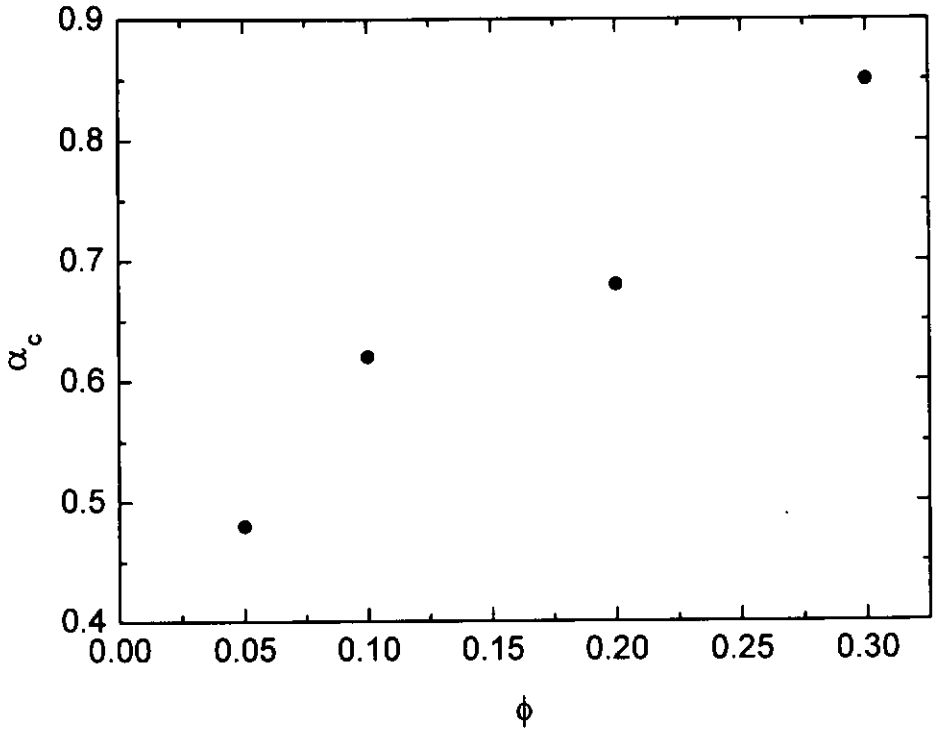

Figure 3.11 The poling ratio α_c of the PT inclusion in the composites as a function of ceramic volume fraction after poling for 1 hour.

3.3.4 Laser Intensity Modulation Method (LIMM)

Laser Intensity Modulation Method (LIMM) introduced by Lang and Das-Gupta [Lang, 1981] is an experimental technique for the high-resolution nondestructive scanning of pyroelectric profiles, which can be applied for the characterization of the polarization depth distribution of ferroelectric materials [Ploss, 1998]. In the present study, the measurement was performed with gold electrode on the two surfaces of a sample exposed in turn to a laser beam of 30 mW $_{r.m.s.}$ power which is intensity modulated in a sinusoidal manner. This causes a sinusoidal variation in the electrode temperature at the sample surface, resulting in a propagation of a thermal wave into the bulk of the sample. The thermal waves are attenuated and retarded in phase as they progress through the sample, thus providing a non-uniformly distributed thermal "force" which interacts with the spatially distributed polarization or space charge to produce sinusoidal pyroelectric current. This current is a unique function of the modulation frequency and the spatial distribution of polarization. The real and imaginary parts of this current are measured with a lock-in amplifier whose reference phase is provided by the same frequency modulator. The frequency modulation can be varied from 10 Hz to 2 MHz and the thermal wave penetrates to shallower depths as the laser modulation frequency is

increased. Spectra of the pyroelectric current were recorded and the pyroelectric profiles were calculated following the thermal scanning function technique [Ploss, 1999]. It is noted that in this measurement, the total amount of energy deposited by the laser beam is independent of frequency and the heat loss from the sample surfaces to the surrounding is neglected.

The experimental arrangement we used for the LIMM measurement is shown in Figure 3.12.

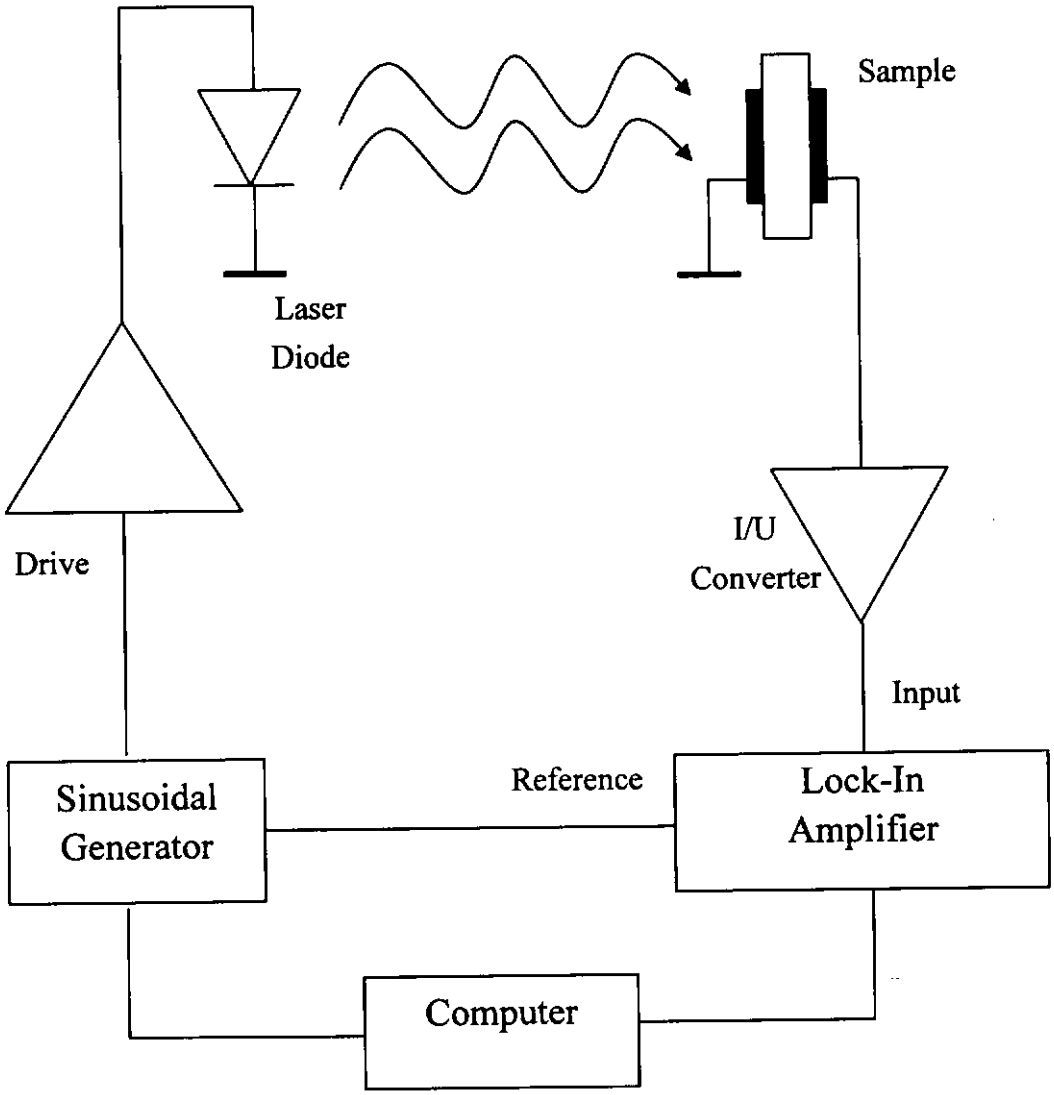

Figure 3.12 Experimental arrangement of the LIMM.

The composites with ceramic volume fraction of 0.1 and 0.3 were polarized under a d.c. electric field of 50 MV/m at 120 °C for 5, 10 and 15 minutes and the pyroelectric profile along the thickness direction was investigated. The profiles of unpoled samples with ceramic volume fraction of 0.1 and 0.3 are shown in Figures 3.13(a) and 3.14(a). Non-uniform pyroelectric profiles were found in both composites after poling for 5 minutes (see Figures 3.13(b) and 3.14(b). The profile of the composite with ceramic volume fraction of 0.3 becomes more uniform after poling for 10 minutes (see Figure 3.14(c)) and is quite constant after poling for 15 minutes (see Figure 3.14(d)). On the other hand, the profiles of the composite with ceramic volume fraction of 0.1 remain non-uniform along the thickness direction even after poling for 15 minutes (see Figure 3.13(d)), especially near the region of anode, i.e. at "thickness" = 0. The LIMM studies show that a poling time of 15 minutes is required to produce a uniform polarization profile in a composite sample with 30 % volume fraction of PT, which is found to be longer than the time development of piezoelectric and pyroelectric activities of the composites with the same ceramic volume fraction.

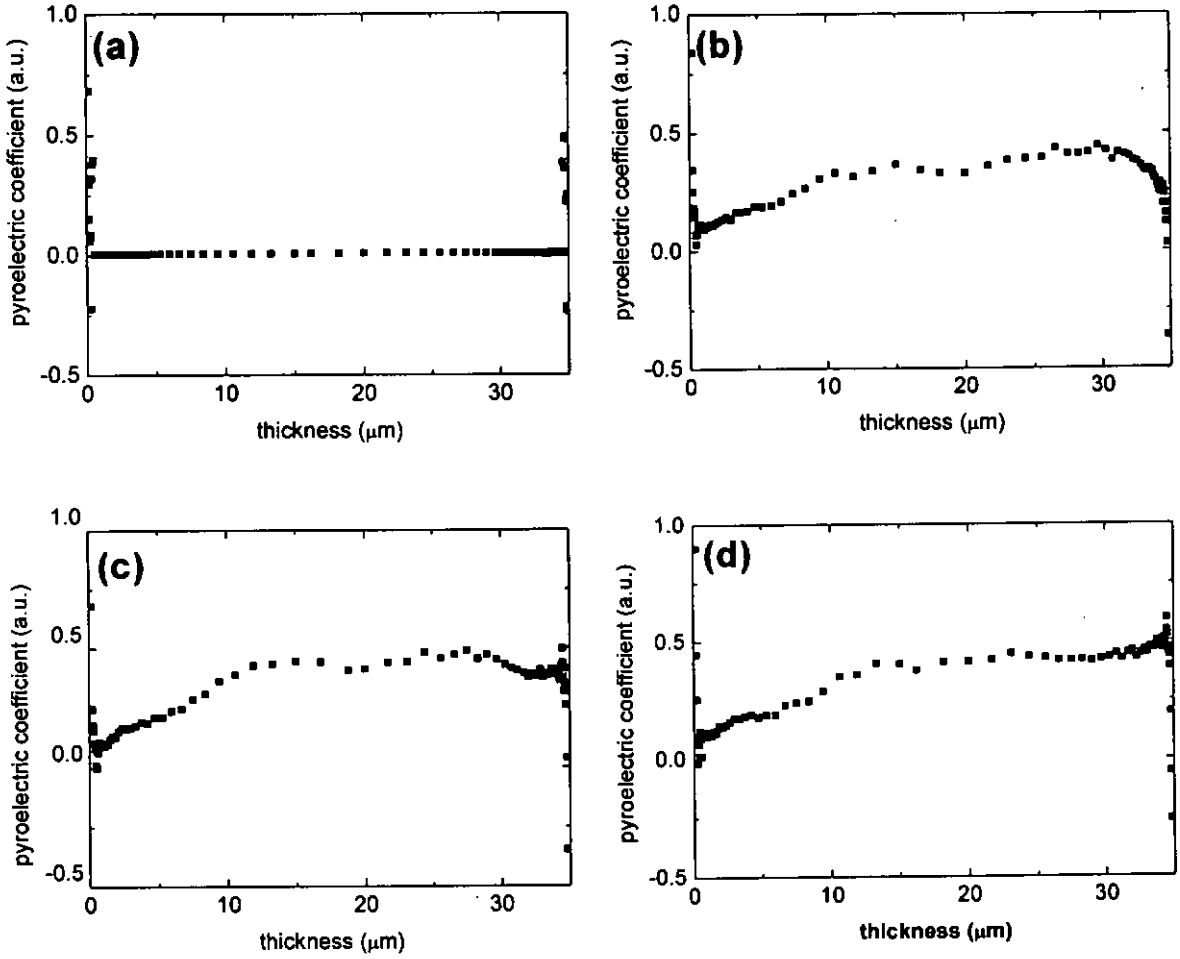

Figure 3.13 The pyroelectric profiles of the composite sample with 10 % volume fraction of PT: (a) Unpoled sample; after poling for (b) 5 minutes, (c) 10 minutes and (d) 15 minutes.

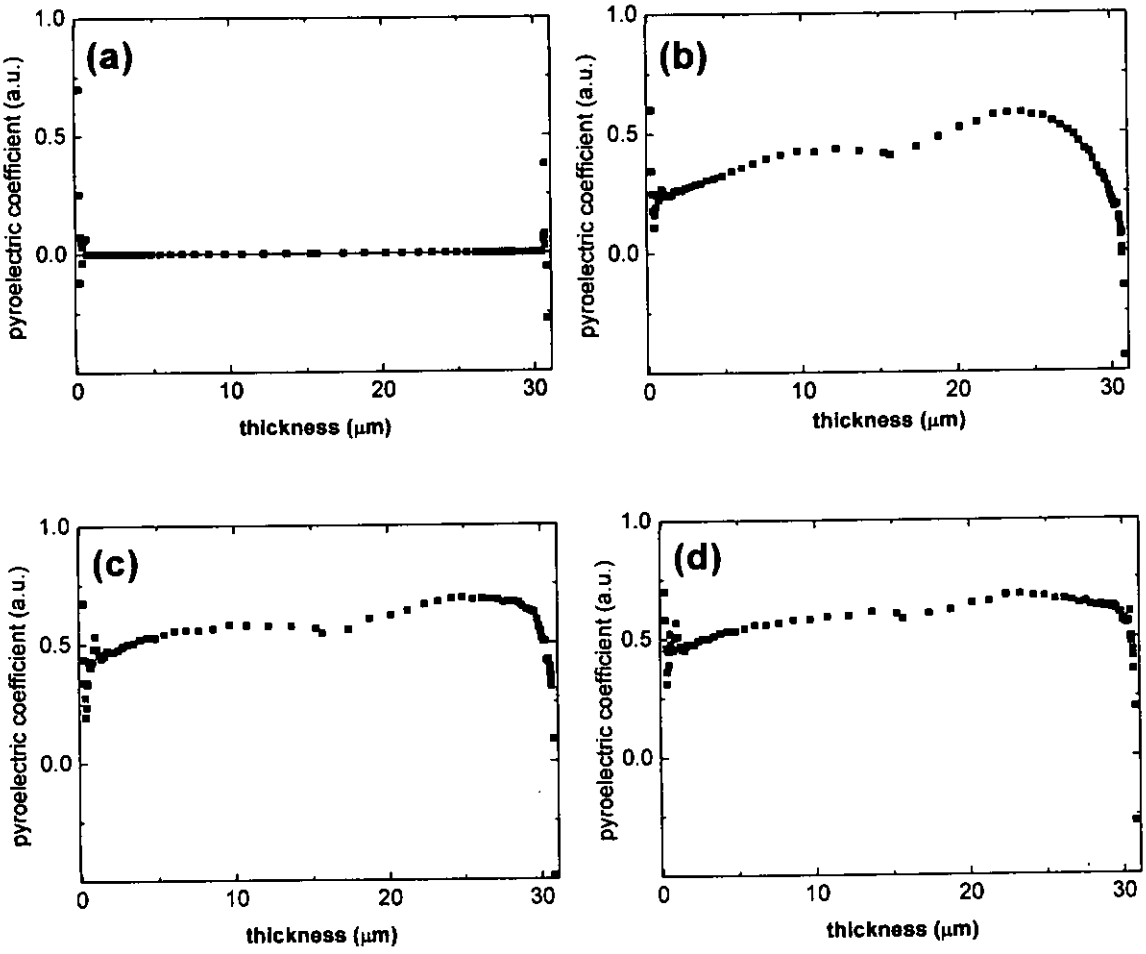

Figure 3.14 The pyroelectric profiles of the composite sample with 30 % volume fraction of PT: (a) Unpoled sample; after poling for (b) 5 minutes, (c) 10 minutes and (d) 15 minutes.

3.4 Conclusion

Thermal poling of PT/P(VDF-TrFE) 0-3 composites was employed in this study. A high d.c. electric field was applied to the samples at elevated temperature, to study the polarization of the composites as a function of poling time. Various characterizations of the poling state of the composites like piezo- and pyroelectric measurements, XRD and LIMM were introduced.

The piezo- and pyroelectric measurements reveal the composites with higher ceramic volume fraction can attain a higher piezoelectric and pyroelectric coefficient, and the build-up time was also shorter than that in the composites with lower ceramic volume fraction. All of them were found to become steady after the poling time of roughly 30 s under identical poling condition, about 2 orders of magnitude shorter than the values reported in the literature.

XRD was used to evaluate the poling ratio of the composites after subjected to poling. It is observed that the poling ratio of the composites with higher ceramic volume fraction attained a higher poling ratio than that of the composites with lower ceramic volume fraction. The poling ratio in the composite with ceramic volume fraction of 0.3 attains a high value of 0.85.

LIMM was employed for scanning of pyroelectric profiles along the

thickness direction of the composites. Profiles of the composites with 10 % and 30 % ceramic volume fraction were measured. The results show that a poling time of 15 minutes is required to produce a uniform polarization profile in a composite sample with 30 % volume fraction of PT, which is longer than the time development of the piezo- and pyroelectric activities in the composites with the same volume fraction.

CHAPTER 4
MODELING STUDIES

4.1 Introduction

This work aims to systematically analyze the physical process(es) pertaining to the poling of the multi-layered composite. Understanding of the physical process behind poling will give an idea on the materials selection and the poling parameters for particular applications. In this chapter, we first give a theoretical description on the poling of multi-layered composite systems by considering the continuity of the total current density going through each ferroelectric layer along the poling direction. A modified model of Miller *et al.* [Miller, 1990, 1991] is used for the description of the *P-E* relation of each ferroelectric layer. The modeling is applied to study the switching of the bilayer PZT/polyvinylidene fluoride-trifluoroethylene P(VDF-TrFE) composite investigated by Furukawa *et al.* [Furukawa, 1986] and the poling of P(VDF-TrFE) with ferroelectric TGS electrodes investigated by Ploss *et al.* [Ploss, 1996]. Then we show the comparison between the experimental results with the theoretical predictions.

A simple model has been developed for studying the piezoelectric and pyroelectric activities of the 0-3 composite systems based on the polarization behaviour of the ceramic inclusion. The model is applied to study the piezoelectric properties of a lead zirconate titanate (PZT) / epoxy system polarized with different poling electric fields [Furukawa, 1976], and our own experimental results on the piezo- and the pyroelectric properties of lead titanate (PT) / polyvinylidene fluoride-trifluoroethylene (P(VDF-TrFE) 70/30 mol-%) with different poling times. This work has demonstrated a novel approach to predict the gross properties of the 0-3 composites in terms of the properties of the constituents.

4.2 Theory for Multilayer Composite

We are going to develop a physical model based on quasi-electrostatic considerations to study the effective polarization response of the ferroelectric multi-layered composite as a function of arbitrary applied electric field. Electrical conductivity of the constituent materials and charge accumulation at the interfaces between constituent phases are taken into account. Also, nonlinear hysteretic *P-E* relations are used for the ferroelectric constituent materials.

Consider a multi-layered composite consisting of n ferroelectric layers connected in series along the thickness direction (see Figure 4.1).

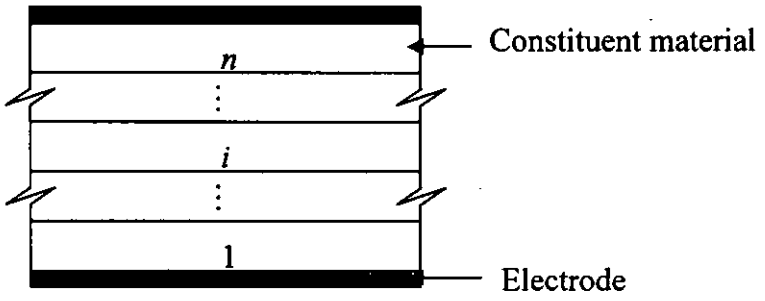

Figure 4.1 Schematic for the multi-layered composite.

The constitutive equation of the i^{th} layer is given by

$$D_i = \varepsilon_i E_i + P_i \tag{4.1}$$

where i is an integer between 1 to n. D, ε, E and P represent the electric displacement, permittivity, electric field and ferroelectric polarization respectively. P_i generally depends on E_i in a complicated manner and a model for describing P-E relations must be used, as will be explained later. In contrast, when some layer, say j^{th} layer, is non-ferroelectric, then $P_j = 0$.

In the measurement of electric displacement of a ferroelectric sample, the Sawyer-Tower circuit is usually adopted, which is merely a capacitor divider where the sample is in series with a standard reference capacitor. Assuming the reference capacitor is a perfect insulator, the measured electric displacement of the ferroelectric sample at a certain time t_o is given by the integration of current density across the reference capacitor:

$$D(t_o) = \int_0^{t_o} J_r dt \tag{4.2}$$

J denotes current density and the subscript r represents reference capacitor.

The overall electric field of the composite is given by [Furukawa, 1986]

$$E = \sum_{i=1}^{n} v_i E_i \tag{4.3}$$

where $v_i = d_i / \sum_{j=1}^{n} d_j$ is the volume fraction of the i^{th} layer. The interfacial charge density q_k between the k^{th} and $k+1^{th}$ layer can be written as, according to the electrostatics or quasi-static boundary conditions,

$$q_k = D_{k+1} - D_k \tag{4.4}$$

where k is an integer between 1 to $n - 1$. Continuity of total current (conduction current plus displacement current) requires

$$J_r = J_k = J_{k+1} = \sigma_k E_k + \frac{\partial D_k}{\partial t} = \sigma_{k+1} E_{k+1} + \frac{\partial D_{k+1}}{\partial t} \tag{4.5}$$

where σ represent the electric conductivity. Here σ serves to allow the accumulation of charge at the interfaces between the constituent phases to stabilize the ferroelectric polarization achieved via poling. The rate with which polarization is developed is very much controlled by σ. Equations (4.1) and (4.5) yield

$$\sigma_k E_k + \varepsilon_k \frac{\partial E_k}{\partial t} + \frac{\partial P_k}{\partial t} = \sigma_{k+1} E_{k+1} + \varepsilon_{k+1} \frac{\partial E_{k+1}}{\partial t} + \frac{\partial P_{k+1}}{\partial t} \tag{4.6}$$

When E changes with time, the relation $\partial P / \partial t = [\partial P / \partial E]\,[\partial E / \partial t]$ may be employed for subsequent calculations.

The P-E relationship of a ferroelectric material is very complex and is the subject of many investigations. We choose to adopt a convenient mathematical model developed by Miller *et al.* [Miller, 1990, 1991], which may be expressed as:

$$\frac{\partial P}{\partial E} = \left(1 - \tanh \sqrt{\frac{P - P_{sat}}{\xi P_s - P}}\right)\left(\frac{\partial P_{sat}}{\partial E}\right) \tag{4.7}$$

where P_{sat} is the polarization on the saturated hysteresis loop at the field of interest, and P and P_s are the magnitudes of the ferroelectric polarization and spontaneous polarization respectively. $\xi = +1$ for an increasing field and $\xi = -1$ for a decreasing

field. The saturated polarization of the hysteresis loop is written as a function of the electric field as

$$P_{sat} = \xi\ P_s \tanh\left[\frac{\xi\ E - E_c}{2E_c}\ln\left(\frac{1+P_r/P_s}{1-P_r/P_s}\right)\right] \tag{4.8}$$

where P_r and E_c are taken as positive quantities representing the magnitude of remanent polarization and coercive field, respectively.

Solving equations (4.3), (4.6) and (4.7) with known applied electric field profile will give the electric field and the ferroelectric polarization in both phases as a function of time, thereby the time development of the electric displacement and the current density of the composite can be evaluated by equations (4.2) and (4.5) accordingly. The interfacial charge density at each interface can be calculated by equation (4.4). In the present work, all these equations were solved by Wolfram Mathematica 4.0.

4.3 Application to Switching of Bilayer PZT/P(VDF-TrFE) Composite

Furukawa *et al.* [Furukawa, 1986] have studied the switching characteristics of a bilayer PZT / P(VDF-TrFE) composite with 75 % ceramic volume fraction. The composite was first pre-polarized in the reverse direction (see Figure 4.2(a)) and the field was released. A d.c. electric field of 1.25 MV/m was then applied on the sample at 100 °C in the forward direction (see Figure 4.2(b)); the electric displacement and the current density were measured with time.

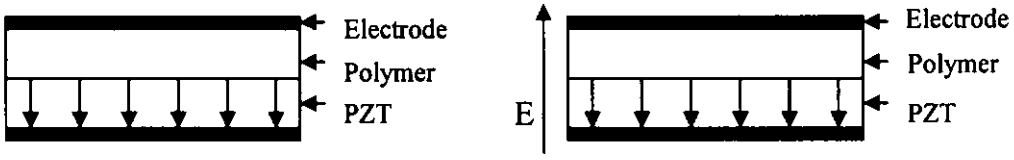

Figure 4.2 (a) PZT ceramic is pre-polarized to $-P_r$. (b) The composite is poled by applying an electric field opposite to the pre-polarized direction.

Assuming *P-E* hysteresis behavior for the PZT ceramic phase is a perfect square loop and the electric displacement is continuous across constituents, Furukawa *et al.* have modeled the switching processes for their bilayer composite

system. Our modeling takes consideration of ceramic / polymer interfacial charge and the nonlinear hysteresis behavior of the ferroelectric constituent.

The *P-E* relationship of PZT ceramic can be simulated by equations (4.7) and (4.8), in which three parameters (P_s, P_r and E_c) are necessary for the prediction. We converted the *D-E* graph of PZT ceramic shown in Ref. [Furukawa, 1986] into a *P-E* graph by use of equation (4.1). Therefore P_s, P_r and E_c can be identified to be 0.35 C/m^2, 0.33 C/m^2 and 0.89 MV/m respectively. Figure 4.3(a) shows the calculated (equations (4.7) and (4.8)) *P-E* saturated hysteresis loop of PZT ceramic and the "experimental" loop from Furukawa *et al.*'s *D-E* measurements. It is found that the two do not fit well. It is noted that the *P-E* loop shape can be quite different even when the material parameters P_s, P_r and E_c are identical. Following Wong *et al.* [Wong, 2001], we make a numerical modification to Miller *et al.*'s model to adjust the *P-E* loop shape. Equation (4.8) is modified as

$$P_{sat} = \xi\, P_s \tanh\left\{\frac{\xi\, E - E_c}{2E_c}\ln\left[\frac{1-(-P_r/P_s)^{1/n}}{1+(-P_r/P_s)^{1/n}}\right]\right\}^n \tag{4.9}$$

where $n \equiv n_1 / n_2$ ranges from 1 / 3 to 1 with n_1 and n_2 being odd-numbers. Figure 4.3(b) shows the experimental loop and the fitting given by equations (4.7) and (4.9) with n equal to 5 / 11. Better agreement is observed between the two loop shapes.

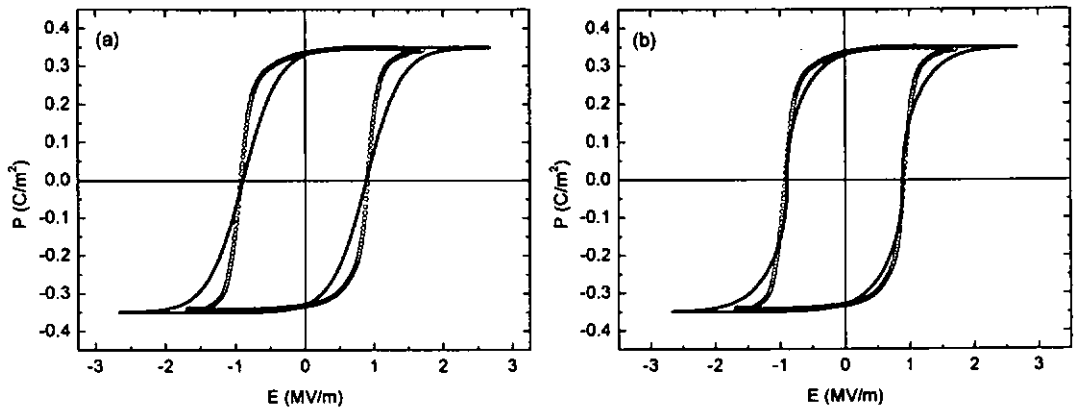

Figure 4.3 (a) *P-E* hysteresis loop of PZT ceramic predicted by Miller's model (solid line) with the experimental result (circles). (b) *P-E* hysteresis loop of PZT ceramic predicted by Miller's model with $n = 5 / 11$ (solid line) and the experimental result (circles).

On the other hand, P(VDF-TrFE) 52/48 mol-% copolymer used in Ref. [Furukawa, 1986] is known to be a ferroelectric copolymer having a Curie temperature near 70 °C. Since the experiment was carried out at 100 °C, the copolymer was in its paraelectric phase. We thus treat it as a linear material.

The material parameters used for the calculations are listed in Table 4.1. We have assumed that the imaginary parts of the permittivities of the constituent materials can be neglected in the computation since they are much smaller than the real parts.

Table 4.1 Properties of constituents for PZT ceramic and P(VDF-TrFE) copolymer.

	P_s (C/m^2)	P_r (C/m^2)	E_c (MV/m)	n	$\varepsilon / \varepsilon_o$ [a]	σ ($\Omega^{-1}m^{-1}$)	ν [a]
PZT	0.35[a]	0.33[a]	0.89[a]	5 / 11	1900	10^{-11} [b]	0.75
P(VDF-TrFE) 56/44 mol-%	—	—	—	—	40	1.8×10^{-8}	0.25

[a] Furukawa, 1986

[b] H.L.W. Chan, W.K. Chan, Y.Chen and C.L. Choy, Ferroelectrics **196**, 141 (1997).

Figure 4.4 shows the experimental results, the predictions given by Furukawa *et al.* (Figures 4.4(b) and 4.4(e)) together with predictions based on our model. According to the latter, the electric field acting on the two phases follows very different trends once the external electric field is applied on the composite. At $t \leq t_1$ (labeled in Figure 4.4), the electric field acting in the ceramic phase would increase but that in the polymer phase would decrease with time. The electric field acting on the ceramic phase would tend to remain constant when it approaches the coercive field of the ceramic. The polarization and the interfacial charge density increase from their initial negative values of $-P_r$ to zero. At the same time, a linear change of electric displacement of the composite with time can be observed. Here the change of electric displacement refers to the difference of the electric displacement between time t and the initial time t = 0 at which the external field is applied. On the other

hand, the total current density follows closely the conduction current of the polymer phase, which is governed by the conductivity of the polymer phase and the electric field acting on it. At $t_1 < t < t_2$, the electric field acting on the ceramic phase further increases. The polarization of the ceramic phase and the interfacial charge density increase from zero to positive values quite gradually because the slope of the ceramic *P-E* curve would decrease after the coercive field is reached (see Figure 4.4(f)). At the same time, the electric field acting on the polymer phase and the total current density gradually decrease. At t equals to t_2, our prediction on the electric field acting on the ceramic reaches a maximum; therefore, the polarization of the ceramic phase, the interfacial charge density and the change of electric displacement of the composite attain maximum and keep constant thereafter. At the same time, the electric field acting on the polymer phase reaches a minimum and the total current density drops to nearly zero. At t_3, the switching process is said to be finished.

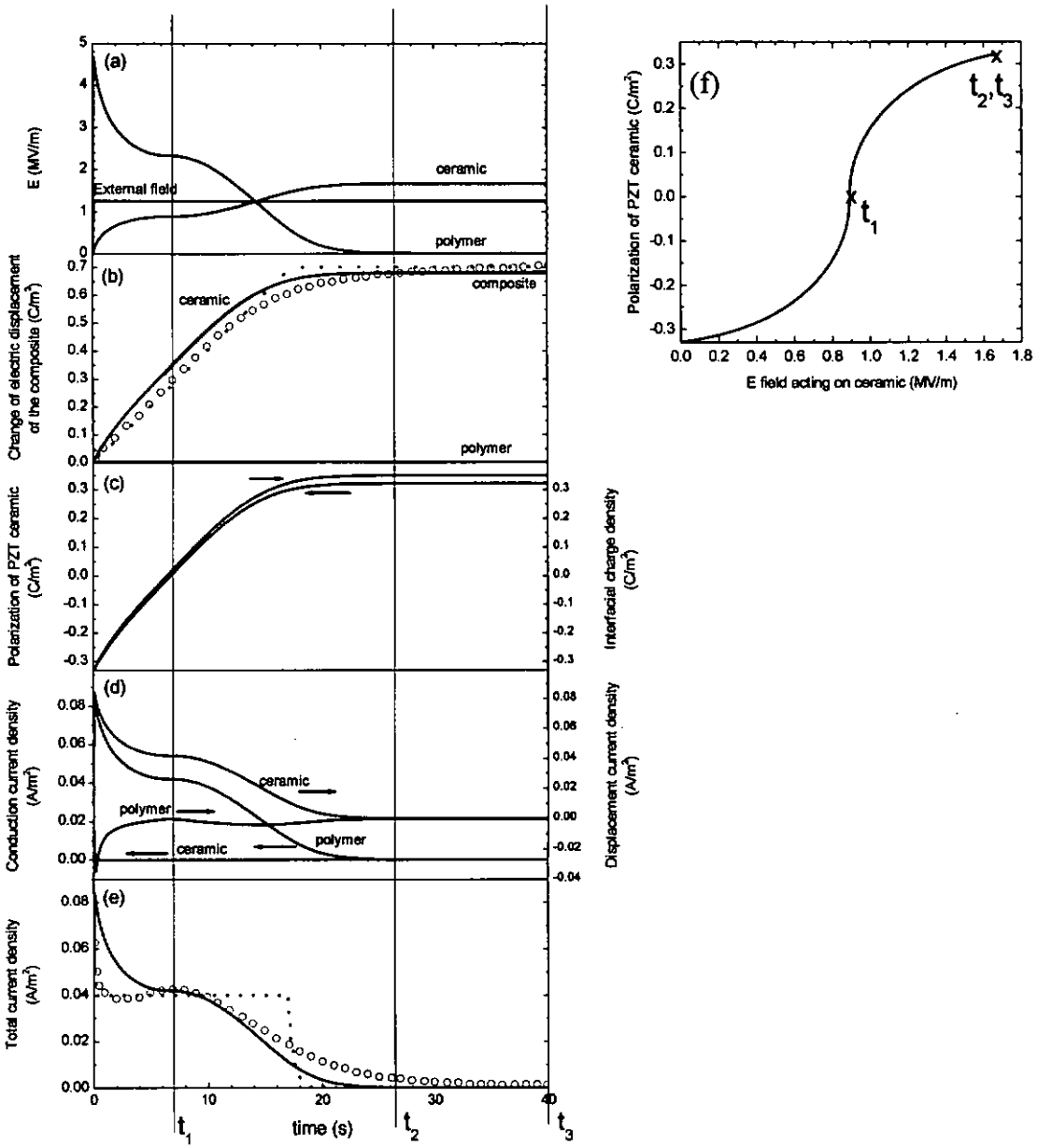

Figure 4.4 Comparison of observed (circles), prediction by Furukawa *et al.* (dotted lines) and our calculated (solid lines) switching characteristics in a PZT/polymer composite.

Furukawa *et al.* have shown an agreement in the change of electric displacement of the composite between their predictions with the experimental result. Due to the assumption of the perfect square loop nature in PZT made by Furukawa *et al.*, their predictions show discontinuity in the change of electric displacement and the current density at particular times [see Figs. 4.4(b) and 4.4(e)]. Significant improvement is obtained in our predicted electric displacement and the current density, which follows quite well the observed result. The improvement is due to the more realistic description of the nonlinear hysteresis nature in PZT by Miller *et al.*'s model. It confirms that consideration of a realistic hysteresis loop is beneficial to the study of the switching characteristics of the ferroelectric composite structures. Qualitative agreement seems to affirm the validity of the basic mechanism we presented for the switching process.

In addition, we have tried different poling parameters in the calculations to find out the dependencies of the poling process. First, we use different conductivity values (1 to 2 orders of magnitude higher than the original values given in Table 4.1) of either phase and re-calculate the switching process under identical driving conditions. Figure 4.5 shows that a higher conductivity of the polymer phase can effectively shorten the build-up time of the electric field acting on the ceramic phase, therefore faster polarization development and change of electric displacement can be

obtained. It is suggested that higher conductivity of the polymer phase can be achieved either by raising the sample temperature or by doping a small amount of a highly conductive third phase such as carbon, germanium, silver or silicon into the polymer phase [Safari, 1986]. On the contrary, a higher conductivity of the ceramic phase results in slower development and lower electric field acting on the ceramic phase, therefore lower polarization of the ceramic phase and lower change of electric displacement are expected.

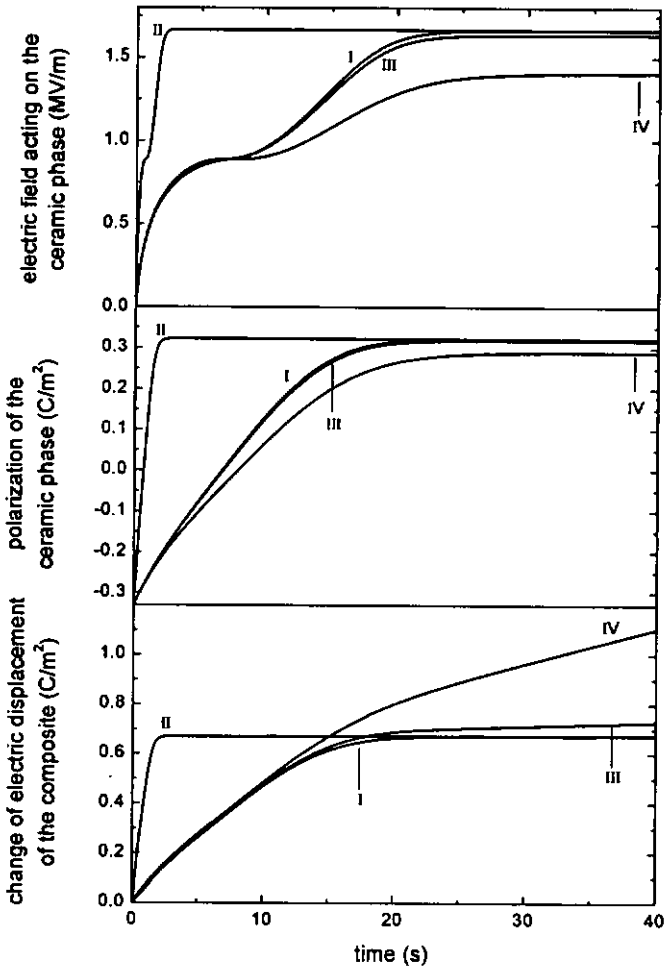

Figure 4.5 Predictions of switching characteristics of PZT/polymer composite with parameters using (I) original value (II) one higher order of magnitude in conductivity of polymer (III) one higher order of magnitude in conductivity of ceramic (IV) two higher order of magnitude in conductivity of ceramic.

It is expected that the permittivity of both phases would not vary by an order of magnitude. We double the original permittivity value of either phase to study the switching process. The predictions shown in Figure 4.6 show that a variation in the permittivity of both phases do not have much effect.

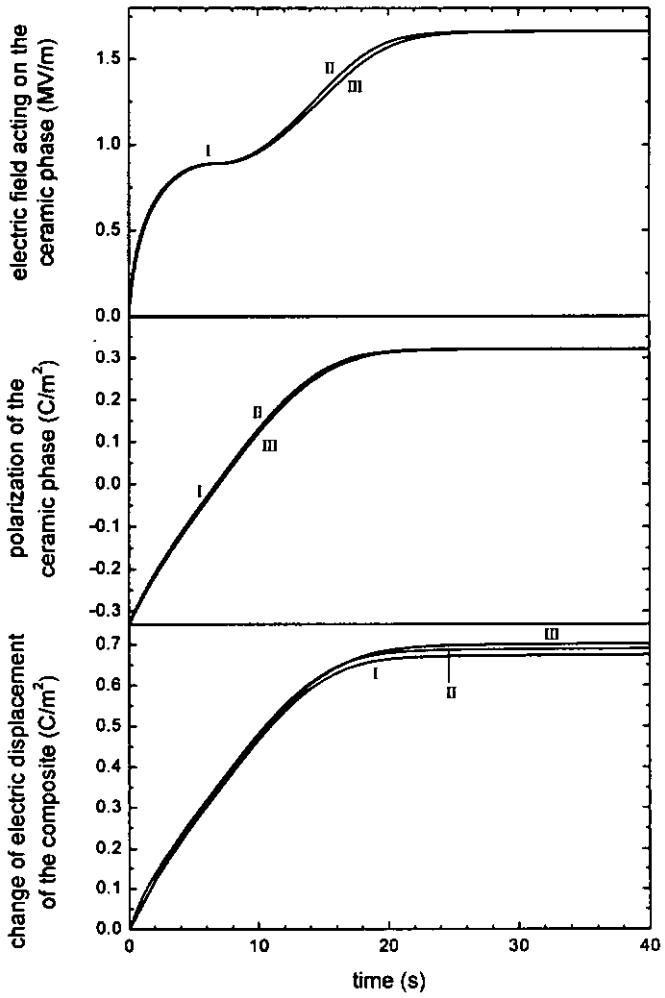

Figure 4.6 Predictions of switching characteristics of PZT/polymer composite with parameters using (I) original value (II) two times higher in the permittivity of polymer (III) two times higher in the permittivity of ceramic.

On the other hand, Figure 4.7 shows the effect of a higher external field (50 % higher than the experimental condition): a faster development, and higher electric field acting on the ceramic phase. A higher polarization and higher electric displacement can be achieved.

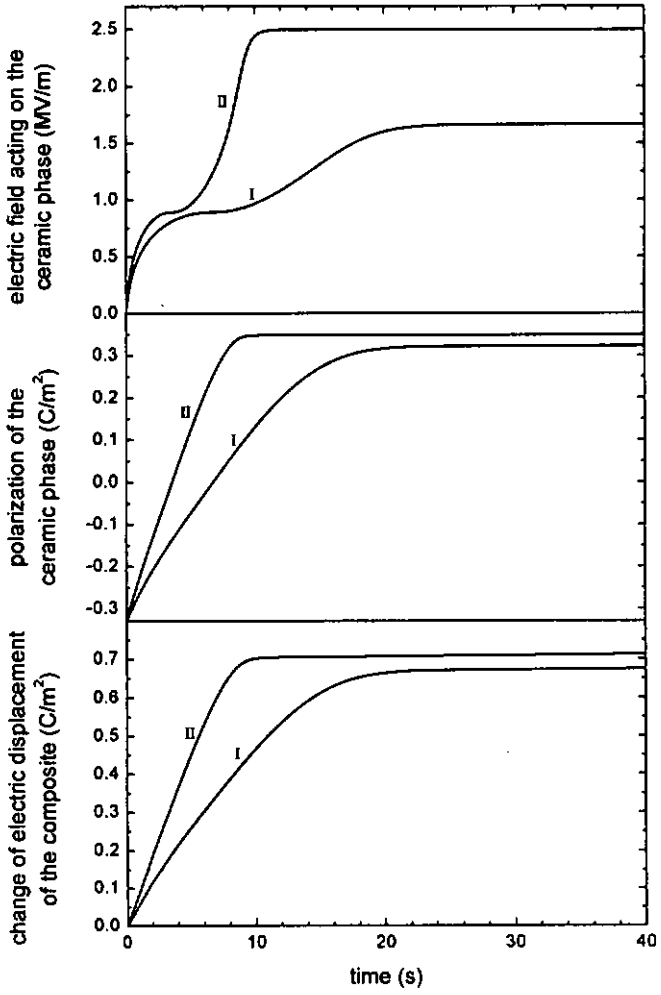

Figure 4.7 Predictions of switching characteristics of PZT/polymer composite with parameters using (I) original value (II) 50% higher external electric field.

Here we conclude that high applied electric field, high conductivity of polymer but low conductivity of ceramic are desirable for fast and high polarization build-up in the ceramic phase of the bilayer ceramic/polymer composite.

4.4 Application to Poling of P(VDF-TrFE) with Ferroelectric TGS Electrodes

A new poling technique was proposed by Ploss *et al.* [Ploss, 1996], in which an unmetallized polymer film was poled in a sandwich between ferroelectric crystals. If a high electrical voltage/field is applied to the stack, the polarization of the ferroelectric crystals is saturated, and the interfaces to the polymer film form well defined sources for a high electric displacement. Here we are going to extend our previous discussion to study the polarization of such a triple-layered composite in a similar manner.

Ploss *et al.* [Ploss, 1996] prepared the 1000 μm thick triglycine sulphate (TGS) crystals as ferroelectric electrodes. The ferroelectric TGS crystals were first pre-polarized to $-P_r$. The 4 μm thick ferroelectric P(VDF-TrFE) 70/30 mol-% copolymer was then stacked between two identical TGS electrodes. One half cycle of a sinusoidal voltage of 1000 V with duration of 2 seconds was applied to the triple-layered composite at room temperature (see Figure 4.8). The applied voltage and the electric displacement were recorded as a function of time using a Sawyer-Tower circuit. The copolymer was then removed and the crystals were brought into contact and a full cycle of a sinusoidal voltage of 1000 V with duration

of 2 seconds was applied to the crystal sandwich (see Figure 4.9), and the applied voltage and the electric displacement were recorded with time. After the negative half cycle, the crystals were allegedly in the initial state ($-P_r$) again.

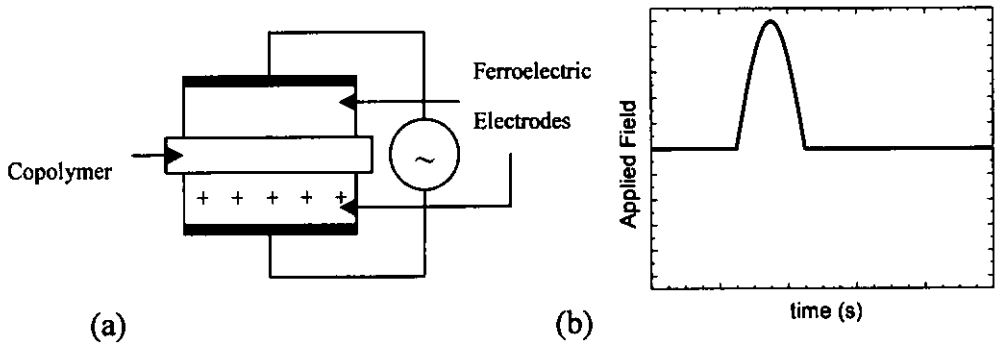

Figure 4.8 Two identical ferroelectric electrodes are first pre-polarized to $-P_r$ and are separated. The unpoled copolymer is inserted between the electrodes shown in (a), to form a triple-layered composite. The composite is poled by applying an external field, shown in (b).

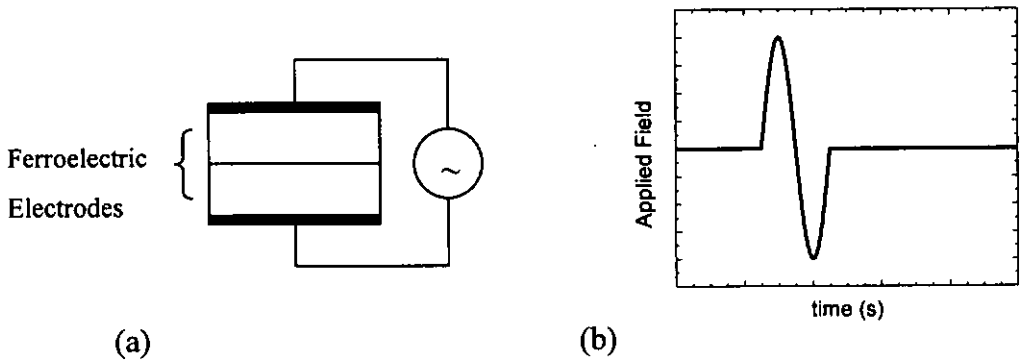

Figure 4.9 After poling, the copolymer is removed and the ferroelectric electrodes are stacked together, as shown in (a). A field, shown in (b), is applied to the stack.

The parameters used in our calculations are listed in Table 4.2.

Table 4.2 Properties of constituents for TGS crystals and P(VDF-TrFE) copolymer.

	P_s[a] (C/m^2)	P_r[a] (C/m^2)	E_c[a] (MV/m)	$\varepsilon / \varepsilon_o$[a]	σ ($\Omega^{-1}m^{-1}$)	n	d (μm)[a]
TGS	0.02865	0.028	0.212	40.67	10^{-10}[b]	11 / 19	1000
P(VDF-TrFE) 70/30 mol-%	0.0572	0.054	43.5	12.3	5×10^{-13}[c]	13 / 19	4

[a] Ploss, 1996

[b] M. Amin, K.A. Darwish and S.S. Ibrahim, Ferroelectrics **76**, 33 (1987).

[c] H.L.W. Chan, Y. Chen and C.L. Choy, Integrated Ferroelectrics **9**, 207 (1995).

The electric field acting on the two phases, the polarization, the change of electric polarization of the two phases and the change of electric displacement of the composite as a function of time are calculated as in the last section and shown in Figures 4.10(a)-(d) respectively. It is found that for the first 1 s, i.e. when the first half cycle of the electric field is applied on the composite, the electric fields acting on both phases increase with time. The maximum electric field acting on the TGS crystals and the copolymer are about 0.35 MV/m and 70 MV/m respectively. During the first 1 s, the polarization of the pre-polarized TGS crystals increases from $-P_r$ (-0.028 C/m^2) to a maximum about 0.025 C/m^2 while that of copolymer increases from 0 to a maximum about 0.047 C/m^2. During the time between 1 s and 2 s, when the applied electric field gradually returns to zero, the electric fields acting on both phases decrease with time. The polarization of the TGS crystals drops slightly from

0.025 C/m^2 to 0.0238 C/m^2 while that of the copolymer is nearly unchanged. At time t = 2 s, i.e. when the applied electric field is at zero, the simulated electric field acting on the TGS crystals undershoots to below zero, i.e. –0.1 MV/m, while the electric field acting on the copolymer lags behind the applied electric field and retains a high value of 45 MV/m. Our calculations are extended to t = 1000 s with the applied field kept at zero. The simulated electric fields acting on both phases are found to approach zero quite gradually. During the time between 2 s and 1000 s, the polarization of the copolymer drops slowly with the diminishing electric field acting on it, while the polarization of the TGS crystals is nearly unchanged at all due to the fact that the field acting on the TGS crystals is now well below the coercive field. The change of the electric displacements of the TGS crystals and the copolymer roughly follow the polarization development of the constituents, and are almost identical at the first 2 s. The simulated result for the change of electric displacement of the TGS/P(VDF-TrFE)/TGS composite is shown in Figure 4.10(d), which roughly follows that of the TGS crystals, providing evidence that the electric displacement of the TGS/P(VDF-TrFE)/TGS composite is somewhat limited by the TGS crystals, as noted by Ploss *et al.* [Ploss, 1996]

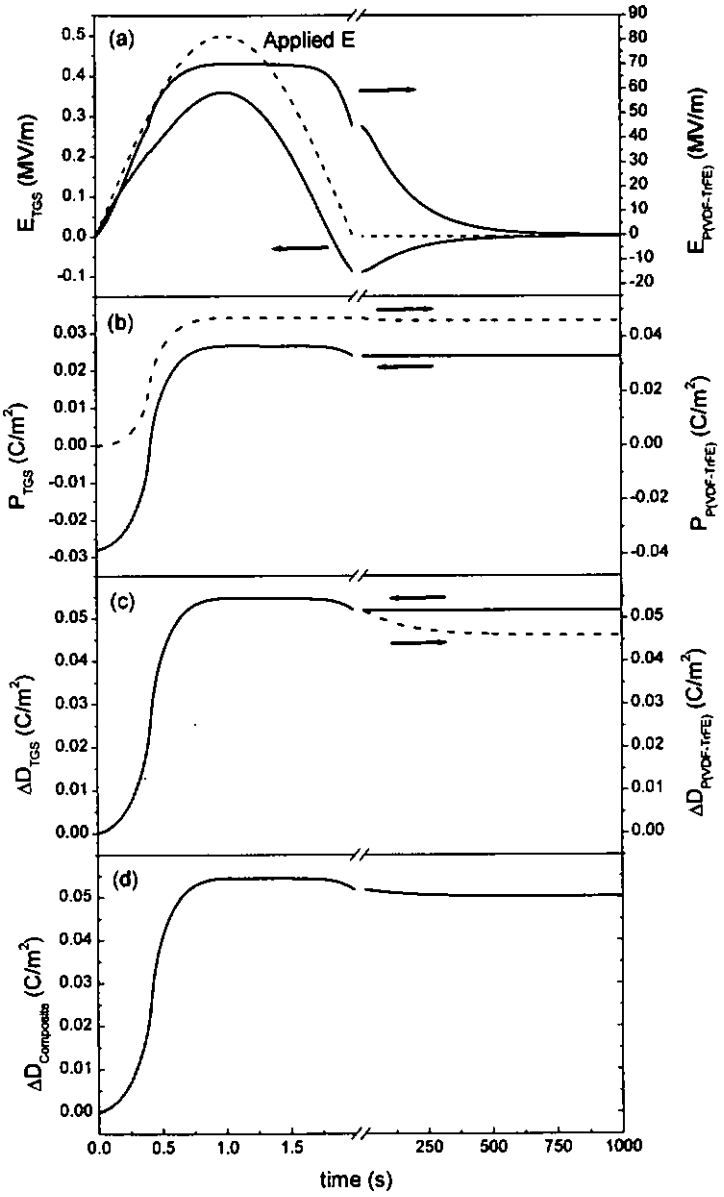

Figure 4.10 The simulated results for the (a) electric field (b) polarization (c) change of electric displacement of the TGS crystals and P(VDF-TrFE) copolymer and (d) the change of electric displacement of the composite as a function of time under the poling procedure shown in Figure 4.8.

The simulated *D-E* curve for the poling of P(VDF-TrFE) with TGS electrodes is compared with the experimental results [Ploss, 1996], shown in Figure 4.11(a). The *D-E* curve of the TGS electrode stack, i.e. TGS/TGS, after removing the copolymer film, is also simulated and compared with the experimental result in Figure 4.11(b).

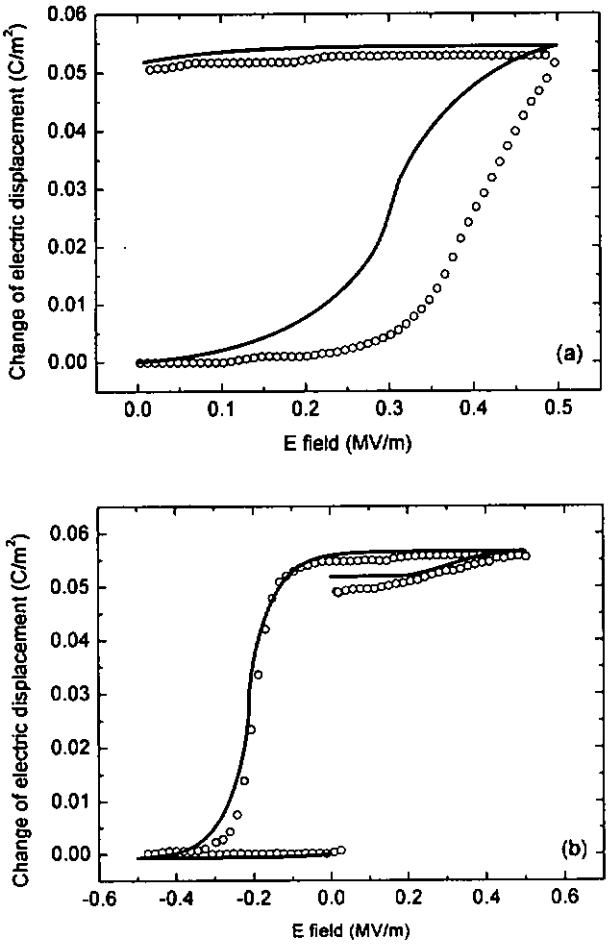

Figure 4.11 The simulated results (solid line) are compared with experimental results (circles). (a) Change of *D* in the TGS/P(VDF-TrFE)/TGS composite during poling under condition shown in Figure 4.8. (b) Change of *D* in the TGS-TGS stack after removing the copolymer, i.e. under condition shown in Figure 4.9.

In Figure 4.11(a), we find that the change of electric displacement of the TGS/P(VDF-TrFE)/TGS composite is slightly narrower than the experimental curve, possibly due to some inadequacies in the prediction of the polarization response of the constituent materials by Miller *et al.*'s model. Moreover, Furukawa *et al.* has noted that a virgin copolymer sample when first ramped by an electric field can support a slightly higher field before noticeable switching is observed [Furukawa, 1983]. After the removable of the film, a full sinusoidal voltage is applied on the electrode stack. Only a small increase of electric displacement occurs during the positive half cycle (see Figure 4.11(b)). This shows that the polarization of the TGS crystals has been nearly completely switched to P_r which confirms that the change of the electric displacement of the TGS/P(VDF-TrFE)/TGS sandwich has been somewhat limited by the TGS crystals. After the negative half cycle the TGS crystals are switched to the initial state, i.e. $-P_r$, therefore the change of electric displacement of the TGS crystal returns to zero. We see that all the general features of the experimental results are reproduced in our calculations. It seems to confirm the validity of our model for studying the poling of multi-layered composite structures.

The *D-E* behavior calculated for each constituent material in the poling process with the experimental *D-E* loop and the simulated *D-E* loop by Miller *et al.*'s model is shown in Figures 4.12.

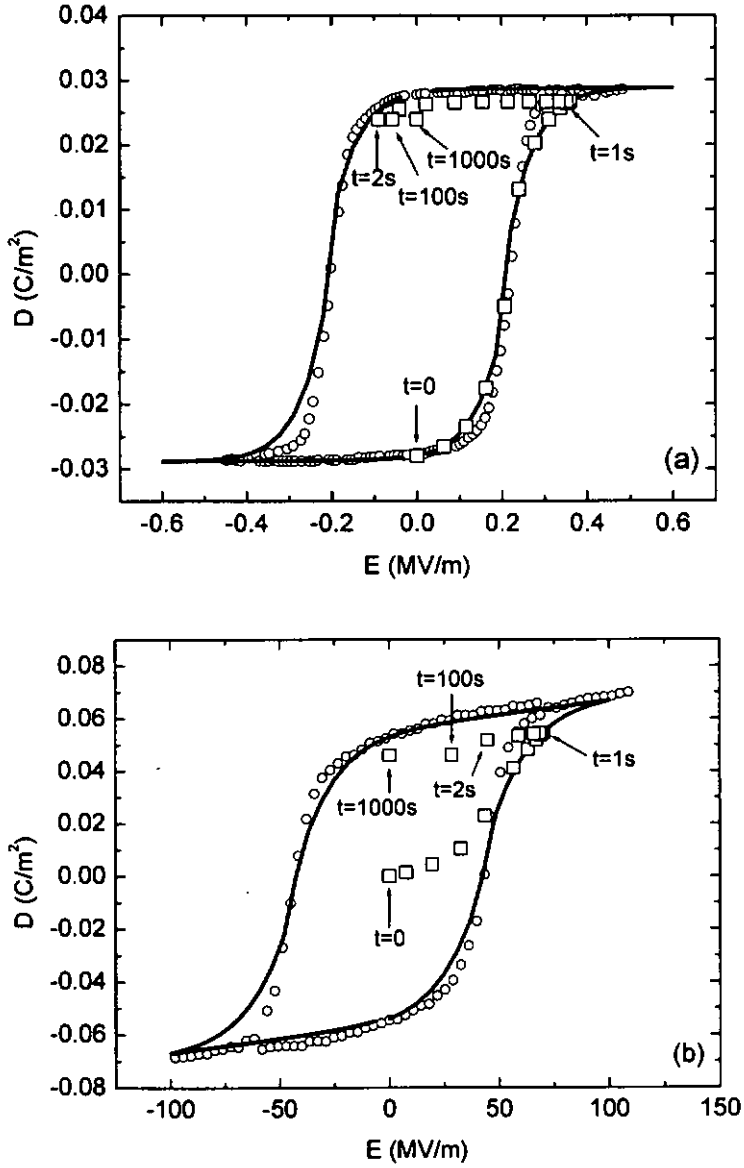

Figure 4.12 The squares denote the simulated *D-E* history in a constituent material during poling of TGS/P(VDF-TrFE)/TGS composite. Corresponding time is labeled in the diagram. The circle and the solid line denote the experimental *D-E* loop and the loop fitted by Miller *et al.*'s model respectively of the constituent materials. (a) TGS and (b) P(VDF-TrFE).

In addition, it is found that the remanent polarization of the copolymer is about 0.046 C/m^2, which is only 83 % of the maximum remanent polarization of the copolymer. It is calculated that the remanent polarization of the copolymer will increase to about 88.8 % and 89.7 % of the maximum if the applied voltage of 1200 V and 1500 V instead of 1000 V is applied on the composite sample. In contrast, the remanent polarization of the copolymer will decrease to about 70 % of the maximum if only 800 V is adopted. Suppose the composite sample can withstand twice the electric field that we used in the present study without dielectric breakdown, i.e. 1 MV/m, the remanent polarization of the copolymer will become 90 % of the maximum. Therefore, we expect that P(VDF-TrFE) copolymer can be polarized to not more than 90 % of its maximum remanent polarization in a stack with TGS crystals, even when the electric field applied to the stack would be doubled.

4.5 Theory for 0-3 Composite

Consider a ferroelectric ceramic/polymer composite with 0-3 connectivity, i.e. the ferroelectric ceramic particles are not in contact with each other while the polymer phase is self-connected in three dimensions. Figure 4.13 shows a schematic diagram of the ceramic/polymer 0-3 composite. The particles are assumed to have a spherical shape.

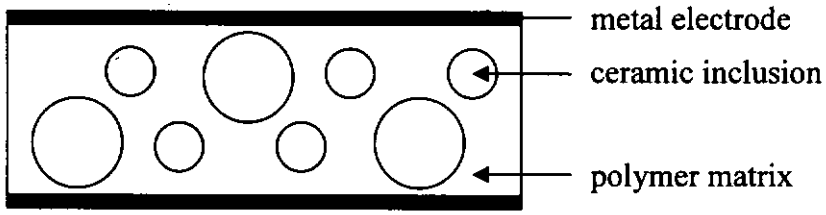

Figure 4.13 Schematic diagram of ceramic/polymer 0-3 composite

The constitutive equations for the ceramic phase and polymer phase are given by [Furukawa, 1986],

$$D_i = \varepsilon_i E_i + P_i \tag{4.10}$$

$$D_m = \varepsilon_m E_m + P_m \tag{4.11}$$

where D, ε, E and P represent the electric displacement, permittivity, electric field and ferroelectric polarization respectively. We generally use subscripts i and m to denote the ceramic inclusion and polymer matrix; for the composite, normally no

subscripts are used. The electric field acting on the respective phases satisfies the following relation for a composite with a small ceramic volume fraction:

$$E = \phi E_i + (1-\phi)E_m \tag{4.12}$$

where ϕ is the ceramic volume fraction. We assume both constituent materials are uniformly polarized and the homogenously polarized sphere is covered with surface charge density q_o at the pole along the polarizing direction (θ=0) with a distribution given by [Ploss, 2001] (see Figure 4.14),

$$q = q_o \cos\theta \tag{4.13}$$

where q represents the surface charge density at an angle θ.

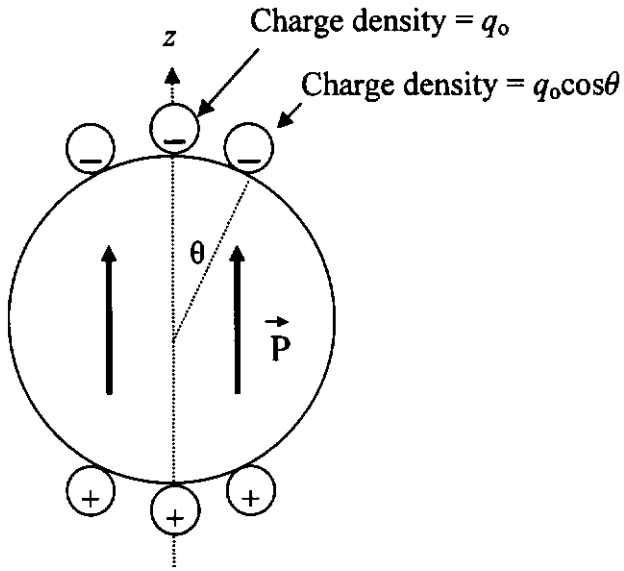

Figure 4.14 Homogeneously polarized sphere covered with "compensating" charge.

For a dilute dispersion of spherical inclusions in a matrix medium of permittivity ε_m and electric conductivity σ_m with a uniform electric field applied along (say) the *Z*-direction, the following equations may be obtained from consideration of the boundary value problem of a single inclusion in an infinite matrix [Wong, 2001]:

$$D_i + 2\varepsilon_m(E_i - E_m) = D_m + q_o \tag{4.14}$$

$$j_i + 2\sigma_m(E_i - E_m) = j_m - \frac{\partial q_o}{\partial t} \tag{4.15}$$

where j is the conduction current density, which is related to electric field by $j = \sigma E$. Differentiating (4.14) w.r.t. time and adding to (4.15) to eliminate q_o, we have

$$\frac{3(\sigma_m E + \varepsilon_m \frac{\partial E}{\partial t})}{(1-\phi)(\varepsilon_i + 2\varepsilon_m) + 3\phi\varepsilon_m} = \frac{E_i}{\tau} + \frac{\partial E_i}{\partial t} + \frac{(1-\phi)(\frac{\partial P_i}{\partial t} - \frac{\partial P_m}{\partial t})}{(1-\phi)(\varepsilon_i + 2\varepsilon_m) + 3\phi\varepsilon_m} \tag{4.16}$$

where $\tau = \dfrac{3\phi\varepsilon_m + (1-\phi)(\varepsilon_i + 2\varepsilon_m)}{3\phi\sigma_m + (1-\phi)(\sigma_i + 2\sigma_m)}$. When E changes with time, the relation $\partial P/\partial t = [\partial P/\partial E]\,[\partial E/\partial t]$ may be employed for subsequent calculations.

Solving equations (4.7) and (4.16) for a given poling E(t), the time development of the electric fields and the polarization in the ceramic inclusions and in the matrix can be evaluated.

4.6 Application to Study the Piezoelectric Properties of PZT/Epoxy 0-3 Composites

Furukawa *et al.* [Furukawa, 1976] prepared PZT / epoxy 0-3 composites with ceramic volume fraction ϕ = 0.048, 0.131 and 0.232. The composites were polarized under different d.c. poling fields at 120 °C for 30 minutes, then kept at the same temperature for 10 minutes under the short circuit condition, and the piezoelectric coefficients d_{31} were measured at 50 °C. The material parameters of PZT and epoxy used in this computation are listed in Table 4.3 and Table 4.4.

Table 4.3 Material parameters of PZT and epoxy at 120 °C.

	P_s (C/m^2)	P_r (C/m^2)	E_c (MV/m)	$\varepsilon/\varepsilon_o$ [a] (unpoled)	σ (Ω^{-1}m^{-1})
PZT	0.35	0.33	0.233	1750	1.5×10^{-10} [b]
Epoxy	...	...	...	4.6	0.65×10^{-11} [c]

[a] Furukawa, 1976

[b] L. Wu, T.S. Wu, C.C. Wei and H.C. Liu, J. Phys. C: Solid State Phys. **16**, 2823 (1983)

[c] C. A. May, *Epoxy resins: chemistry and technology*, (M. Dekker, New York, 1988).

Table 4.4 Dielectric, elastic and piezoelectric constants of PZT and epoxy at 50 °C.

	$\varepsilon/\varepsilon_o$ [a] (poled)	Y (GPa)[a]	ν [b]	$-d_{31}$ [a] (pC/N)	d_{33} [b] (pC/N)
PZT	1700	36	0.3	177	400
Epoxy	4.2	1.8	0.35	...	...

[a] Furukawa, 1976

[b] Wong, 2001

The "remanent" polarization in the ceramic inclusion as a function of applied electric field can be calculated by solving equation (4.16) with appropriate *P-E* hysteresis behaviour for the PZT ceramic involved. Here the *P-E* hysteresis loop of PZT ceramic can be simulated by Miller *et al.*'s model with the materials parameters shown in Table 4.3. It is noted that $P_m = 0$ because epoxy is not ferroelectric.

Figure 4.15 shows the simulated *P-E* hysteresis loop for PZT ceramic by the modified Miller *et al.*'s model (equations (4.7) and (4.9)) with $n = 5 / 11$. It is noted that the PZT ceramic is reported to have been fully polarized under a field of 0.7 MV/m, by Furukawa *et al.* [Furukawa, 1976]. Therefore, we assume its E_c is one-third of this value, i.e. 0.233 MV/m, in the following computation.

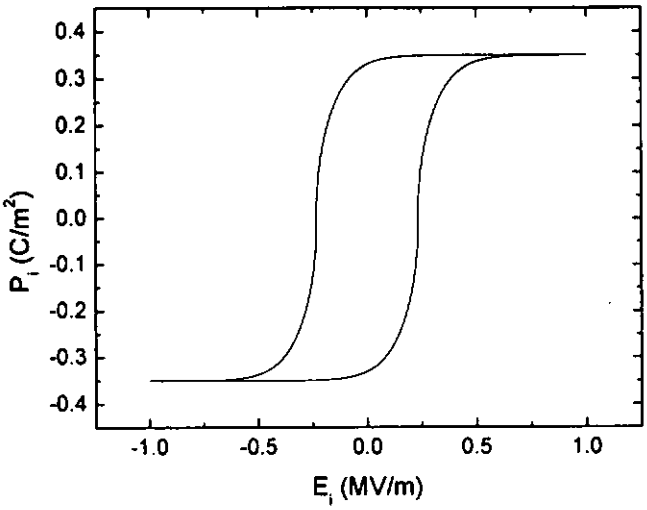

Figure 4.15 Adopted *P-E* hysteresis loop of PZT ceramic [Eq. (4.7) and (4.9) with $n_1/n_2 = 5/11$] for model calculation.

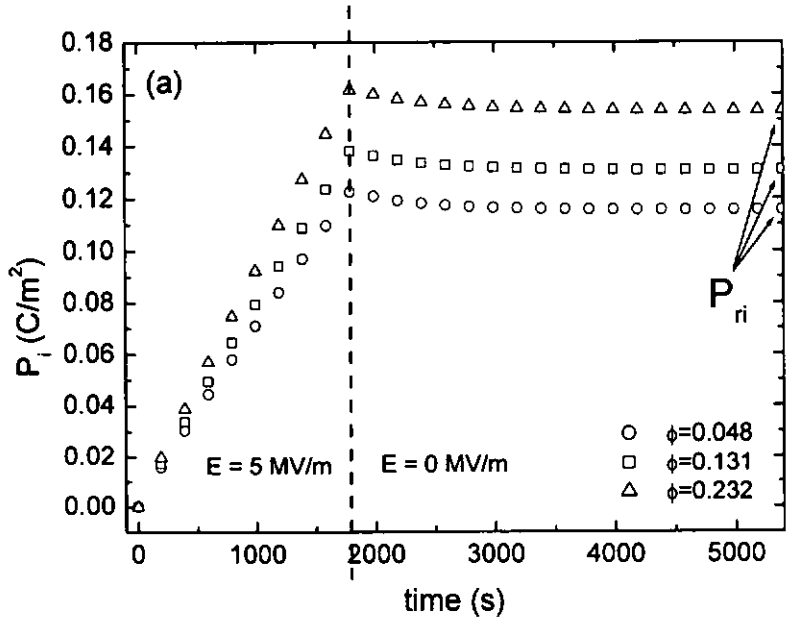

Figure 4.16(a) The polarization in PZT inclusions of PZT/epoxy 0-3 composites with $\phi = 0.048$ (circle), 0.131 (square) and 0.232 (triangle) as a function of time. The final "remanent" polarization attained in the total process is denoted by P_{ri}.

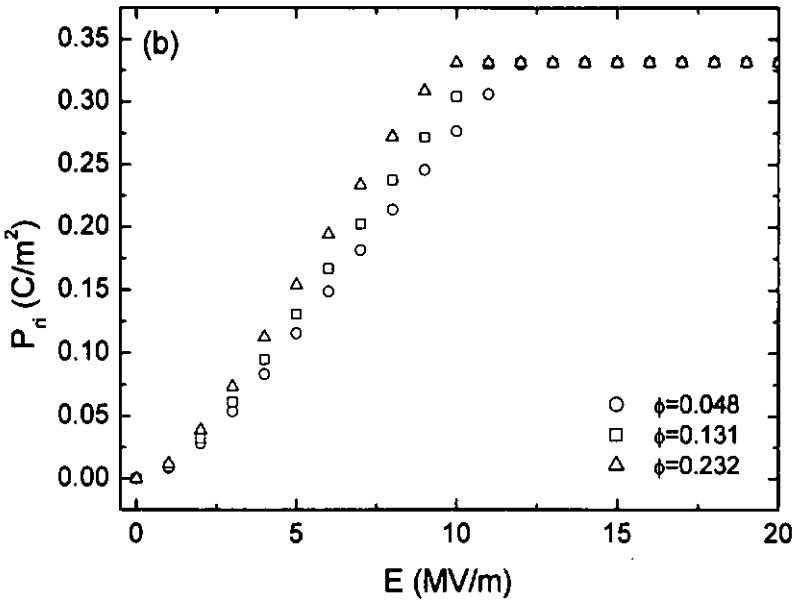

Figure 4.16(b) The simulated results for the "remanent" polarization in PZT inclusions of PZT/epoxy 0-3 composites with ϕ = 0.048 (circle), 0.131 (square) and 0.232 (triangle) as a function of poling field.

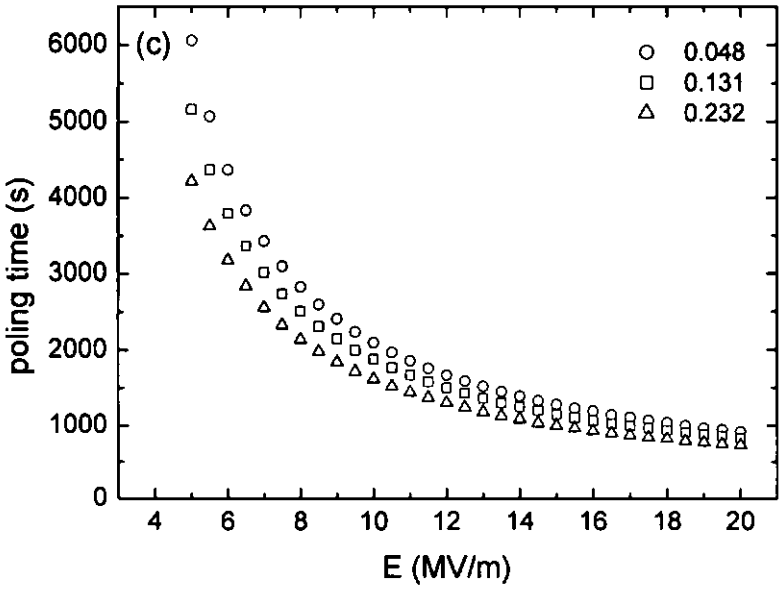

Figure 4.16(c) The simulated results for the poling time for achieving of 95 % of the maximum achievable remanent polarization in PZT inclusions of PZT/epoxy 0-3 composites with ϕ = 0.048 (circle), 0.131 (square) and 0.232 (triangle) as a function of poling field.

Here it is seen (Figure 4.16(a)) that the ceramic polarization basically increases with the poling time after the application of the poling field of 5 MV/m and relaxes slightly after the release of the field. The final "remanent" polarization attained in the total process is denoted by P_{ri} in the following discussion. Figure 4.16(b) shows the simulated results for the "remanent" polarization in the ceramic inclusion P_{ri} as a function of poling field. Generally speaking, a higher poling field results in a higher P_{ri}, particularly in the composites with higher ϕ. It is seen that P_{ri} increases quite linearly with the increase in poling field. Saturation in P_{ri} can be obtained when poling fields of about 10 MV/m and 12 MV/m are applied for 1800 s on the composites with ϕ = 0.232 and 0.048, respectively, reflecting a 20 % difference between the two. In addition, the relationship between the poling field and poling time for the achievement of 95 % of maximum achievable P_{ri} and is calculated and shown in Figure 4.16(c). It is evident that the higher the poling field, the shorter the poling time to attain the high P_{ri}. Moreover, the composites with higher ϕ require a shorter time to attain a high P_{ri} for the same poling field.

To further discuss the gross piezoelectric properties of the poled composites based on our simulated polarization behaviour of the ceramic inclusion, a main problem is the unknown relationship between P_{ri} and the piezo- and pyroelectric properties of the ceramic material. Therefore, in the following, we make the simple

assumption that the piezoelectric coefficient of the inclusion is directly proportional to its P_{ri}. The expression for the piezoelectric coefficient of the inclusion can therefore be written as

$$d_{3ki} = \frac{P_{ri}}{P_{ri}^{f}} d_{3k}^{f} \qquad \text{k=1,2,3} \tag{4.17}$$

where P_{ri}^{f} and d_{3k}^{f} denote the remanent polarization and the piezoelectric coefficient of a fully polarized ceramic at the measuring temperature.

Many theoretical works have been carried out to express the gross piezoelectric properties of the 0-3 composite system in terms of the piezoelectric properties of the constituents. The expressions we adopt in the present work for the piezoelectric constant is developed by Wong *et al.* [Wong, 2001] and given as

$$d_{31} = \phi\ L_E \left\{ \left(L_T^{\perp} + L_T^{//} \right) d_{31i} + L_T^{\perp} d_{33i} \right\} \tag{4.18}$$

$$d_{33} = \phi L_E \left\{ 2 L_T^{\perp} d_{31i} + L_T^{//} d_{33i} \right\} \tag{4.19}$$

where

$$\begin{cases} L_E = \dfrac{1}{\phi}\ \dfrac{\varepsilon - \varepsilon_m}{\varepsilon_i - \varepsilon_m} \\ L_T^{\perp} = \dfrac{1}{\phi}\left\{ \dfrac{1}{3}\ \dfrac{k^{-1} - k_m^{-1}}{k_i^{-1} - k_m^{-1}} - \dfrac{1}{3}\ \dfrac{\mu^{-1} - \mu_m^{-1}}{\mu_i^{-1} - \mu_m^{-1}} \right\} \\ L_T^{//} = \dfrac{1}{\phi}\left\{ \dfrac{1}{3}\ \dfrac{k^{-1} - k_m^{-1}}{k_i^{-1} - k_m^{-1}} + \dfrac{2}{3}\ \dfrac{\mu^{-1} - \mu_m^{-1}}{\mu_i^{-1} - \mu_m^{-1}} \right\} \end{cases} \tag{4.20}$$

For 0-3 composites with spherical inclusion, ε may be calculated from the Bruggeman formula [Bruggeman, 1935]

$$\frac{\varepsilon_i - \varepsilon}{\varepsilon^{1/3}} = (1-\phi)\frac{\varepsilon_i - \varepsilon_m}{\varepsilon_m^{1/3}} \tag{4.21}$$

The bulk modulus k and the shear modulus μ of the composite are calculated by

$$k = k_m + \frac{\phi\ (k_i - k_m)}{1 + (1-\phi)(k_i - k_m)/(k_m + 4\mu_m/3)} \tag{4.22}$$

$$\mu_l = \mu_m \left\{ 1 + \frac{15(1-\nu_m)(\mu_i/\mu_m - 1)\phi}{7 - 5\nu_m + 2(4-5\nu_m)\left[\mu_i/\mu_m - (\mu_i/\mu_m - 1)\ \phi\right]} \right\} \tag{4.23}$$

$$\mu_u = \mu_m \left[1 + \left(\frac{\mu_i}{\mu_m} - 1 \right) \frac{\beta}{\alpha + \beta\ \gamma} \phi \right] \tag{4.24}$$

where

$$\begin{cases} \alpha = \dfrac{42}{5\mu_m}\ \dfrac{\mu_m - \mu_i}{1-\nu_m}\ \phi\ \left(\phi^{2/3} - 1\right)^2 \\ \beta = \left[(7-10\nu_i) - (7-10\nu_m)\ \vartheta\right] 4\phi^{7/3} + 4\ (7-10\nu_m)\ \vartheta \\ \gamma = \dfrac{\mu_i}{\mu_m} + \dfrac{7-5\nu_m}{15(1-\nu_m)}\left(1 - \dfrac{\mu_i}{\mu_m}\right) + \dfrac{2(4-5\nu_m)}{15(1-\nu_m)}\left(1 - \dfrac{\mu_i}{\mu_m}\right)\phi \\ \vartheta = \dfrac{(7+5\nu_i)\mu_i + 4(7-10\nu_i)\mu_m}{35(1-\nu_m)\mu_m} \end{cases} \tag{4.25}$$

Subscripts u and l for the effective shear modulus denote upper bound and lower bound respectively. ν represents Poisson's ratio.

By using equations (4.17) and (4.18) with our simulated P_{ri} results shown in Figure 4.16, the d_{31} coefficients of the PZT/epoxy composites as a function of poling field can be evaluated. Figure 4.17 shows our predictions together with the experimental results investigated by Furukawa *et al.* [Furukawa, 1976]. Apart from the sample with $\phi = 0.232$, it is seen that fairly good agreement is achieved with most

of the data points falling within our predicted bounds. For the sample with $\phi = 0.232$, fairly good agreement is obtained at poling fields smaller than 4 MV/m, but not for larger fields. The discrepancy may come from the assumption of simple proportionality of the d_{31} coefficient of the inclusion with P_{ri}, which becomes inadequate at high poling field.

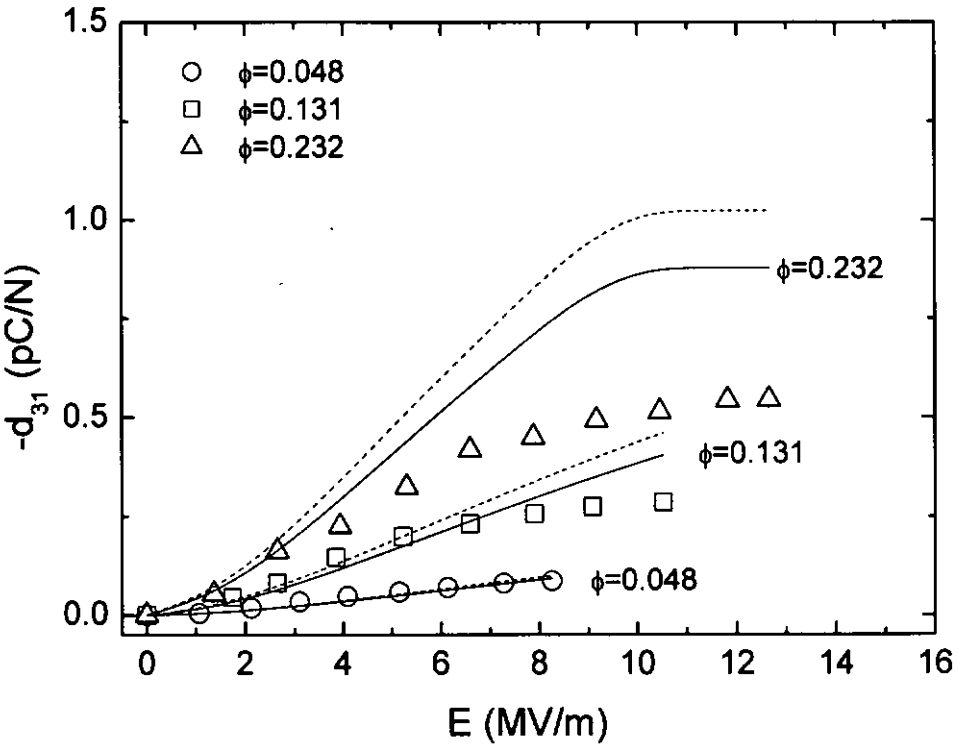

Figure 4.17 Experimental results for the piezoelectric coefficients of the PZT/epoxy composites with $\phi = 0.048$ (circle), 0.131 (square) and 0.232 (triangle) as a function of poling field are shown together with the simulated curves. The solid lines and the dash lines denote the calculated lower bound and upper bound, respectively.

4.7 Application to Study the Piezoelectric and Pyroelectric Properties of PT/P(VDF-TrFE) 0-3 Composites

The experimental results of the piezoelectric and the pyroelectric coefficients of the PT/P(VDF-TrFE) 0-3 composites as a function of poling time have been reported in the previous chapter. In this section, we are going to simulate the gross piezo- and pyroelectric properties of these composites based on the calculated polarization behaviour of the ceramic inclusion, in a manner similar to Section 4.6.

Tables 4.5 and 4.6 show the materials parameters for the constituents used for modeling the piezoelectric and pyroelectric coefficients of the above composites.

Table 4.5 Material parameters of PT and P(VDF-TrFE) at 120 °C.

	P_s (C/m^2)[a]	P_r (C/m^2)[b]	E_c (MV/m)[c]	$\varepsilon/\varepsilon_o$	σ (Ω^{-1}m^{-1})
PT	0.57	0.50	5	200	10^{-10}
P(VDF-TrFE)	...	...	...	50[#]	2.5×10^{-9} [d]

[a] M. E. Lines and A. M. Glass, *Principles and Applications of Ferroelectrics and Related Materials* (Oxford, New York, 1977), p.249.

[b] B. Ploss, B. Ploss, F.G. Shin, H.L.W. Chan and C.L. Choy, Proceedings of the 2000 12th IEEE International Symposium on Applications of Ferroelectrics, 2000, (ISAF 2000), Vol.1, p. 301.

[c] H.L.W. Chan, W.K. Chan, Y. Chen and C.L. Choy, Ferroelectrics **196**, 141 (1997).

[d] H.L.W. Chan, Y. Chen and C.L. Choy, Integrated Ferroelectrics **9**, 207 (1995)

[#] Measured data in the present study.

Table 4.6 Dielectric, elastic, piezoelectric and pyroelectric constants of PZT and P(VDF-TrFE) at room temperature.

	$\varepsilon/\varepsilon_o$	Y (GPa) [b]	ν [b]	$-d_{31}^f$ (pC/N)	d_{33}^f (pC/N)	$p^{f\,a}$ (μC/cm^{2}K)
PT	200[a]	126.7	0.22	12.5	100	300
P(VDF-TrFE)	11.6[#]	2.32	0.39	...	...	...

[a] M. E. Lines and A. M. Glass, *Principles and Applications of Ferroelectrics and Related Materials* (Oxford, New York, 1977), p.250.

[b] Furukawa, 1976

[#] Data measured in the present study.

The simulated *P-E* hysteresis loop for PT ceramic (obtained by the modified Miller *et al.*'s model) with equations (4.7) and (4.9)) is shown in Figure 4.18.

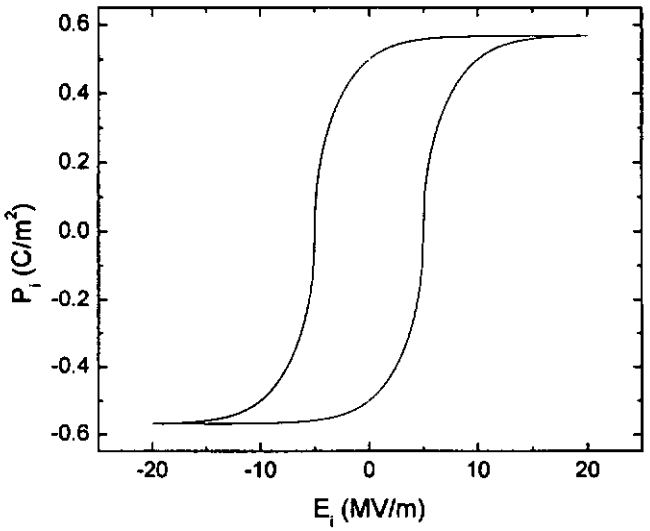

Figure 4.18 Adopted *P-E* hysteresis loop of PT ceramic [Eq. (4.7) and (4.9) with $n_1/n_2 = 5/11$] for model calculation.

The calculated P_{ri} with different poling times (equations (4.7) and (4.16)) under the poling procedure described in Chapter 3 is shown in Figure 4.19.

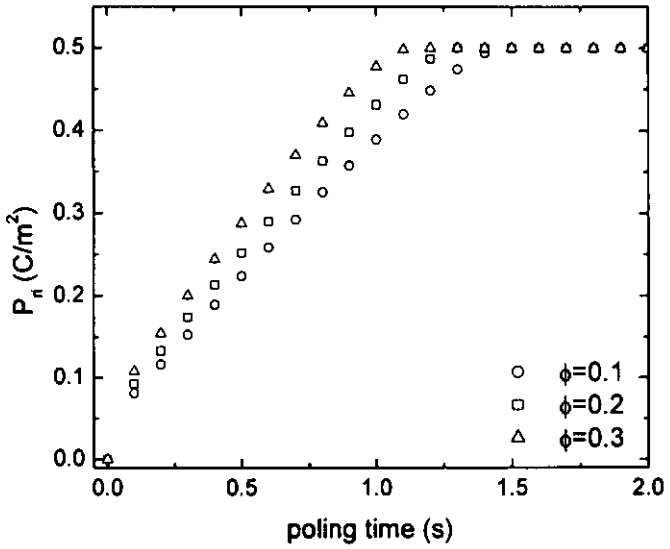

Figure 4.19 The simulated results for the "remanent" polarization in PT inclusions of PT/P(VDF-TrFE) 0-3 composites with ϕ = 0.1 (circle), 0.2 (square) and 0.3 (triangle) as a function of poling time.

It is found that the "remanent" polarization of the inclusions in the composites increase quite linearly with the poling time between 0 and 1.5 s. Moreover, ceramic inclusions in the composites with higher ϕ can be polarized more rapidly than in composites with lower ϕ, because of a shorter τ of the former. The P_{ri} in the composites with ϕ = 0.3 and 0.1 attain maximum after the poling time of 1.1 s and 1.5 s respectively. These simulated results revealed the time scale for fully

polarizing a 0-3 composite is at least 3 orders of magnitude shorter than the poling times adopted by many investigations.

By using equations (4.17) and (4.19) with our simulated P_{ri} results shown in Figure 4.19, the piezoelectric coefficients d_{33} of the composites as a function of poling time are evaluated and shown in Figure 4.20. Good agreement with the experimental results at poling time of 1 s is achieved in all our predicted d_{33} coefficients. Composites with higher ϕ attain a higher d_{33} value under the same poling condition. Apart from the samples with ϕ = 0.1, our predictions show good agreement with the experimental data in the sense that all these data points fall within our predicted bounds. As for the experimental and predicted d_{33} values for ϕ = 0.1, we note that there could be larger measurement errors due to the relatively smaller electrical signal in the measurement. Both experimental results and our predicted d_{33} values of the composites as a function of poling time reveal that these composites can be fully polarized quite rapidly under the poling conditions mentioned above, i.e. less than 10 s, consistent with our simulated time development of P_{ri}. The present work seems to affirm that a prolonged poling time is not necessary for the development of high P_{ri}.

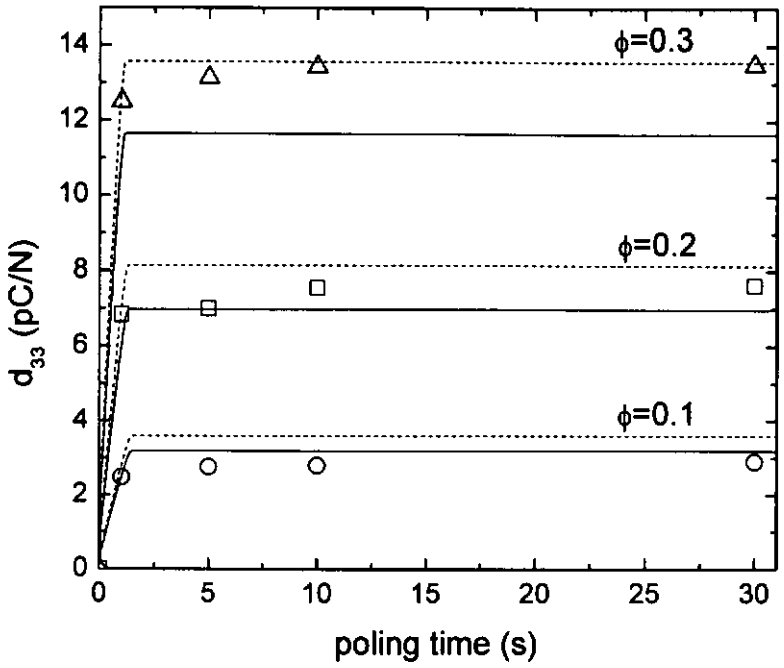

Figure 4.20 The experimental results of piezoelectric coefficients d_{33} of the PT/P(VDF-TrFE) 0-3 composites with ϕ = 0.1 (circle), 0.2 (square) and 0.3 (triangle) as a function of poling time are shown together with the simulated curves. The solid lines and the dash lines denote the calculated lower bound and the upper bound, respectively.

In the polarized samples presently investigated, we assume the electric fields in the matrix and inclusions attain zero values (lowest field energy state) so that the difference in the polarizations of the two phases is completely compensated by charge at the inclusion-matrix interfaces, i.e. $P_{ri} = q_o$ (refer to Fig. 4.14). The pyroelectric coefficient p of the composite is given by [Ploss, 2001]

$$p = \phi L_E p_i \tag{4.26}$$

It is noted that $p_m = 0$ as the P(VDF-TrFE) 70/30 mol-% copolymer cannot be polarized at a temperature above the Curie transition temperature (106 °C). Following the idea of the previous section, we take

$$p_i = \frac{P_{ri}}{P_{ri}^{\ f}} p^f \tag{4.27}$$

where p^f refers to the pyroelectric coefficient of a fully polarized ceramic at the measuring temperature. L_E has been defined in equation (4.20).

The pyroelectric coefficients p of the PT/P(VDF-TrFE) 0-3 composites as a function of poling time can therefore be evaluated by using equations (4.26) and (4.27) with our simulated P_{ri} results shown in Figure 4.19. Similar to our predictions on d_{33} coefficients of the composites versus poling time, it is seen (Figure 4.21) that both our predicted p and the experimental p increase quite rapidly within the first second of poling. Composites with higher ϕ attain a higher p under the same poling condition. Our predictions show reasonably good agreement with the experimental data in that all data points follow roughly the predicted trends. Both experimental results and our predictions reveal the composites in the present work attain maximum pyroelectric coefficient at poling times of less than 10 s, consistent with the time scale of development of our simulated P_{ri} and the d_{33} coefficients results.

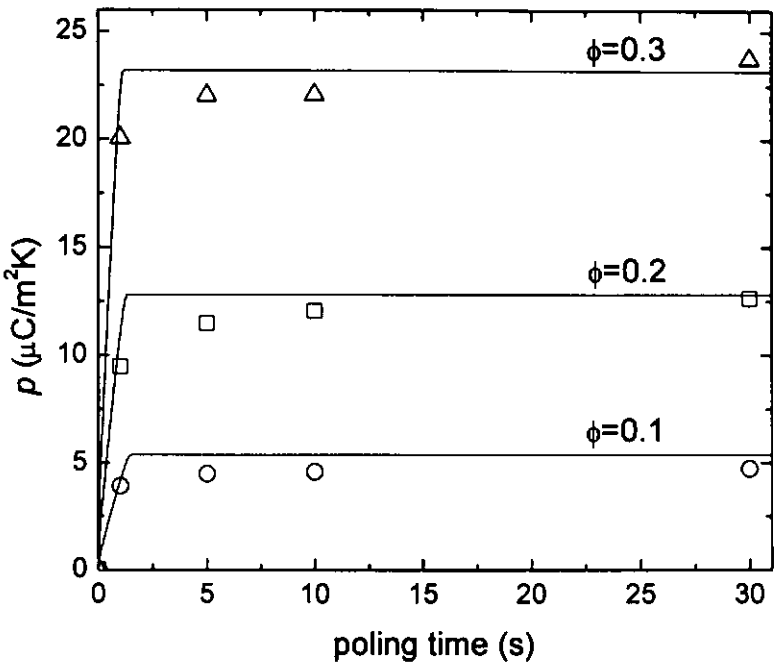

Figure 4.21 The experimental results of pyroelectric coefficients p of the PT/P(VDF-TrFE) 0-3 composites with ϕ = 0.1 (circle), 0.2 (square) and 0.3 (triangle) as a function of poling time are shown together with the simulated curve (solid line).

Quite aside from the above understanding of the poling results, we find that the time of development of the piezo- and pyroelectric activities of the composites is faster than that of the "poling ratio" of the inclusions observed via XRD (refer to Section 3.3.3). We therefore expect that the rapid development of the remanent polarization in the inclusions is mainly due to the 180° domain switching, which would show no obvious effect under the XRD investigations. For the composites polarized for long poling time, say 1 hour, 90° domain switching was identified under XRD. However, their piezoelectric and pyroelectric coefficients show only

comparable values to those composites poled for a short time. Therefore we conclude the piezoelectric and pyroelectric properties of the composites are mainly contributed by the 180° domain switching in the ceramic inclusions in the poling process.

4.8 Conclusion

A model for studying the poling of ferroelectric multi-layered composite systems is discussed by considering the continuity of the total current density going through the layers along the poling direction. The *P-E* relation of each ferroelectric layer is described by using a modified Miller *et al.*'s model. The model is applied to study the switching of the bilayer PZT/polyvinylidene fluoride-trifluoroethylene P(VDF-TrFE) composite and the poling of the triple-layered TGS/P(VDF-TrFE)/TGS composite system reported in literature. All the broad experimental features are reproduced by the simulations and fairly good qualitative agreement is observed. The bilayer PZT/P(VDF-TrFE) study reveals the finite conductivity in the polymer phase is playing an important role in the poling of such composites. A higher conductivity of the polymer phase and higher applied electric field facilitate the development of a high electric field at the ceramic phase, therefore poling of the ceramic phase in such composite systems can be more efficient. The polarization behavior of the triple-layered TGS/P(VDF-TrFE)/TGS composite is also discussed. It is seen that the change of electric displacement in TGS is somewhat limiting the change of the displacement of the TGS/P(VDF-TrFE)/TGS composite. Our calculation reveals the P(VDF-TrFE) copolymer can be polarized to not more

than 90 % of its maximum remanent polarization in a stack with TGS crystals, even when the electric field applied to the stack would be doubled. Comparison is made between the experimental results and the predictions, fairly good agreement is also achieved.

The effective d_{31}, d_{33} and p for 0-3 composites of ferroelectric particles in a linear matrix have been studied in terms of the dielectric, elastic, piezoelectric and pyroelectric properties of the constituents as well as the state of polarization of the dispersed particles. The composites are subjected to a variety of poling schedules and the time development and final values of the ceramic polarization are calculated by use of a similar model but for 0-3 geometry. Comparison with the experimental data indicates that fairly good agreement is achieved. This work shows fairly realistic predictions for the piezoelectric coefficients d_{31} of the PZT/epoxy 0-3 composites at low poling electric field. In the study of the piezoelectric and pyroelectric properties of PT/P(VDF-TrFE) 0-3 composites, the overall simulated results can account quite well the experimental results. The time scale for fully polarizing the PT composites is found to be in the order of 10 s, which is much shorter than that reported in the literature. Qualitative agreement seems to affirm our modeling technique can be used for predicting the piezoelectric and pyroelectric properties of 0-3 composites, which

would be a significant help in materials selection and designing poling parameters for ceramic/polymer composites.

CHAPTER 5
CONCLUSIONS AND SUGGESTIONS FOR FUTURE WORK

5.1 Conclusions

300 nm diameter lead titanate (PT) powder was derived from the metal alkoxide sol-gel route and sintered at 600 °C for one hour. The microstructure and the crystal structure were characterized by SEM and XRD respectively. Roughly spherical shape and good tetragonal crystallite structure of the ceramic inclusion were observed. The PT ceramic powder was incorporated into the P(VDF-TrFE) copolymer, followed by solution casting and compression molding into 30 μm thick PT/P(VDF-TrFE) 0-3 composite films of ceramic volume fraction from 0.05 to 0.3. Gold electrodes of 5 mm diameter were deposited on both sample surfaces. Ceramic dispersion in the copolymer matrix was investigated by SEM and the dielectric properties of the composite samples were studied in the temperature range of -20 °C to 120 °C. The measurement results were compared with predictions based on the Bruggeman formula, and a good agreement between the two was found.

Thermal poling was employed in the present study to polarize the ceramic

inclusions only for different poling times. Characterization of the poling state of the composites was carried out in different ways. The piezo- and pyroelectric measurements reveal the composites can be polarized almost fully within 10 s. The XRD measurement was employed to investigate the domain switching before and after poling. It is found that for those composites polarized for a short time (say less than 30 s), 90° domain switching was identified to take place only sparingly as compared to composites polarized for a long time (say 1 hour). Also, the piezo- and pyroelectric coefficients of the composites polarized for long poling time was comparable to those polarized for short poling time. Therefore the rapid polarization development, the piezoelectric and the pyroelectric properties of the composites were expected to originate from 180° domain switching. On the other hand, the pyroelectric profiles along the thickness direction of the composites were studied by laser intensity modulation method. Composites with 30 % PT ceramic volume showed uniform profiles after poling for 15 minutes, which is longer than the time development of their piezo- and pyroelectric activities.

A physical model was developed based on quasi-electrostatic considerations to study the effective polarization response of the ferroelectric composite systems as a function of arbitrary applied electric field. Electrical conductivity of the constituent materials and charge accumulation at interfaces between constituent phases are taken

into account. Also nonlinear, hysteretic *P-E* relations are used for the ferroelectric constituent materials.

To verify our theoretical description on the poling process, the model was first applied as a test to ferroelectric composites with simple geometric structure, i.e. multi-layered composites. We modeled the polarization behavior of ferroelectric multi–layered composite structures including the bilayer PZT/P(VDF-TrFE) composite and the triple-layered TGS/P(VDF-TrFE)/TGS composite under the action of variable fields. The model takes into consideration the continuity of the total current density going through each ferroelectric layer along the poling direction, the ceramic/polymer interfacial charge and the nonlinear hysteresis nature (by use of the modified Miller model) of the ferroelectric constituent materials. The polarization response of the multi-layered composite systems was simulated and compared with published experimental results. Model predictions showed agreement in the electric displacement of the composites as a function of time and poling field considered by Furukawa and Ploss respectively. All the broad experimental features were reproduced by the simulations and fairly good qualitative agreement was observed. The good agreement is mainly due to the more realistic *P-E* hysteresis behaviour involved in this computation. The study of the poling of the multi-layered composite systems reveals the finite conductivity in the polymer phase is playing an important

role in the poling of such composite structures. A higher conductivity of the polymer phase and higher applied electric field are favorable for building up a high electric field at the ceramic phase, therefore poling of the ceramic phase in such a composite system can be more efficient. Overall speaking, qualitative agreement affirms the validity of the basic mechanism we presented for the poling process of the multi-layered composite structures.

The modeling was further extended to study the poling process of a ferroelectric composite system with more complicated geometric structure, i.e. 0-3 composite. Theoretical description was given to the poling process of dilute 0-3 composite systems, which has built up from considerations of a single inclusion problem in which a single ferroelectric sphere is surrounded by a linear matrix medium under the action of a uniform electric field. Similarly, a modified Miller model is used for the description of the *P-E* relation of the ferroelectric constituent. The "remanent" polarization of the 0-3 composites under the poling field was then simulated. A simple but quite realistic assumption was made: that the piezoelectric and pyroelectric properties of the poled dispersed ceramic particles are directly proportional to its "remanent" polarization. The gross piezoelectric and pyroelectric properties of the composites were estimated from the properties acquired by the constituent materials after the poling process. The modeling was first applied to the

published experimental work of Furukawa. Reasonably good prediction of the piezoelectric d_{31} coefficient of the PZT/epoxy 0-3 composite as a function of poling field was observed. Finally the modeling was applied to our own PT/P(VDF-TrFE) 0-3 composite system. The simulated piezoelectric and pyroelectric properties of the PT composites after the poling process were found to be in qualitative agreement with the experimental results. Similar to our finding in the poling of multi-layered composite systems, a high conductivity of the polymer matrix (at high temperature) would provide a desirable condition for developing a high electric field in the dispersed ceramic inclusion, therefore a large and fast polarization response of the 0-3 composite system. Both the simulation and our own experimental results show the time scale for fully polarizing the 0-3 composite is in the order of 10 s, which is 2 to 3 orders of magnitude shorter than what is commonly believed. The ability to predict the gross properties of 0-3 composites in terms of the poling field and poling time may be especially helpful in the making of practical composites with particular properties.

Our modeling contributes to an understanding of the time-dependent response of a ferroelectric composite system under a poling field. The importance of the electrical conductivity of the host matrix material and the role of interfacial charge was identified. Electrical conductivity serves to allow the accumulation of charge at

interfaces between constituent phases to stabilize the ferroelectric polarization achieved via poling. The rate with which polarization is developed is very much controlled by conductivity, i.e. charge transport, as shown in Chapter 4. Such an understanding of poling if already a significant help in materials selection and in designing poling parameters for ceramic/polymer composites.

5.2 Suggestions for Future Work

It is suggested that the present work can be extended as follows:

1. Investigate the pyroelectric profiles along the thickness direction of the composites after poling for short times.

2. Study the second order dielectric permittivity of the composites, which should provide a very sensitive method for the investigation of polarization.

3. Study theoretically the piezoelectric and pyroelectric properties in relation to the poling of composites where the ferroelectric ceramic inclusions and the ferroelectric polymer matrix are polarized in parallel or in anti-parallel directions.

REFERENCES

Abdullah, M.J., A study of electro-active properties of polymer/ceramic composites, PHD Thesis, University of Wales-SEECS, Bangor, 1989.

Amin, M., Balloomal, L.S., Darwish, K.A., Osman, H., Kamal, B., "Pyroelectricity in rubber composite films", Ferroelectrics, Vol. 81, pp.1345, 1988.

Amin, M., Osman, H., Baloomal, L., Darwish, K.A., Kamal, B., "Electrical properties of acrylonitrile-butadiene rubber-barium titanate composites", Ferroelectrics, Vol. 81, pp. 1351, 1988.

Bahalla, A. S., Newnham, R. E. and Cross, L. E., Schulze, W. A., "Pyroelectric PZT-polymer composites", Ferroelectrics, Vol. 33, pp. 139-146, 1981.

Banno, H. and Saito, S., "Piezoelectric Properties of composites of synthetic rubber and PbTiO3 or PZT", J. Appl. Phys., Vol. 22, pp. 67, 1983.

Berlincourt, D. and Kruger, H. H. A., "Domain process in lead titanate zirconate and barium titanate ceramics", J. Appl. Phys., Vol. 30, pp. 1804-1810, 1959.

Birks, L. S. and Friedman, H., "Particle size determination from X-ray line boardening". J. Appl. Phys., Vol. 17, pp. 687-692, 1946.

Bloomfield, P.E. and Preis, S., "Piezoelectric and dielectric properties of heat treated and polarized VF2/VF3 Copolymer", IEEE Trans. on Dielectrics and Electrical Insulation, Vol. EI-21, No.3, pp. 533-537, 1986.

Blum, J. B. and Gurkovich, S. R., "Sol-Gel Derived PbTiO3", J. Mater. Sci., Vol. 20, pp.4470, 1985.

Bruggeman, DAG, Berechnung verschoiedener Konstanten von heterogenen Substanzen: 1, 1935.

Budd, K. D., Dey, S. and Payne, D., "Sol-Gel Processing of PbTiO3, PbZrO3, PZT and PLZT Thin Films," Br. Ceram. Proc., Vol. 36, pp.107-121, 1985.

Callister, W. D., "Materials Science and Engineering An Introduction", Wiley, New York, 1996.

Chan, H. L. W., Chan, W. K., Zhang, Y. and Choy, C. L., "Pyroelectric and piezoelectric properties of lead titanate/polyvinylidene fluoride-trifluoroethylene 0-3 Composites", IEEE Trans on Dielectrics and Electrical Insulation, Vol. 5, pp. 505-512, 1998

Chan, H. L. W., Ng, P. K. L. and Choy, C. L., "Effect of poling procedure on the properties of lead zirconate titanate/vinylidene fluoride-trifluoroethylene composites", Appl. Phys. Letters, Vol. 74, pp. 3029-3031, 1999.

Chan, H.L.W., Ng, P.K.L and Choy, C.L., "Permittivity and electrical conductivity of PZT/P(VDF-TrFE) 0-3 Composites", Ferroelectrics, Vol. 201, pp. 225-234, 1997.

Chen, Y., Chan, H. L. W. and Choy, C. L., "Properties of PT/P(VDF-TrFE) 0-3 nanocomposites", Journal of the Korean Physical Society, Vol. 32, pp. S1072-1075, 1998.

Chen, Y., Chan, H. L. W., N. M., Wong, Y. W. and Choy, C. L., "Response of nanocomposite pyroelectric detectors", Sensors and Actuators A, Vol. 69, pp. 155-165, 1998.

Damjanovic, D. "Ferroelectric, dielectric and piezoelectric properties of ferroelectric thin films and ceramic", Rep. Prog. Phys 61, pp.1267-1324, 1998.

Das-Gupta, D. K., "Piezoelectricty and Pyroelectricity", Key Engineering Materials Vols. 92-93, pp. 1-14, 1994.

Dias, C., Simon, M., Quad, R. and Das-Gupta D. K., J. Phys. D: Appl. Phys. 26, pp. 106-110, 1983.

Dias, C. J and Das Gupta, D. K., "Inorganic ceramic/polymer ferroelectric composite electrets", IEEE Trans. on Dielectrics and Electrical Insulation, Vol. 3, pp. 706-734, 1996.

Dias, C. J. and Das-Gupta, D. K., "Piezo-and pyroelectricity in ferroelectric ceramic/polymer composites", Key Engineering Materials Vol. 92-93, pp.217-218, 1994.

Dias, C. and Das-Gupta, D.K., Proceeding of 6th Int. Conf. On Dielectric Materials, Measurements and Applications, DMMA6 ed. IEE, Manchester, pp. 393-396, 1992.

Fang, C., Wang, M. and Zhou, H., "Pyroelectric properties of a new composite material-PVDF-TGS film", Proceedings of 7th International Symposium on Electrets (ISE7), pp.507-511, 1991.

Furukawa, T., Fujino, K., and Fukada, E., "Electromechanical Properties in the Composites of Epoxy Resin and PZT Ceramics", Jpn. J. Appl. Phys., Vol. 15, pp.2119-2129, 1976.

Furukawa, T., Ishida, K., and Fukada, E., "Piezoelectric properties in the composite systems of polymers and PZT ceramics", J. Appl. Phys., Vol. 50, pp. 4904-4912, 1979.

Furukawa, T., Lovinger, A. J., Davis, G. T. and Broadhurst, M. G., "Dielectric hysteresis and nonlinearity in a 52/48 mol-percent co-polymer of vinylidene fluoride and trifluoroethylene", Macromolecules, Vol. 16, pp.1885, 1983.

Furukawa, T., Suzuki K. and Date, M., "Switching process in composite systems of PZT cermaics and polymers", Ferroelectrics, Vol. 68, pp.33-44, 1986.

Garner, G. M., Shorrocks, N. M., Whatmore, R. W., Goosey, M. T., Seth, P. and Ainger, F. W., "0-3 piezoelectric composites for large area hydrophones", Ferroelectrics, Vol. 93, pp. 169-176, 1989.

Giniewicz J. R., "(Pb,Bi)(Ti,Fe)/Polymer 0-3 composite materials for hydrophone applications", M.S. thesis, Pennsylvania State University, University Park, Pennsylvania, 1985.

Giniewicz, J. R., Newnham, R. E. and Safari, A., "(Pb,Bi)-(Ti(Fe,Mn))O3 of polymer 0-3 composites for hydrophone applications", Ferroelectrics, Vol. 66, 1986.

Harrison, W. B., "Flexible piezoelectric organic composites", Proceedings of the workshop on solar transducer materials, Naval Research Laboratories, 1976.

Hippel, V. and Authur, R., Dielectrics and Waves, Wiley, New York, 1954.
IEEE standard definitions of primary ferroelectric terms, ANSI/IEEE Std, pp. 180, 1986.

Jaffe., B., Cook, W.R. and Jaffe, H.L.C., Piezoelectric Ceramics, Academic Press Publishers, New York, 1971.

Kyiatama, T., "Flexible piezoelectric materials", Seramikkusu, Vol. 14, pp.209, 1979.

Lang, S. B. and Das-Gupta, D. K., "A technique for determining the polarization distribution in thin polymer electrets using periodic heating", Ferroelectrics, Vol. 39, pp.1249, 1981.

Lines, M. E. and Glass, A. M., "Principle and Applications of Ferroelectrics and Related Materials", Oxford, 1977.

Meyer, R. J., "High Frequency (15-70MHZ) 1-3 PZT Fiber/Polymer Composites: Fabrication and Characterization", Ph. D. Thesis, Materials, The Pennsylvania State University, 1998.

Miller, S. L., Schwank, J.R., Nasby R.D. and Rodgers, M.S., "Modeling ferroelectric capacitor switching with asymmetric nonperiodic input signals and arbitrary initial conditions", J. Appl. Phys., Vol. 70, pp. 2849-2860, 1991.

Miller, S.L., Nasby, R.D., Schwank, R.D., Rodgers, M.S. and Dressendorfer, P.V., "Device modeling of ferroelectric capacitors", J. Appl. Phys., Vol. 68, pp. 6463-6470, 1990.

Moulson, A.J. and Herbert, J.M., Electroceramics: materials, properties, applications. London: Chapman and Hall, 1990.

Newnham, R. E., Safari, A., Giniewucz, J. and Fox, B. H., "Piezoelectric Sensors", Ferroelectrics, Vol. 60, pp.15, 1984.

Newnham, R.E., Safari, A., Sa-Gong, G. and Guniewucz, J., "Flexible Composite Piezoelectric Sensors", IEEE Ultrasonic Symposium Proceedings, pp.501, 1984.

Newnham, R.E., Skinner, D.P. and Cross, L.E., "Connectivity and Piezoelectric -Pyroelectric Composites", Mat. Res. Bull., Vol. 13, pp.525, 1978.

Ngoma, J. B., Cavaille, J. Y., Paletto, J., Perez, J. and Macchi, F., "Dielectric and piezoelectric properties of copolymer-ferroelectric composite", Ferroelectrics, Vol. 109, pp.205-210, 1990.

Nye, J. F. "Physical properties of Crystal", London, England: Oxford University Press pp. 78-189, 1957.

Pauer, L. A., "Flexible composite materials", IEEE Intl. Conv. Rec., Vol. 1, 1973.

Ploss, B. and Emmerich, R. and Bauer, S., "Thermal wave probing of pyroelectric distributions in the surface region of ferroelectric materials: a new method for the analysis", J Appl. Phys. Vol. 72, pp.5363, 1992.

Ploss, B. and Ploss, B., "Poling of P(VDF-TrFE) with Ferroelectrically Applied Dielectric Displacement", Ferroelectrics, Vol. 184, pp. 107-116, 1996.

Ploss, B., "Handbook of Low and high dielectric constant materials and their applications", Vol. 2, Ed.: H.S. Nalwa, Academic Press, San Diego, pp. 209-287, 1999.

Ploss, B., Hassler, W., Hulz, H. and Kobernik, G., "Investigation of the polarization depth distribution of PZT thick films by LIMM", Proceedings of the Eleventh IEEE International Symposium on Applications of Ferroelectrics (ISAF 98), pp. 207-210, 1998.

Ploss, B., Ng, W. Y., Chan, H. L. W., Ploss, B. and Choy, C. L., "Poling study of PZT/P(VDF-TrFE) composite", Composites Science and Technology, Vol. 61, pp. 957, 2001.

Ploss, B., Ploss, B., Shin, F. G., Chan, H. L. W. and Choy, C. L., "Internal fields in PT/P(VDF-TrFE) 0-3 composites", Proceedings of the 12th IEEE International Symposium on Applications of Ferroelectrics (ISAF 2000), pp. 301-304, 2001.

Safari, A., Sa-Gong, G., Giniewicz, J. and Newnham, R. E., "Composite piezoelectric sensors", Proceedings of the 21st University Conference on Ceramic Science, Vol. 20, pp. 445-454, 1986.

Scaife, B. K. P., Principle of Dielectrics, Clarendon Press, Oxford, pp. 75-112, 1989.
Sessler, G. M., "Electrets: Selected Topics", Springer, Heidelberg, pp. 20-39, 1987.

Tajitsu, Y., Ogura, H., Chiba, A. and Furukawa, T., "Investigation of switching characteristics of vinylidene fluoride/trifluoroethylene copolymers in relation to their structures", Jpn. J. Appl. Phys., Vol. 26, pp. 554-560, 1987.

Tashiro, K., Takano, K., Kobayashi, M., Chatani, Y. and Todokoro, H., "Structure study on ferroelectric phase transition of vinylidene fluoride-trifluoroethylene copolymers (III) dependence of transitional behaviour on VDF molar content", Ferroelectrics, Vol. 57, pp. 297-326, 1984.

Wagner, K., "Erjkarung der dielektrischen nachwirkungsvorgange auf grund maxwellscher Vorstellungen", Archiv. Elektrotech., Vol. 2, pp. 371, 1914.

Wong, C. K., Wong, Y. W. and Shin, F. G., "Effect of interfacial charge on polarization switching of lead zirconate titanate particles in lead zirconate titanate/polyurethane composites", J. Appl. Phys., Vol. 92, No.8, pp. 3974-3978, 2002.

Wong, C. K., Wong, Y. W. and Shin, F. G., "Explicit formulas for effective piezoelectric coefficients of ferroelectric 0-3 composites", J. Appl. Phys., Vol. 90, No. 9, pp. 4690-4700, 2001.

Xu, Y., "Pervoskite-type ferroelectrics: Part I", Ferroelectric Materials and Their Applications, Elserivier Science Publishers B.V., The Netherlands, pp. 101-159, 1991

Yamada, T., Ueda, T. and Kitayama, T., "Piezoelectrcity of a high-content lead zirconate titanate/polymer composites" J. Appl. Phys., Vol. 53, pp.4328-4332, 1982.

Yamazaki, H. and Kitayama. T., "Pyroelectric properties of polymer-ferroelectric composites", Ferroelectrics, Vol. 33, pp.147-153, 1981.

Zhang, Q. Q., Chan, H. L. W., Ploss, B. and Choy, C. L., "PCLT/P(VDF-TrFE) nanocomposite pyroelectric sensors", IEEE Transactions on Ultrasonic, Ferroelectrics and Frequency Control, Vol. 48, pp.154-160, 2001.

LIST OF PUBLICATIONS

Conference Paper

1. Y.T. Or, B. Ploss, F.G. Shin, H.L.W. Chan and C.L. Choy, "Poling of ferroelectric PT/P(VDF-TrFE) 0-3 composite", *Proceedings of International Symposium on Integrated Ferroelectrics (ISIF 2002)*, in press.

Journal Paper

2. Y.T. Or, C.K. Wong, B. Ploss and F.G. Shin, "Polarization behaviour of ferroelectric multi-layered composite structures", submitted to *Journal of Applied Physics*.

3. Y.T. Or, C.K. Wong, B. Ploss and F.G. Shin, "Poling and modeling of piezoelectric and pyroelectric properties of 0-3 composites of ferroelectric inclusions in linear matrix", submitted to *Journal of Applied Physics*.